Electronic Thesis and Dissertation Repository

6-27-2014 12:00 AM

Plasmonic Optical Sensors: Performance Analysis and Engineering Towards Biosensing

Peipei Jia
The University of Western Ontario

Supervisor
Jun Yang
The University of Western Ontario

Graduate Program in Biomedical Engineering
A thesis submitted in partial fulfillment of the requirements for the degree in Doctor of Philosophy
© Peipei Jia 2014

Follow this and additional works at: https://ir.lib.uwo.ca/etd

Part of the Biomedical Devices and Instrumentation Commons, Biotechnology Commons, Membrane Science Commons, Nanoscience and Nanotechnology Commons, Nanotechnology Fabrication Commons, and the Optics Commons

Recommended Citation

PLASMONIC OPTICAL SENSORS: PERFORMANCE ANALYSIS AND
ENGINEERING TOWARDS BIOSENSING

(Thesis format: Integrated Article)

by

Peipei <u>Jia</u>

Biomedical Engineering Graduate Program

A thesis submitted in partial fulfillment
of the requirements for the degree of
Doctor of Philosophy

The School of Graduate and Postdoctoral Studies
The University of Western Ontario
London, Ontario, Canada

Abstract

Surface plasmon resonance (SPR) sensing for quantitative analysis of chemical reactions and biological interactions has become one of the most promising applications of plasmonics. This thesis focuses on performance analysis for plasmonic sensors and implementation of plasmonic optical sensors with novel nanofabrication techniques.

A universal performance analysis model is established for general two-dimensional plasmonic sensors. This model is based on the fundamental facts of surface plasmon theory. The sensitivity only depends on excitation light wavelength as well as dielectric properties of metal and dielectrics. The expression involves no structure-specified parameters, which validates this formula in broad cases of periodic, quasiperiodic and aperiodic nanostructures. Further analysis reveals the intrinsic relationship between plasmonic sensor performance and essential physics of surface plasmon. The analytical results are compared to the sensitivities of previously reported plasmonic sensors in the field. This universal model is a promising qualification criterion for plasmonic sensors.

Plasmonic optical sensors are engineered into high-performance on-chip sensors, plasmonic optical fibers and freestanding nanomembranes. (1) Periodic nanohole arrays are patterned on chip by a simple and robust template-transfer approach. A spectral analysis approach is also developed for improving the sensor performance. This sensor is applied to demonstrate the on-chip detection of cardiac troponin-I. (2) Plasmonic optical fibers are constructed by transferring periodic metal nanostructures from patterned templates onto endfaces of optical fibers using an epoxy adhesive. Patterned metal structures are generally extended from nanohole arrays to nanoslit arrays. A special plasmonic fiber is designed to simultaneously implement multimode refractive index sensing with remarkably narrow linewidth and high figure of merit. A real-

time immunoassay relying on plasmonic fiber is demonstrated. Plasmonic optical fibers also take advantages of consistent optical responses, excellent stability during fiber bending and capability of spectrum filtering. (3) Large-area freestanding metal nanomembranes are implemented using a novel fabrication approach. The formed transferrable membranes feature high-quality and uniform periodic nanohole arrays. The freestanding nanomembranes exhibit remarkably higher transmission intensity in comparison to the nanohole arrays with same features on the substrate. These three modalities of plasmonic sensors possess different applicability to fulfill various plasmonic sensing tasks in respective scenarios.

Keywords

surface plasmon resonance, refractive index sensitivity, 2-D nanostructure, periodic, quasicrystalline, aperiodic, template transfer, nanohole array, nanoslit, plasmonics optical fiber, surface topography, multimode, real-time biosensing, freestanding metal nanomembrane

Co-Authorship Statement

This PhD thesis has been prepared by P. Jia and reviewed by Dr. J. Yang according to the regulations for an integrated article format thesis specified by the Faculty of Graduate and Postdoctoral Studies at the Western University and has been co-authored as follows:

Chapter 3: Universal Optical Performance Analysis

All the theoretical analyses and data analyses were conducted by P. Jia under the supervision of Dr. J. Yang. A paper co-authored by P. Jia and J. Yang is to be submitted.

Chapter 4: Plasmonic Nanohole Array Sensors Fabricated by Template Transfer

All the experiments and data analyses were conducted by P. Jia under the supervision of Dr. J. Yang. Dr. J. Sabarinathan provided the optical setup for measurement. Dr. H. Jiang helped to design and implement optical measurement. A paper entitled ***Plasmonic nanohole array sensors fabricated by template transfer with improved optical performance*** (P. Jia, H. Jiang, J. Sabarinathan and J. Yang) has been published in the ***Nanotechnology***, 2013.

Chapter 5: Plasmonic Optical Fiber

All the experiments and simulations were conducted by P. Jia under the supervision of Dr. J. Yang. A paper entitled ***Integration of large-area metallic nanohole arrays with multimode optical fibers for surface plasmon resonance sensing*** (P. Jia and J. Yang) has been published in the ***Applied Physics Letters***, 2013. Another paper entitled ***A plasmonic optical fiber patterned by template transfer as a high-performance flexible nanoprobe for real-time biosensing*** (P. Jia and J. Yang) has been published in the ***Nanoscale***, 2014.

Chapter 6: Freestanding Metal Nanomembrane as Plasmonic Sensor

All the experiments and data analyses were conducted by P. Jia under the supervision of Dr. J. Yang. A paper co-authored by P. Jia and J. Yang is to be submitted.

Acknowledgments

I would like to sincerely thank my advisor, Prof. Jun Yang for his extensive support and guidance in this research. It is his trust and motivation from beginning to end that enables me to focus my mind and efforts on my research regardless of challenges and roadblocks at the moment. The most important thing I have learned from him is how to be an eligible scientist, which would pave the way for my academic life in future.

Without the help from my colleagues, the research presented in this thesis could not have happened. I would like to appreciate all generous help from Dr. Tingjie Li, Dr. Qiuquan Guo, and Dr. Binyu Yu. I express my gratitude to Dr. Meiku Fan for his introduction of this fantastic field at the very beginning. Other group members also deserve my gratitude for their valuable comments and suggestions. I am grateful to Dr. Hao Jiang and Prof. Jayshri Sabarinathan for our successful collaboration to guide me in the right direction. I also thank the staffs from Western Nanofab including Dr. Todd Simpson, Tim Goldhawk and Dr. Rick Glew for their technical assistance.

Yet most importantly, my little family gives me happiness, courage and perspective that always encourage me. I dedicate this thesis and all the hard work it presents, to my wife, Ying, for her love and all the experience we have gone through together, and to my son, Evan, for his joy and smile. Finally, I am deeply grateful to my parents and hope they know that without their endless love, I would never have made it this far.

Table of Contents

List of Tables

List of Figures

List of Appendices

Chapter 1

1   Introduction

This chapter introduces the basics of surface plasmon resonance sensing and the different implementation of plasmonic sensors. The advanced nanofabrication techniques used in plasmonics including top-down lithography and unconventional methods are also discussed. Based on the limitation of current plasmonic sensing techniques, we define the objectives and scope of this research.

1.1   Surface Plasmon Resonance Sensing

Surface plasmon resonance (SPR) is collective oscillation resulting from the coupling of electromagnetic waves with free electrons.[1-2] Such interaction is bound to the metal/dielectric interface and leads to significant field enhancement phenomena. Surface plasmon (SP) waves are therefore exceptionally sensitive to dielectric properties near the metal surface. In turn, the refractive index change at the interface will modulate the high-concentrated electromagnetic fields generated by SPR. This unique aspect gives rise to a direct means to monitor surface events which could induce dielectric changes for plasmonic applications.

Typical biosensing related to genomic or proteomic applications with SPR probes rely on the highly specific binding of a target analyte to a previously immobilized receptor at the metal sensor surface.[3-4] The size of the most common analytes and receptors, such as proteins or DNA, is in the range of a few nanometers. In consequence, the recognition

process takes place in a few nanometers above the metal surface, where SPR puts the electromagnetic field into effect. The principle advantage of SPR biosensing is its 'label-free' whereby the targets maintain their original properties and functions since no labels, e.g. fluorescent markers or magnetic beads, are involved.[5-6] As a direct consequence, plasmonic sensors allow for real-time monitoring binding events on the sensor surface, thereby providing a distinct advantage over endpoint detection methods, such as ELISA (enzyme-linked immunosorbent assay). This feature constitutes the key of the importance of plasmonic sensors in biosensing applications.

1.1.1 Propagating Plasmon Sensors

The advances in SPR sensing technology have been remarkable since the introduction of SPR biomolecular sensing based on propagating SPs on flat thin metal films.[7] Meanwhile, the commercialization of instruments such as Biacore Inc. has significantly expanded the scope of plasmonic utilization. In this technique, propagating SPs are typically produced by illuminating thin metal films through a prism in Kretschmann configuration based on attenuated total reflection (ATR).[8-9] The prism is used to meet momentum matching condition which is required to excite SPR. The analysis target could be antibodies, antigens, DNA, viruses, cells, bacterial toxins.[10] When analyte binds to the immobilized capture molecules on the sensor surface, changes of the dielectric environment at the surface of metal film alter the magnitude and the position of recorded SPR. The shift of SPR can be measured by angular monitoring, wavelength interrogation, or intensity measurements.

Combined with effective surface chemistry and advanced microfluidic systems, this well-established technique enables real-time detection and measurement of analyte binding and

provides quantitative information on interaction specificity, affinity constants, reaction kinetics and concentration as well as identifies binding partners.[11-12] The conventional SPR sensor has played a considerable role in life science,[10] food industry [13]and medical diagnosis[14]. As a mature technique, propagating SPR sensing now serves as a benchmark for novel nanoplasmonic sensor solutions. In the research aspect, various high-sensitive and miniaturized SPR sensor platforms have emerged including the phase-sensitive SPR sensor[15], waveguide SPR sensors[16-18], and optical fiber SPR sensor[19-22].

1.1.2 Nanoplasmonic Sensors

Currently most research effort on plasmonic sensor is being put onto the development of plasmonic nanostructures for performing real-time and label-free analyses.[4, 6, 23] In particular, the discovery of extraordinary optical transmission (EOT) through subwavelength aperture arrays in optical thick metal films has prompted new research activities for applying optical nanostructures in the field of plasmonic sensor.[24] Dielectric changes around nanostructured metals produce measurable variations of the SPR peak position and magnitude that can be recorded to perform label-free biosensing in real time. In comparison to propagating SPR excited using special illumination configurations, an important advantage of nanoplasmonic sensors on chip is the relaxed SPR excitation conditions, e.g. ordinary white light under normal incident, so that instruments can be made more compact and portable.[25] Another favorite factor of nanoplasmonic sensors is the short penetration depth of evanescent field wave, making the sensor less sensitive to bulk dielectric environment changes induced by temperature fluctuations in the solvent far from the metal surface.

The performance of plasmonic sensor depends on the material, shape, size, pattern of nanostructures and surrounding dielectric environment.[26] The selection of an appropriate material is of utmost importance to performance optimization for a plasmonic device. However, metal suffer from intrinsic ohmic losses and interband transition in the visible and ultraviolet regime. To date, gold and silver are still the most commonly used materials in plasmonics. In contrast, plasmonic structure has much more accommodation. A variety of periodic metal structures such as nanoparticle,[27-30] nanohole arrays,[25, 31-45] and nanoslit arrays[46-54] have been applied in plasmonic sensing. Apart from periodic nanostructures, quasiperiodic and aperiodic and fractal aperture arrays have also been investigated and drawn lots of attention in plasmonics due to the absence of periodicity.[55-65] In essence, it is possible to engineer plasmonic structures to possess desired optical properties by means of state-of-the-art nanofabrication techniques.

1.2 Fabrication of Plasmonic Nanostructures

Advanced nanofabrication technology has been promoting the rapid growth of photonics, electronics, optoelectronics and nanophotonics. In particularly, the development of nanoplasmonics tightly relies on our ability of tailoring metal nanostructures in a controllable way with sub-100 nm resolution.[4] The optical properties of metal nanostructures can be tuned conveniently by making use of the nanofabrication methods to adjust their size, shape and structure patterns.[26, 66] Plasmonic nanostructures are typically created using either conventional top-down techniques or emerging unconventional lithography methods.[4] Top-down approaches involve using advanced techniques such as electron-beam lithography and focused-ion beam milling to pattern

metal nanostructures onto planar substrates. On the other hand, unconventional fabrication technologies enable high-resolution patterning at low costs whereby more researchers have opportunities to access the plasmonics. The availability of nanofabrication techniques will further promote basic research of plasmonics as well as lead to new applications in a wide range of areas such as plasmonic sensing and more. This section will introduce in detail the utilization of these approaches to manufacture representative metal nanostructures that feature special optical properties to support surface plasmon applications such as SPR sensing.

1.2.1 Conventional Top-Down Approaches

1.2.1.1   Electron-Beam Lithography

Electron-beam lithography (EBL) utilizes a beam of electrons focused by modified electron microscopes to pattern nanostructures with arbitrary shapes. The focused beam of electrons is scanned over a surface covered with the electron-sensitive resist, thereby altering the solubility of the resist. The electron exposure enables selective removal of either the exposed or non-exposed regions by immersing the resist in a solvent. The patterned resist can be used as a sacrificial layer to generate nanostructures with well-controlled geometries on the target through deposition processes. By the subsequent process of metallization, the pattern can be transformed into designed metal nanostructures for plasmonic application. Due to its versatility and super resolution (smaller than 10 nm),[67] e-beam lithography has been one of favorite fabrication method for advanced research in the plasmonics.[68-74]

However, the major drawback of EBL is the low-throughput and high-cost. Each nanostructure is lithographically defined in a serial manner. In addition, the involved lift-off process for metallization restricts the creation of nanostructures with high aspect ratios. Moreover, the dependence of the exposure effect on the substrate conductivity limits the choice of substrates.

1.2.1.2 Focused-Ion Beam Milling

Focused-ion beam (FIB) milling is a fabrication technique that impinges a focused beam of ions (typically Ga) onto the substrate to directly write patterns. As a maskless and high-resolution approach, FIB milling is extensively used for direct patterning of metallic nanostructures. Various metal nanostructures such as nanoholes arrays,[24, 39, 75-77] nanoslit gratings,[78-79] circular slits[80] and V-grooves[81] have been demonstrated for research in the field of plasmonics by FIB. In comparison to EBL, FIB milling provides the ability of both 2D and 3D patterning. As a result, this advantage enables us to control the light with plasmonic nanostructure more flexibly.

However some limitations also exist. Traditional FIB technique mills the structures one by one in the same serial manner as EBL. Therefore large-area patterning is not feasible, in particular, for metal nanostructures. One obvious drawback is Ga ions are implanted into the sample surface along with FIB bombardment.[82] This can reduce the performance of patterned plasmonic nanostructure.

1.2.2 Unconventional Lithography Techniques

1.2.2.1   Nanosphere Lithography

Nanosphere lithography (NSL) is a bottom-up nanofabrication technique capable of producing well-ordered two-dimensional nanoparticle arrays.[83-84] NSL begins with self-assembly of monodisperse nanospheres to form a two-dimensional deposition mask. After metal deposition in plasmonic applications, the nanosphere is removed by sonication of the sample in a solvent, leaving behind the patterned metal nanostructure arrays on the substrate. These plasmonic structures are extensively used for localized SPR (LSPR) sensing[85-88] and surface-enhanced Raman spectroscopy (SERS)[89-90]. Detection of tumor markers[91] and disease-related antibody[92] were demonstrated based on extinction spectra of visible light passing through gold nanohole array and nanoparticles formed by NSL. Using nanoparticle-antibody conjugates, a LSPR biosensor was developed to amplify the wavelength shift for more sensitive detection of low-concentration analytes.[93]   By transferring the NSL patterned metalized nanospheres to a flexible substrate, a tunable plasmonic structure can support the polarization-dependent optical response.[94] Recently, a novel 3D Au nanohole arrays fabricated by NSL exhibits much improved optical properties performance in comparison to conventional nanohole arrays.[95]

1.2.2.2   Soft Lithography

In this rapidly emerging technology, soft elastic stamps are used to replicate features by printing or molding nanoscale patterns.[96] Metal nanostructures are patterned using either of self-assembled monolayers (SAM) of molecules or polymer template as an etch mask.

Large-area, free-standing nanohole arrays were fabricated by soft lithography used high-resolution composite PDMS stamps as conformable phase masks.[97] Direct evidence was disclosed for surface plasmon-mediated enhanced light transmission through these metallic nanohole arrays.[98] A high performance plasmonic crystal structure was formed by using soft lithography with an elastomeric mold and subsequent metal deposition.[99] This quasi-3D plasmonic sensor is used for multispectral sensing with submonolayer binding sensitivity[100] and imaging of molecular binding events with spatial resolution of tens of microns[101]. Although soft lithography techniques can pattern metals over large areas, the resolution and aspect ratio of the formed nanostructures is limited.

1.2.2.3   Nanoimprint Lithography

Nanoimprint Lithography (NIL) accomplishes pattern transfer by imprint a hard stamp with nanoscale surface-relief features into a resist cast on a substrate at a controlled temperature and pressure.[102] Unlike photon- or electron-induced resist reaction in traditional lithography approaches, NIL relies on the mechanical deformation. Thus the resolution of NIL is not limited by light diffraction or beam scattering, but depends solely on the smallest attainable features by stamp fabrication. The ultimate resolution of NIL is on the order of sub-10 nm.[103] Being a next generation lithography candidate, NIL has the merits of high-throughput and low-cost, thereby being suitable for large-scale patterning of plasmonic structures.[104] Large-area subwavelength aperture arrays fabricated using NIL show high refractive index sensitivities.[105] Resonant metal gratings fabricated using NIL was incorporated into micromechanical and microfluidic devices.[106] Extraordinary light transmission was also demonstrated with subwavelength holes blocked by metal disks

above the opaque thin metal film.[107] A metal/dielectric/metal stack "fishnet" structure fabricated by NIL reveals a SP induced negative refractive index at near and mid-IR range.[108] The obvious drawback of NIL is molds often get contaminated by liquid resists and may be damaged due to high pressure during pattern transfer.

1.2.2.4 Nanostencil Lithography

Nanostencil lithography (NSL) transfers nanoscale patterns to any planar surface by direct deposition of materials through a stencil as shadow-mask in a single step. NSL enables fabrication of plasmonic metal nanostructures with high reliability and uniformity. The resolution and area of final pattern depend on the pre-patterned stencil which is fabricated on suspended membrane using EBL of FIB milling. The major advantage of NSL is that the stencil can be reuse to pattern the same nanostructures with high repeatability, which facilitates high throughput nanofabrication applications. Since no resists is involved in NSL, it allows for patterning nanostructures on different types of substrates[109] and eliminate the possibility of contaminations. The presented nanostructures demonstrated a major improvement in resolution down to ~50 and ~20 nm. Meanwhile this lift-off free technique enables fabrication of nanostructures with high aspect ratios. The Infrared plasmonic nanorod antenna arrays fabricated by NSL were demonstrated to support spectrally sharp collective resonances in vibration spectroscopy.[110] NSL can also achieve nanopatterning on a wide range of unconventional and non-planar substrates.[111] By patterning plasmonic nanorod arrays on thin flexible films, their optical responses can be actively tuned by mechanical stretching the substrate. On the other hand, high-resolution patterning requires a suspended thin membrane on stencil mask which can be easily broken.

Furthermore, the evaporation of metal through the mask may gradually clog the apertures on the stencil.

One similar technique as NSL is a lift-off free nanofabrication method, which explores the additive metal nanostructures left on the stencil after deposition rather than those on the substrate.[112] This approach sacrifices the recyclability of NSL mask due to using the nanostructure with the stencil together. However, the suspended plasmonic nanostructures feature very high optical performance and targeted delivery of analytes due to throughout nanohole openings,[113] which are both of great importance for biosensing application. The integrated nanoplasmonic-nanofluidic biosensors can actively transport virus analytes for rapid and ultrasensitive detection[31] and even enable seeing protein monolayers with naked eye[32]. In addition, this integration facilitates the implementation of plasmonic sensing on lightweight and portable device for point-of-care applications in resource-limited settings.[114]

1.2.2.5 Interference Lithography

Interference lithography (IL) makes use of interference of laser beams incident from different directions to generate interference patterns, which consists of a periodic standing wave and is recorded on the photoresist. Thus IL requires no advanced exposure optics or photomask. IL has proven its ability to generate uniform two dimensional patterns over a large area.[115] The obvious drawback is IL cannot produce complex shape or pattern due to the limitation of interference pattern. However, regular nanostructures in plasmonics consist of simple periodic patterns (e.g. periodic arrays of particles, holes, slits) and do not require arbitrary pattern generation. In this context, IL is a simple and useful method for

fabrication of these types of plasmonic nanostructures in large area. Nanohole arrays were fabricated by IL as high-resolution surface plasmon resonance sensor with linewidth-optimized transmittance[116] and spectral sensitivity[117]. A bimetallic nanodot array was obtained by a lift-off procedure after IL for tuning surface plasmon resonance.[118] Multiscale nanohole arrays in thin gold films patterned by IL combined with soft lithography were used to study the dispersion properties of plasmonic lattices consisting of near-infinite arrays and superlattices.[119] With the same method, nanopyramidal gratings were developed to improve the sensitivities of plasmonic biosensors using the angle-dependent resonances of molded plasmonic crystals,[120-121] and anisotropic three-dimensional nanohole arrays were used to selectively excited and manipulate surface plasmons on the same substrate.[122] Moreover, large-scale plasmonic microarrays was patterned for label-free high-throughput screening of large libraries of pharmaceutical compounds and biomolecular interactions.[123] Recently, a plasmonic gold mushroom arrays developed by IL exhibited refractive index sensing figures of merit approaching the theoretical limit.[124]

1.3 Motivation

Many excellent plasmonic sensors have been demonstrated in the field of biosensing, chemical imaging and spectroscopy due to present rapid advances in nanofabrication technologies and computational electrodynamics. Nonetheless, some unsolved basic theoretical problems still restrict our understanding of the intrinsic physics and principle behind phenomena. For instance, the plasmonic sensor performance intensively depends on the pattern of the nanostructures due to nature of SPR. We can certainly compare the

performance of different sensors using indicators such as refractive index sensitivity and figure of merit. However whether the experimental performance of one sensor achieves that it intrinsically has, is unclear. Thus a universal performance analysis model for general plasmonic nanostructures is of theoretic importance and highly desirable for performance assessment. On the other hand, extensive utilization of plasmonic sensors requires effective and high-quality fabrication techniques to pattern metal nanostructures in various modalities. Meanwhile practical application demands that plasmonic sensor systems own the merit of flexibility and robustness for different scenarios. The implementation of such plasmonic sensors would have great promises to far extend the scope of plasmonics utilization in biological and chemical community.

1.4   Objectives and Outline

The overall objectives of this thesis are (i) to address the performance analysis for general two-dimensional plasmonic nanostructures and (ii) to develop novel nanofabrication methods and platforms for plasmonic sensing.

The main body of the thesis is organized into the independent portions of the original research performed towards the aforementioned objectives. An overview of the following chapters describes the content and link of each chapter with the objectives.

Chapter 2 introduces the theoretical background including dielectric constant of metals, dispersion relation of surface plasmon and extraordinary optical transmission of nanohole arrays, which are necessary for understanding SPR fundamentals.

Chapter 3 proposes the universal performance analysis model based on momentum matching condition for SPR excitation. A sensitivity expression is established using the momentum matching condition of SPR excitation for any tow-dimensional nanohole Bravais lattices. The sensitivity only depends on excitation light wavelength as well as dielectric properties of metal and dielectrics. A series of phenomena in plasmonic sensing are successfully explained using this quantitative model. The nanohole arrays are proved to have larger intrinsic sensitivity compared to nanoparticle LSPR sensors. The expression involves no structure-specified parameters, which validates this formula in broad cases of periodic, quasiperiodic and aperiodic nanostructures. The analytical results are compared to the sensitivities of previously reported plasmonic sensors in the field.

Chapter 4 describes a high-performance on-chip plasmonic nanohole array sensor fabricated by a novel template transfer scheme for simple and repeatable production of high-quality nanostructures on substrates for biosensing. By the sensitivity comparison between two nanohole array sensors with different morphology, the in-hole surface is verified to have higher sensitivity. A spectral analysis approach is also developed for improving the sensor performance. This sensor is applied to demonstrate the on-chip detection of cardiac troponin-I.

Chapter 5 describes the implementation of plasmonic optical fiber as a high-performance flexible nanoprobe for real-time biosensing. Plasmonic optical fibers are constructed by transferring periodic metal nanostructures from patterned templates onto endfaces of optical fibers. Patterned metal structures are generally extended from nanohole arrays to nanoslit arrays. By adjusting the viscosity of adhesive layers, surface topography of metal structures can be controlled. The specially designed plasmonic fiber can work in multimode at the same

time in refractive index sensing with remarkably narrow linewidth and high figure of merit. A real-time immunoassay relying on plasmonic fiber is demonstrated. Plasmonic optical fibers also take advantages of consistent optical responses, excellent stability during fiber bending and capability of spectrum filtering.

Chapter 6 presents a large-area freestanding metal nanomembrane implemented using a novel fabrication approach. This technique is same applicable to freestanding nanoslit fabrication. The formed membranes feature high-quality, uniform and throughout periodic nanohole arrays and is transferrable to unconventional surfaces. The freestanding nanomembranes exhibit remarkably enhanced transmission intensity in comparison to the nanohole arrays with same features on the substrate.

Chapter 7 concludes the previous work towards performance analysis and engineering of plasmonic sensing, along with directions of future research.

References

1.   Ritchie, R., Plasma losses by fast electrons in thin films. *Physical Review* **1957,** *106* (5), 874.

2.   Barnes, W. L.; Dereux, A.; Ebbesen, T. W., Surface plasmon subwavelength optics. *Nature* **2003,** *424* (6950), 824-830.

3.   Homola, J., Surface plasmon resonance sensors for detection of chemical and biological species. *Chemical Reviews* **2008,** *108* (2), 462-493.

4.   Stewart, M. E.; Anderton, C. R.; Thompson, L. B.; Maria, J.; Gray, S. K.; Rogers, J. A.; Nuzzo, R. G., Nanostructured plasmonic sensors. *Chemical Reviews* **2008,** *108* (2), 494-521.

5.   Anker, J. N.; Hall, W. P.; Lyandres, O.; Shah, N. C.; Zhao, J.; Van Duyne, R. P., Biosensing with plasmonic nanosensors. *Nat Mater* **2008,** *7* (6), 442-53.

6.   Mayer, K. M.; Hafner, J. H., Localized surface plasmon resonance sensors. *Chemical Reviews* **2011,** *111* (6), 3828-3857.

7.   Liedberg, B.; Nylander, C.; Lunström, I., Surface plasmon resonance for gas detection and biosensing. *Sensors and actuators* **1983,** *4*, 299-304.

8.   Löfås, S.; Malmqvist, M.; Rönnberg, I.; Stenberg, E.; Liedberg, B.; Lundström, I., Bioanalysis with surface plasmon resonance. *Sensors and Actuators B: Chemical* **1991,** *5* (1), 79-84.

9.   Karlsson, R.; Michaelsson, A.; Mattsson, L., Kinetic analysis of monoclonal antibody-antigen interactions with a new biosensor based analytical system. *Journal of immunological methods* **1991,** *145* (1), 229-240.

10.   Karlsson, R., SPR for molecular interaction analysis: a review of emerging application areas. *Journal of Molecular Recognition* **2004,** *17* (3), 151-161.

11.   Campbell, C. T.; Kim, G., SPR microscopy and its applications to high-throughput analyses of biomolecular binding events and their kinetics. *Biomaterials* **2007,** *28* (15), 2380-2392.

12.   Wassaf, D.; Kuang, G.; Kopacz, K.; Wu, Q.-L.; Nguyen, Q.; Toews, M.; Cosic, J.; Jacques, J.; Wiltshire, S.; Lambert, J., High-throughput affinity ranking of antibodies using surface plasmon resonance microarrays. *Analytical biochemistry* **2006,** *351* (2), 241-253.

13.   Taylor, A. D.; Ladd, J.; Yu, Q.; Chen, S.; Homola, J.; Jiang, S., Quantitative and simultaneous detection of four foodborne bacterial pathogens with a multi-channel SPR sensor. *Biosensors and Bioelectronics* **2006,** *22* (5), 752-758.

14.   Estmer Nilsson, C.; Abbas, S.; Bennemo, M.; Larsson, A.; Hämäläinen, M.; Frostell-Karlsson, Å., A novel assay for influenza virus quantification using surface plasmon resonance. *Vaccine* **2010,** *28* (3), 759-766.

15.   Patskovsky, S.; Meunier, M.; Prasad, P. N.; Kabashin, A. V., Self-noise-filtering phase-sensitive surface plasmon resonance biosensing. *Optics express* **2010,** *18* (14), 14353-14358.

16.   Stöcker, P.; Menges, B.; Langbein, U.; Mittler, S., Multimode waveguide mode surface plasmon coupling: a sensitivity and device realizability study. *Sensors and Actuators A: Physical* **2004,** *116* (2), 224-231.

17.   Homola, J.; Čtyroký, J.; Skalský, M.; Hradilova, J.; Kolářová, P., A surface plasmon resonance based integrated optical sensor. *Sensors and Actuators B: Chemical* **1997,** *39* (1), 286-290.

18.   Berini, P., Bulk and surface sensitivities of surface plasmon waveguides. *New J Phys* **2008,** *10* (10), 105010.

19.   Jorgenson, R.; Yee, S., A fiber-optic chemical sensor based on surface plasmon resonance. *Sensors and Actuators B: Chemical* **1993,** *12* (3), 213-220.

20.   Slavík, R.; Homola, J.; Čtyroký, J., Miniaturization of fiber optic surface plasmon resonance sensor. *Sensors and Actuators B: Chemical* **1998,** *51* (1), 311-315.

21.   Slavık, R.; Homola, J.; Brynda, E., A miniature fiber optic surface plasmon resonance sensor for fast detection of staphylococcal enterotoxin B. *Biosensors and Bioelectronics* **2002,** *17* (6), 591-595.

22.   Suzuki, H.; Sugimoto, M.; Matsui, Y.; Kondoh, J., Effects of gold film thickness on spectrum profile and sensitivity of a multimode-optical-fiber SPR sensor. *Sensors and Actuators B: Chemical* **2008,** *132* (1), 26-33.

23.   Anker, J. N.; Hall, W. P.; Lyandres, O.; Shah, N. C.; Zhao, J.; Van Duyne, R. P., Biosensing with plasmonic nanosensors. *Nature materials* **2008,** *7* (6), 442-453.

24.   Ebbesen, T. W.; Lezec, H. J.; Ghaemi, H. F.; Thio, T.; Wolff, P. A., Extraordinary optical transmission through sub-wavelength hole arrays. *Nature* **1998,** *391* (6668), 667-669.

25.   Brolo, A. G.; Gordon, R.; Leathem, B.; Kavanagh, K. L., Surface plasmon sensor based on the enhanced light transmission through arrays of nanoholes in gold films. *Langmuir* **2004,** *20* (12), 4813-4815.

26.   Lindquist, N. C.; Nagpal, P.; McPeak, K. M.; Norris, D. J.; Oh, S.-H., Engineering metallic nanostructures for plasmonics and nanophotonics. *Reports on Progress in Physics. Physical Society (Great Britain)* **2012,** *75* (3), 036501.

27.   McFarland, A. D.; Van Duyne, R. P., Single silver nanoparticles as real-time optical sensors with zeptomole sensitivity. *Nano Letters* **2003,** *3* (8), 1057-1062.

28.   Haes, A. J.; Van Duyne, R. P., A nanoscale optical biosensor: sensitivity and selectivity of an approach based on the localized surface plasmon resonance spectroscopy of triangular silver nanoparticles. *Journal of the American chemical society* **2002,** *124* (35), 10596-10604.

29.   Sherry, L. J.; Chang, S.-H.; Schatz, G. C.; Van Duyne, R. P.; Wiley, B. J.; Xia, Y., Localized surface plasmon resonance spectroscopy of single silver nanocubes. *Nano Letters* **2005,** *5* (10), 2034-2038.

30.   Sannomiya, T.; Hafner, C.; Voros, J., In situ sensing of single binding events by localized surface plasmon resonance. *Nano Letters* **2008,** *8* (10), 3450-3455.

31.   Yanik, A. A.; Huang, M.; Kamohara, O.; Artar, A.; Geisbert, T. W.; Connor, J. H.; Altug, H., An optofluidic nanoplasmonic biosensor for direct detection of live viruses from biological media. *Nano Letters* **2010,** *10* (12), 4962-4969.

32.   Yanik, A. A.; Cetin, A. E.; Huang, M.; Artar, A.; Mousavi, S. H.; Khanikaev, A.; Connor, J. H.; Shvets, G.; Altug, H., Seeing protein monolayers with naked eye through plasmonic Fano resonances. *Proceedings of the National Academy of Sciences* **2011,** *108* (29), 11784-11789.

33.   Brolo, A. G.; Kwok, S. C.; Moffitt, M. G.; Gordon, R.; Riordon, J.; Kavanagh, K. L., Enhanced fluorescence from arrays of nanoholes in a gold film. *Journal of the American chemical society* **2005,** *127* (42), 14936-14941.

34.   De Leebeeck, A.; Kumar, L. S.; de Lange, V.; Sinton, D.; Gordon, R.; Brolo, A. G., On-chip surface-based detection with nanohole arrays. *Analytical Chemistry* **2007,** *79* (11), 4094-4100.

35.   Ferreira, J.; Santos, M. J.; Rahman, M. M.; Brolo, A. G.; Gordon, R.; Sinton, D.; Girotto, E. M., Attomolar protein detection using in-hole surface plasmon resonance. *Journal of the American chemical society* **2008,** *131* (2), 436-437.

36.   Eftekhari, F.; Escobedo, C.; Ferreira, J.; Duan, X.; Girotto, E. M.; Brolo, A. G.; Gordon, R.; Sinton, D., Nanoholes as nanochannels: flow-through plasmonic sensing. *Analytical Chemistry* **2009,** *81* (11), 4308-4311.

37.   Escobedo, C.; Brolo, A. G.; Gordon, R.; Sinton, D., Flow-through vs flow-over: analysis of transport and binding in nanohole array plasmonic biosensors. *Analytical Chemistry* **2010,** *82* (24), 10015-10020.

38.   Escobedo, C.; Brolo, A. G.; Gordon, R.; Sinton, D., Optofluidic concentration: plasmonic nanostructure as concentrator and sensor. *Nano Letters* **2012,** *12* (3), 1592-1596.

39.   Sannomiya, T.; Scholder, O.; Jefimovs, K.; Hafner, C.; Dahlin, A. B., Investigation of plasmon resonances in metal films with nanohole arrays for biosensing applications. *Small* **2011,** *7* (12), 1653-1663.

40.   Feuz, L.; Jönsson, P.; Jonsson, M. P.; Höök, F., Improving the limit of detection of nanoscale sensors by directed binding to high-sensitivity areas. *ACS Nano* **2010,** *4* (4), 2167-2177.

41.   McMahon, J. M.; Henzie, J.; Odom, T. W.; Schatz, G. C.; Gray, S. K., Tailoring the sensing capabilities of nanohole arrays in gold films with Rayleigh anomaly-surface plasmon polaritons. *Optics express* **2007,** *15* (26), 18119-18129.

42.   Im, H.; Wittenberg, N. J.; Lesuffleur, A.; Lindquist, N. C.; Oh, S.-H., Membrane protein biosensing with plasmonic nanopore arrays and pore-spanning lipid membranes. *Chemical Science* **2010,** *1* (6), 688-696.

43.   Im, H.; Lee, S. H.; Wittenberg, N. J.; Johnson, T. W.; Lindquist, N. C.; Nagpal, P.; Norris, D. J.; Oh, S.-H., Template-stripped smooth Ag nanohole arrays with silica shells for surface plasmon resonance biosensing. *ACS Nano* **2011,** *5* (8), 6244-6253.

44.   Im, H.; Sutherland, J. N.; Maynard, J. A.; Oh, S.-H., Nanohole-based surface plasmon resonance instruments with improved spectral resolution quantify a broad range of antibody-ligand binding kinetics. *Analytical Chemistry* **2012,** *84* (4), 1941-1947.

45.   Lee, S. H.; Lindquist, N. C.; Wittenberg, N. J.; Jordan, L. R.; Oh, S.-H., Real-time full-spectral imaging and affinity measurements from 50 microfluidic channels using nanohole surface plasmon resonance. *Lab on a Chip* **2012,** *12* (20), 3882-3890.

46.   Lee, K.-L.; Lee, C.-W.; Wang, W.-S.; Wei, P.-K., Sensitive biosensor array using surface plasmon resonance on metallic nanoslits. *Journal of biomedical optics* **2007,** *12* (4), 044023-044023-5.

47.   Lee, K.-L.; Lee, C.-W.; Wei, P.-K., Sensitive detection of nanoparticles using metallic nanoslit arrays. *Applied Physics Letters* **2007,** *90* (23), 233119-233119-3.

48.   Lee, K.-L.; Wang, W.-S.; Wei, P.-K., Sensitive label-free biosensors by using gap plasmons in gold nanoslits. *Biosensors and Bioelectronics* **2008,** *24* (2), 210-215.

49.   Lee, K.-L.; Wang, W.-S.; Wei, P.-K., Comparisons of surface plasmon sensitivities in periodic gold nanostructures. *Plasmonics* **2008,** *3* (4), 119-125.

50.   Lee, K.-L.; Wu, S.-H.; Wei, P.-K., Intensity sensitivity of gold nanostructures and its application for high-throughput biosensing. *Optics express* **2009,** *17* (25), 23104-23113.

51.   Lee, K.-L.; Wei, P.-K., Optimization of periodic gold nanostructures for intensity-sensitive detection. *Applied Physics Letters* **2011,** *99* (8), 083108.

52.   Lee, K.-L.; Chen, P.-W.; Wu, S.-H.; Huang, J.-B.; Yang, S.-Y.; Wei, P.-K., Enhancing surface plasmon detection using template-stripped gold nanoslit arrays on plastic films. *ACS Nano* **2012,** *6* (4), 2931-2939.

53.   Lee, K. L.; Chih, M. J.; Shi, X.; Ueno, K.; Misawa, H.; Wei, P. K., Improving Surface Plasmon Detection in Gold Nanostructures Using a Multi‐Polarization Spectral Integration Method. *Advanced Materials* **2012,** *24* (35), OP253-OP259.

54.   Wu, S. H.; Lee, K. L.; Chiou, A.; Cheng, X.; Wei, P. K., Optofluidic Platform for Real‐Time Monitoring of Live Cell Secretory Activities Using Fano Resonance in Gold Nanoslits. *Small* **2013,** *9* (20), 3532-3540.

55.   Przybilla, F.; Genet, C.; Ebbesen, T., Enhanced transmission through Penrose subwavelength hole arrays. *Applied Physics Letters* **2006,** *89* (12), 121115.

56.   Rockstuhl, C.; Lederer, F.; Zentgraf, T.; Giessen, H., Enhanced transmission of periodic, quasiperiodic, and random nanoaperture arrays. *Applied Physics Letters* **2007,** *91* (15), 151109.

57.   Bao, Y.-J.; Zhang, B.; Wu, Z.; Si, J.-W.; Wang, M.; Peng, R.-W.; Lu, X.; Shao, J.; Li, Z.-f.; Hao, X.-P., Surface-plasmon-enhanced transmission through metallic film perforated with fractal-featured aperture array. *Applied Physics Letters* **2007,** *90* (25), 251914.

58.   Bravo-Abad, J.; Fernandez-Dominguez, A.; Garcá-Vidal, F.; Martń-Moreno, L., Theory of extraordinary transmission of light through quasiperiodic arrays of subwavelength holes. *arXiv preprint cond-mat/0606121* **2006**.

59.   Matsui, T.; Agrawal, A.; Nahata, A.; Vardeny, Z. V., Transmission resonances through aperiodic arrays of subwavelength apertures. *Nature* **2007,** *446* (7135), 517-521.

60.   Pacifici, D.; Lezec, H. J.; Sweatlock, L. A.; Walters, R. J.; Atwater, H. A., Universal optical transmission features in periodic and quasiperiodic hole arrays. *Optics express* **2008,** *16* (12), 9222-9238.

61.   Zhou, W.; Gao, H.; Odom, T. W., Toward broadband plasmonics: tuning dispersion in rhombic plasmonic crystals. *ACS Nano* **2010,** *4* (2), 1241-1247.

62.   Lubin, S. M.; Hryn, A. J.; Huntington, M. D.; Engel, C. J.; Odom, T. W., Quasiperiodic Moiré Plasmonic Crystals. *ACS Nano* **2013,** *7* (12), 11035-11042.

63.   Xue, J.; Dong, B.-Q.; Wang, X.; Yang, R.; Xu, Z.-C.; Chen, Y.; Huq, E.; Zeng, W.; Qu, X.-P.; Liu, R., Surface plasmon enhanced transmission through gold planar crystals with various aperture arrangements. *Microelectronic Engineering* **2010,** *87* (5), 1340-1343.

64.   Xue, J.; Zhou, W.-Z.; Dong, B.-Q.; Wang, X.; Chen, Y.; Huq, E.; Zeng, W.; Qu, X.-P.; Liu, R., Surface plasmon enhanced transmission through planar gold quasicrystals fabricated by focused ion beam technique. *Microelectronic Engineering* **2009,** *86* (4), 1131-1133.

65.   Huang, X.; Xiao, S.; Ye, D.; Huangfu, J.; Wang, Z.; Ran, L.; Zhou, L., Fractal plasmonic metamaterials for subwavelength imaging. *Optics express* **2010,** *18* (10), 10377-10387.

66.   Henzie, J.; Lee, J.; Lee, M. H.; Hasan, W.; Odom, T. W., Nanofabrication of Plasmonic Structures*. *Annual Review of Physical Chemistry* **2009,** *60* (1), 147-165.

67.   Broers, A.; Molzen, W.; Cuomo, J.; Wittels, N., Electron‑beam fabrication of 80‑Å metal structures. *Applied Physics Letters* **2008,** *29* (9), 596-598.

68.   Sharpe, J. C.; Mitchell, J. S.; Lin, L.; Sedoglavich, N.; Blaikie, R. J., Gold nanohole array substrates as immunobiosensors. *Analytical Chemistry* **2008,** *80* (6), 2244-2249.

69.   Ji, J.; O'Connell, J. G.; Carter, D. J.; Larson, D. N., High-throughput nanohole array based system to monitor multiple binding events in real time. *Analytical Chemistry* **2008,** *80* (7), 2491-2498.

70.   Lee, K. L.; Wei, P. K., Enhancing surface plasmon detection using ultrasmall nanoslits and a multispectral integration method. *Small* **2010,** *6* (17), 1900-1907.

71.   Braun, J.; Gompf, B.; Weiss, T.; Giessen, H.; Dressel, M.; Hübner, U., Optical transmission through subwavelength hole arrays in ultrathin metal films. *Phys Rev B* **2011,** *84* (15), 155419.

72.   Wu, C.; Khanikaev, A. B.; Adato, R.; Arju, N.; Yanik, A. A.; Altug, H.; Shvets, G., Fano-resonant asymmetric metamaterials for ultrasensitive spectroscopy and identification of molecular monolayers. *Nature materials* **2012,** *11* (1), 69-75.

73.   Adato, R.; Altug, H., In-situ ultra-sensitive infrared absorption spectroscopy of biomolecule interactions in real time with plasmonic nanoantennas. *Nature communications* **2013,** *4*.

74.   Adato, R.; Yanik, A. A.; Amsden, J. J.; Kaplan, D. L.; Omenetto, F. G.; Hong, M. K.; Erramilli, S.; Altug, H., Ultra-sensitive vibrational spectroscopy of protein monolayers with plasmonic nanoantenna arrays. *Proceedings of the National Academy of Sciences* **2009,** *106* (46), 19227-19232.

75. Poujet, Y.; Salvi, J.; Baida, F. I., 90% Extraordinary optical transmission in the visible range through annular aperture metallic arrays. *Optics letters* **2007,** *32* (20), 2942-2944.

76. Stark, P.; Halleck, A. E.; Larson, D., Short order nanohole arrays in metals for highly sensitive probing of local indices of refraction as the basis for a highly multiplexed biosensor technology. *Methods* **2005,** *37* (1), 37-47.

77. Ji, J.; Yang, J.-C.; Larson, D. N., Nanohole arrays of mixed designs and microwriting for simultaneous and multiple protein binding studies. *Biosensors and Bioelectronics* **2009,** *24* (9), 2847-2852.

78. Gonzalez, M.; Weeber, J.-C.; Baudrion, A.-L.; Dereux, A.; Stepanov, A.; Krenn, J.; Devaux, E.; Ebbesen, T., Design, near-field characterization, and modeling of 45 surface-plasmon Bragg mirrors. *Phys Rev B* **2006,** *73* (15), 155416.

79. López-Tejeira, F.; Rodrigo, S. G.; Martín-Moreno, L.; García-Vidal, F. J.; Devaux, E.; Ebbesen, T. W.; Krenn, J. R.; Radko, I.; Bozhevolnyi, S. I.; González, M. U., Efficient unidirectional nanoslit couplers for surface plasmons. *Nature physics* **2007,** *3* (5), 324-328.

80. Chang, C.-K.; Lin, D.-Z.; Yeh, C.-S.; Lee, C.-K.; Chang, Y.-C.; Lin, M.-W.; Yeh, J.-T.; Liu, J.-M., Experimental analysis of surface plasmon behavior in metallic circular slits. *Applied Physics Letters* **2007,** *90* (6), 061113.

81. Volkov, V. S.; Bozhevolnyi, S. I.; Devaux, E.; Laluet, J.-Y.; Ebbesen, T. W., Wavelength selective nanophotonic components utilizing channel plasmon polaritons. *Nano Letters* **2007,** *7* (4), 880-884.

82. Mayer, J.; Giannuzzi, L. A.; Kamino, T.; Michael, J., TEM sample preparation and FIB-induced damage. *Mrs Bulletin* **2007,** *32* (05), 400-407.

83. Hulteen, J. C.; Van Duyne, R. P., Nanosphere lithography: a materials general fabrication process for periodic particle array surfaces. *Journal of Vacuum Science & Technology A* **1995,** *13* (3), 1553-1558.

84. Haynes, C. L.; Van Duyne, R. P., Nanosphere lithography: a versatile nanofabrication tool for studies of size-dependent nanoparticle optics. *The Journal of Physical Chemistry B* **2001,** *105* (24), 5599-5611.

85. Huang, W.; Qian, W.; El-Sayed, M. A., Coherent vibrational oscillation in gold prismatic monolayer periodic nanoparticle arrays. *Nano Letters* **2004,** *4* (9), 1741-1747.

86. Das, A.; Zhao, J.; Schatz, G. C.; Sligar, S. G.; Van Duyne, R. P., Screening of type I and II drug binding to human cytochrome P450-3A4 in nanodiscs by localized surface plasmon resonance spectroscopy. *Analytical Chemistry* **2009,** *81* (10), 3754-3759.

87. Prikulis, J.; Hanarp, P.; Olofsson, L.; Sutherland, D.; Käll, M., Optical spectroscopy of nanometric holes in thin gold films. *Nano Letters* **2004,** *4* (6), 1003-1007.

88. Ctistis, G.; Patoka, P.; Wang, X.; Kempa, K.; Giersig, M., Optical transmission through hexagonal arrays of subwavelength holes in thin metal films. *Nano Letters* **2007,** *7* (9), 2926-2930.

89. Li, M.; Cushing, S. K.; Zhang, J.; Suri, S.; Evans, R.; Petros, W. P.; Gibson, L. F.; Ma, D.; Liu, Y.; Wu, N., Three-dimensional hierarchical plasmonic nano-architecture enhanced surface-enhanced Raman scattering immunosensor for cancer biomarker detection in blood plasma. *ACS Nano* **2013,** *7* (6), 4967-4976.

90. Lee, S. H.; Bantz, K. C.; Lindquist, N. C.; Oh, S.-H.; Haynes, C. L., Self-assembled plasmonic nanohole arrays. *Langmuir* **2009,** *25* (23), 13685-13693.

91. Gao, D.; Chen, W.; Mulchandani, A.; Schultz, J. S., Detection of tumor markers based on extinction spectra of visible light passing through gold nanoholes. *Applied Physics Letters* **2007,** *90* (7), 073901.

92. Haes, A. J.; Hall, W. P.; Chang, L.; Klein, W. L.; Van Duyne, R. P., A localized surface plasmon resonance biosensor: First steps toward an assay for Alzheimer's disease. *Nano Letters* **2004,** *4* (6), 1029-1034.

93.   Hall, W. P.; Ngatia, S. N.; Van Duyne, R. P., LSPR Biosensor Signal Enhancement Using Nanoparticle− Antibody Conjugates. *The Journal of Physical Chemistry C* **2011,** *115* (5), 1410-1414.

94.   Zhu, X.; Xiao, S.; Shi, L.; Liu, X.; Zi, J.; Hansen, O.; Mortensen, N. A., A stretch-tunable plasmonic structure with a polarization-dependent response. *Optics express* **2012,** *20* (5), 5237-5242.

95.   Ai, B.; Yu, Y.; Möhwald, H.; Zhang, G., Novel 3D Au nanohole arrays with outstanding optical properties. *Nanotechnology* **2013,** *24* (3), 035303.

96.   Xia, Y.; Whitesides, G. M., Soft lithography. *Annual review of materials science* **1998,** *28* (1), 153-184.

97.   Kwak, E.-S.; Henzie, J.; Chang, S.-H.; Gray, S. K.; Schatz, G. C.; Odom, T. W., Surface plasmon standing waves in large-area subwavelength hole arrays. *Nano Letters* **2005,** *5* (10), 1963-1967.

98.   Gao, H.; Henzie, J.; Odom, T. W., Direct evidence for surface plasmon-mediated enhanced light transmission through metallic nanohole arrays. *Nano Letters* **2006,** *6* (9), 2104-2108.

99.   Malyarchuk, V.; Hua, F.; Mack, N.; Velasquez, V.; White, J.; Nuzzo, R.; Rogers, J., High performance plasmonic crystal sensor formed by soft nanoimprint lithography. *Optics express* **2005,** *13* (15), 5669-5675.

100.   Stewart, M. E.; Mack, N. H.; Malyarchuk, V.; Soares, J. A.; Lee, T.-W.; Gray, S. K.; Nuzzo, R. G.; Rogers, J. A., Quantitative multispectral biosensing and 1D imaging using quasi-3D plasmonic crystals. *Proceedings of the National Academy of Sciences* **2006,** *103* (46), 17143-17148.

101.   Yao, J.; Stewart, M. E.; Maria, J.; Lee, T. W.; Gray, S. K.; Rogers, J. A.; Nuzzo, R. G., Seeing molecules by eye: Surface plasmon resonance imaging at visible wavelengths with high spatial resolution and submonolayer sensitivity. *Angewandte Chemie* **2008,** *120* (27), 5091-5095.

102.   Chou, S. Y.; Krauss, P. R.; Renstrom, P. J., 25-nanometer resolution. *Science* 272 **1996**, 85-87.

103.   Chou, S. Y.; Keimel, C.; Gu, J., Ultrafast and direct imprint of nanostructures in silicon. *Nature* **2002,** *417* (6891), 835-837.

104.   Lucas, B. D.; Kim, J. S.; Chin, C.; Guo, L. J., Nanoimprint Lithography Based Approach for the Fabrication of Large‐Area, Uniformly‐Oriented Plasmonic Arrays. *Advanced Materials* **2008,** *20* (6), 1129-1134.

105.   Skinner, J. L.; Hunter, L. L.; Talin, A. A.; Provine, J.; Horsley, D. A., Large-area subwavelength aperture arrays fabricated using nanoimprint lithography. *Nanotechnology, IEEE Transactions on* **2008,** *7* (5), 527-531.

106.   Horsley, D. A.; Talin, A.; Skinner, J. L., Micromechanical and microfluidic devices incorporating resonant metallic gratings fabricated using nanoimprint lithography. *Journal of Nanophotonics* **2008,** *2* (1), 021785-021785-11.

107.   Li, W.-D.; Hu, J.; Chou, S. Y., Extraordinary light transmission through opaque thin metal film with subwavelength holes blocked by metal disks. *Optics express* **2011,** *19* (21), 21098-21108.

108.   Wu, W.; Kim, E.; Ponizovskaya, E.; Liu, Y.; Yu, Z.; Fang, N.; Shen, Y. R.; Bratkovsky, A. M.; Tong, W.; Sun, C., Optical metamaterials at near and mid-IR range fabricated by nanoimprint lithography. *Applied Physics A* **2007,** *87* (2), 143-150.

109.   Vazquez-Mena, O.; Sannomiya, T.; Tosun, M.; Villanueva, L. G.; Savu, V.; Voros, J.; Brugger, J., High-resolution resistless nanopatterning on polymer and flexible substrates for plasmonic biosensing using stencil masks. *ACS Nano* **2012,** *6* (6), 5474-5481.

110.   Aksu, S.; Yanik, A. A.; Adato, R.; Artar, A.; Huang, M.; Altug, H., High-throughput nanofabrication of infrared plasmonic nanoantenna arrays for vibrational nanospectroscopy. *Nano Letters* **2010,** *10* (7), 2511-2518.

111.   Aksu, S.; Huang, M.; Artar, A.; Yanik, A. A.; Selvarasah, S.; Dokmeci, M. R.; Altug, H., Flexible plasmonics on unconventional and nonplanar substrates. *Advanced Materials* **2011,** *23* (38), 4422-4430.

112.   Yanik, A. A.; Huang, M.; Artar, A.; Chang, T.-Y.; Altug, H., Integrated nanoplasmonic-nanofluidic biosensors with targeted delivery of analytes. *Applied Physics Letters* **2010,** *96* (2), 021101.

113.   Huang, M.; Galarreta, B. C.; Cetin, A. E.; Altug, H., Actively transporting virus like analytes with optofluidics for rapid and ultrasensitive biodetection. *Lab on a Chip* **2013,** *13* (24), 4841-4847.

114.   Cetin, A. E.; Coskun, A. F.; Galarreta, B. C.; Huang, M.; Herman, D.; Ozcan, A.; Altug, H., Handheld high-throughput plasmonic biosensor using computational on-chip imaging. *Light: Science & Applications* **2014,** *3* (1), e122.

115.   Beesley, M.; Castledine, J., The use of photoresist as a holographic recording medium. *Applied optics* **1970,** *9* (12), 2720-2724.

116.   Tetz, K. A.; Pang, L.; Fainman, Y., High-resolution surface plasmon resonance sensor based on linewidth-optimized nanohole array transmittance. *Optics letters* **2006,** *31* (10), 1528-1530.

117.   Pang, L.; Hwang, G. M.; Slutsky, B.; Fainman, Y., Spectral sensitivity of two-dimensional nanohole array surface plasmon polariton resonance sensor. *Applied Physics Letters* **2007,** *91* (12), 123112.

118.   Liu, C.; Hong, M.; Cheung, H.; Zhang, F.; Huang, Z.; Tan, L.; Hor, T., Bimetallic structure fabricated by laser interference lithography for tuning surface plasmon resonance. *Optics express* **2008,** *16* (14), 10701-10709.

119.   Henzie, J.; Lee, M. H.; Odom, T. W., Multiscale patterning of plasmonic metamaterials. *Nature nanotechnology* **2007,** *2* (9), 549-554.

120.   Gao, H.; Henzie, J.; Lee, M. H.; Odom, T. W., Screening plasmonic materials using pyramidal gratings. *Proceedings of the National Academy of Sciences* **2008,** *105* (51), 20146-20151.

121.   Gao, H.; Yang, J.-C.; Lin, J. Y.; Stuparu, A. D.; Lee, M. H.; Mrksich, M.; Odom, T. W., Using the angle-dependent resonances of molded plasmonic crystals to improve the sensitivities of biosensors. *Nano Letters* **2010,** *10* (7), 2549-2554.

122.   Yang, J.-C.; Gao, H.; Suh, J. Y.; Zhou, W.; Lee, M. H.; Odom, T. W., Enhanced optical transmission mediated by localized plasmons in anisotropic, three-dimensional nanohole arrays. *Nano Letters* **2010,** *10* (8), 3173-3178.

123.   Chang, T.-Y.; Huang, M.; Yanik, A. A.; Tsai, H.-Y.; Shi, P.; Aksu, S.; Yanik, M. F.; Altug, H., Large-scale plasmonic microarrays for label-free high-throughput screening. *Lab on a Chip* **2011,** *11* (21), 3596-3602.

124.   Shen, Y.; Zhou, J.; Liu, T.; Tao, Y.; Jiang, R.; Liu, M.; Xiao, G.; Zhu, J.; Zhou, Z.-K.; Wang, X., Plasmonic gold mushroom arrays with refractive index sensing figures of merit approaching the theoretical limit. *Nature communications* **2013,** *4*.

Chapter 2

2   Fundamentals of Plasmonics

In this chapter, the most important facts and phenomena of plasmonics is summarized, including dielectric function of metals, dispersion relation of surface plasmon, spatial properties of surface plasmon field and extraordinary optical transmission of nanohole arrays. The purpose of this introduction is to give a background for the theory analysis in Chapter 3 for convenience.

2.1   Dielectric Constant of Metals

The interaction between metals and electromagnetic fields can be explained based on classic Maxwell's equations. Even metal nanostructures down to sizes of about ten nanometers can be successfully described without a need of quantum mechanics.[1] Many of the fundamental optical properties of the metal are firmly understood by a plasma concept, where the free electrons of a metal are treated as an electron liquid with bulk number density n moving against a fixed background of positive ion cores. The "volume plasmons" will oscillate in response to an external electromagnetic field. This motion is damped by each other's collisions of electrons with a characteristic frequency γ. By solving kinetic equation of oscillation and substituting the result into Maxwell's equations, we arrive at a complex dielectric function of the free electron liquid:

$$\varepsilon(\omega) = 1 - \frac{\omega_p^2}{\omega^2 + i\gamma\omega} \tag{2-1}$$

where $\omega_p = \sqrt{\dfrac{ne^2}{\varepsilon_0 m}}$ is the plasma frequency of the free electron with mass m and elementary charge e, ε_0 is the electric permittivity of vacuum. This dielectric function $\varepsilon(\omega)$ known as the Drude model[2] describes the dispersive properties of metal, which provides the basis of all discussed optical phenomena. For large frequencies close to ω_p, $\varepsilon(\omega)$ is predominantly real,

$$\varepsilon(\omega) = 1 - \frac{\omega_p^2}{\omega^2} \tag{2-2}$$

which can be regarded as the dielectric function of the undamped free electron.

2.2 Dispersion Relation of Surface Plasmon

Surface plasmon (SP) is an important conceptual extension of the bulk plasmon.[3] Maxwell's theory shows electron charges on a metal boundary can perform coherent oscillation.[4] The oscillation frequency ω is associated to its wave vector k by a dispersion relation $\omega(k)$. Given the simplest configuration (Figure 2-1) of a semi-infinite plane metal surface with the dielectric function $\varepsilon_m = \varepsilon_m' + \varepsilon_m''$, adjacent to a dielectric ε_d such as air or vacuum, one can obtain the following equations by solving Maxwell's equations with boundary conditions,

$$\frac{k_{z1}}{\varepsilon_m} + \frac{k_{z2}}{\varepsilon_d} = 0 \tag{2-3}$$

$$k_{sp}^2 + k_{z1}^2 = \varepsilon_m \left(\frac{\omega}{c}\right)^2 \tag{2-4}$$

$$k_{sp}^2 + k_{z2}^2 = \varepsilon_d \left(\frac{\omega}{c}\right)^2 \tag{2-5}$$

where k_{z1} and k_{z2} are the respective component of the wave vector perpendicular to the interface in the metal and dielectric, k_{sp} is the wave vector of SP, c is the velocity of light in vacuum.
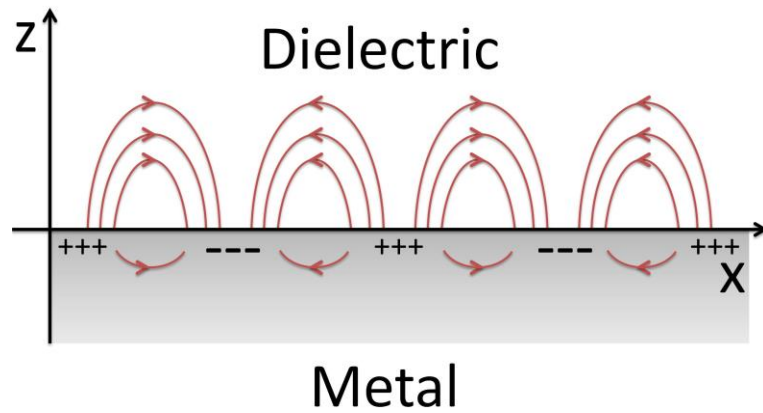
Figure 2-1 Configuration for SPs at the interface between a metal and a dielectric.

From these equations, the dispersion relation of SP can be written as

$$k_{sp} = \frac{\omega}{c}\sqrt{\frac{\varepsilon_m \varepsilon_d}{\varepsilon_m + \varepsilon_d}} \tag{2-6}$$

The real part of k_{sp} is

$$k_{sp}' = \frac{\omega}{c}\sqrt{\frac{\varepsilon_m' \varepsilon_d}{\varepsilon_m' + \varepsilon_d}} \tag{2-7}$$

To get a real k'_{sp}, one needs $\varepsilon'_m < 0$ and $|\varepsilon'_m| > \varepsilon_d$, which can be fulfilled in a metal such as Ag and Au. The imaginary part of k_{sp} is

$$k''_{sp} = \frac{\omega}{c} \sqrt{\left(\frac{\varepsilon'_m \varepsilon_d}{\varepsilon'_m + \varepsilon_d}\right)^3 \frac{\varepsilon''_m}{2(\varepsilon'_m)^2}} \qquad \text{(2-8)}$$

which determines the internal damping and absorption. Insert the free electron dielectric function (2-2) into (2-6), and we can get the characteristic surface plasmon frequency when $k_{sp} \to \infty$

$$\omega_{sp} = \frac{\omega_p}{\sqrt{1 + \varepsilon_d}} \qquad \text{(2-9)}$$

The dispersion curve k_{sp} lies right of the light line (see Figure 2-2), which means that surface plasmons have a longer wave vector than light waves of the same energy, so that freely propagating light cannot directly excite the SPs due to such wave vector gap. Therefore momentum-matching techniques such as prism or grating coupling are required to compensate the missing momentum for the excitation of SP oscillation. These charge oscillations momentarily trap an electromagnetic field which decay exponentially into the space perpendicular (z direction) to the surface and have their maximum at the interface, as is characteristic for surface waves. This implies the evanescent nature of SPs, which explains their sensitivity to dielectric environment at the surface.
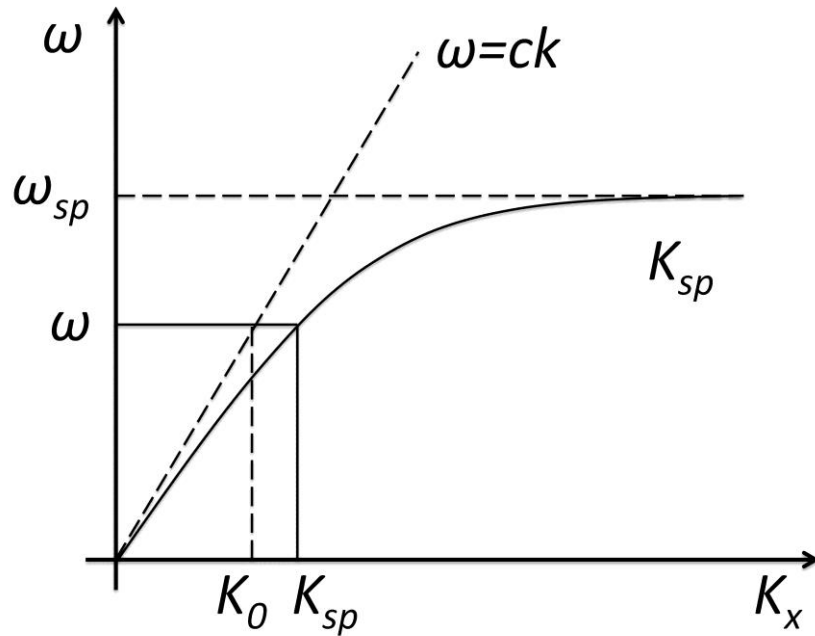
Figure 2-2 Dispersion curve of SP, always lying right of the light line, with surface plasmon frequency ω_{sp}.

2.3 Field Penetration Depth

As mentioned above, the field intensity of the SPs decreases exponentially as $e^{-|k_{zi}||z|}$ (Figure 2-3), normal to the surface. The penetration depth is a measure of how deep electromagnetic field can penetrate into a material. It is defined as the depth at which the field intensity falls to $1/e$ (about 37%) of its original value at the interface. In this context,

$$|z_i| = \frac{1}{|k_{zi}|} \qquad \text{(2-10)}$$

For metal with ε_m,

$$z_1 = -\frac{c}{\omega}\sqrt{\frac{|\varepsilon_m'+\varepsilon_d|}{\varepsilon_m'^2}} \qquad \text{(2-11)}$$

For dielectric with ε_d

$$z_2 = \frac{c}{\omega}\sqrt{\frac{|\varepsilon_m'+\varepsilon_d|}{\varepsilon_d^2}} \qquad \text{(2-12)}$$

The field distribution in z direction determined by penetration depth is of critical importance to plasmonic sensor performance, which will be discussed in Chapter 3.
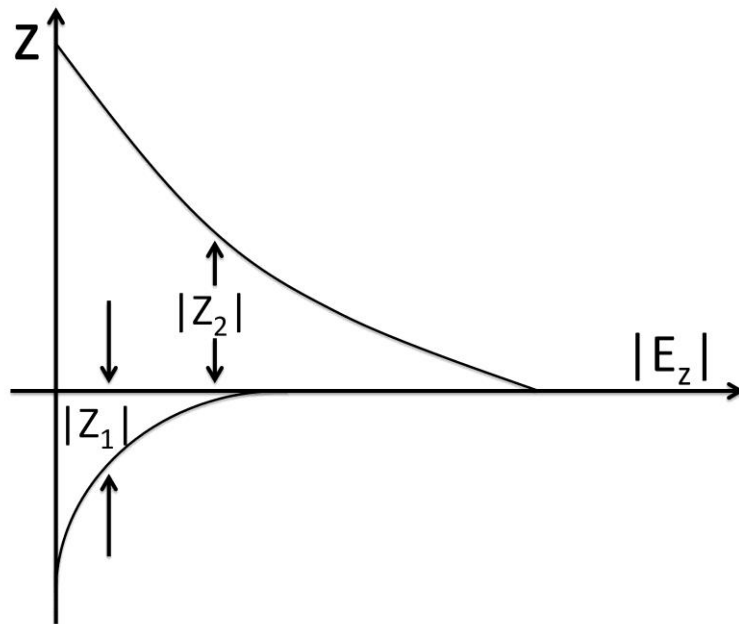
Figure 2-3 Field distribution in the z direction perpendicular to the interface, implying an evanescent feature.

2.4 Propagation Length

The intensity of SP wave propagating along a smooth surface decreases according to

$e^{-2k''_{sp}x}$. The propagation length is defined as L after which the intensity decreases to $1/e$.

$$L = \frac{1}{2k''_{sp}} = \frac{\lambda}{2\pi}\sqrt{\left(\frac{\varepsilon'_m+\varepsilon_d}{\varepsilon'_m\varepsilon_d}\right)^3\frac{(\varepsilon'_m)^2}{\varepsilon''_m}} \qquad (2\text{-}13)$$

The propagation length of Au and Ag in air is plotted in Figure 2-4 using the respective

dielectric constants for Au and Ag.[5] Obviously Ag has larger propagation length than that

of Au. In the visible and near-infrared region, the larger the wavelength of exciting light is,

the longer propagation length SPs have.
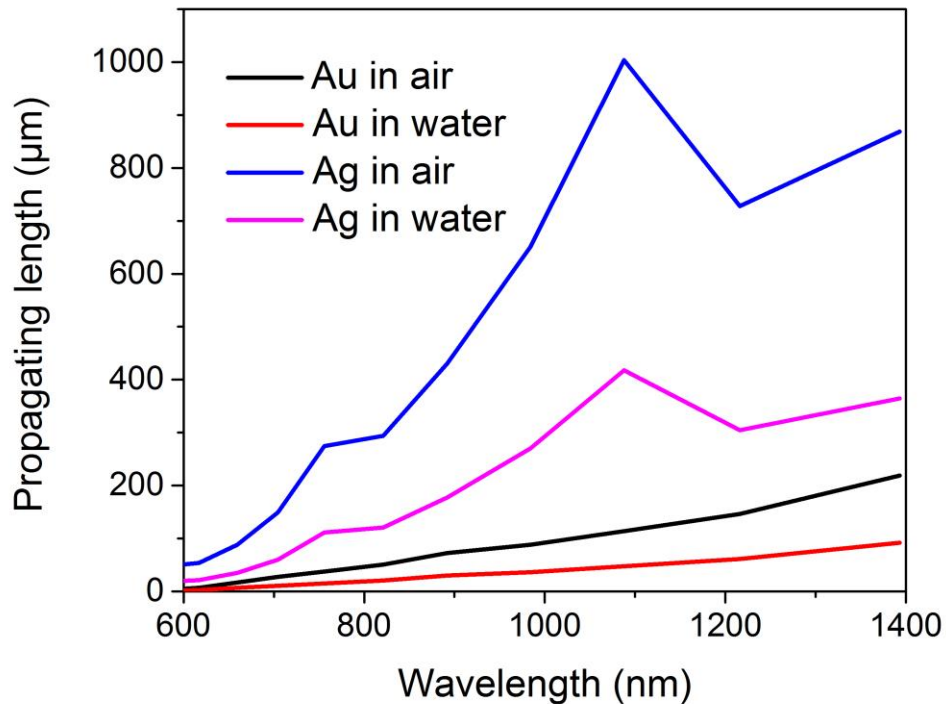
Figure 2-4 SPs propagation lengths of Au and Ag in air and water respectively, showing a strong dependence on excitation wavelength.

2.5 Extraordinary Optical Transmission

Among numerous plasmonic nanostructures, periodic nanohole arrays have so far been one of most intensively investigated structures owing to their extraordinary optical transmission, where the transmission efficiency can exceed unity normalized to the area of the holes.[6-9] Such phenomena are attributed to surface plasmon resonance (SPR) induced by periodic surface patterns with which their spectral properties can be tuned and scaled. As mentioned above, these two-dimensional periodic gratings can indeed transform light into SPs by providing the additional momentum for the coupling process. The process can

be understood to have three steps: the resonant coupling of light to SPs on the input surface,

tunneling through the holes to the output surface and re-emission from the output surface.
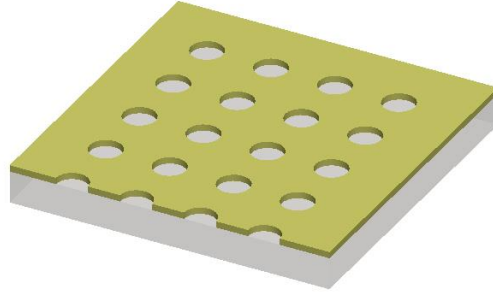
Figure 2-5 Periodic nanohole array supporting extraordinary optical transmission.

By applying the above momentum-matching condition to a two-dimensional square array

of nanoholes with lattice constant P, the coupling process follows the law of momentum

conservation:

$$k_0 \, sin \, \theta \pm iG_x \pm jG_y = k_{sp} \tag{2-14}$$

where k_0 is the wave vector of the incident light with incident angle θ, G_x and G_y the

reciprocal lattice vectors for a square lattice with $G_x = G_y = 2\pi/P$, and i, j are the

scattering orders that couple the incident light.

$$\sqrt{\left(\frac{2\pi}{\lambda} \, sin \, \theta + i \frac{2\pi}{P}\right)^2 + \left(j \frac{2\pi}{P}\right)^2} = \frac{\omega}{c} \sqrt{\frac{\varepsilon'_m \varepsilon_d}{\varepsilon'_m + \varepsilon_d}} \tag{2-15}$$

In a first approximation that the film has no significant change in the plasmon dispersion and no coupling between the front and back surfaces of the metal film, the transmission peak position λ_m at normal incidence ($\theta = 0$) are given by:[10]

$$\lambda_m = \frac{P}{\sqrt{i^2+j^2}} \sqrt{\frac{\varepsilon_m' \varepsilon_d}{\varepsilon_m' + \varepsilon_d}} \tag{2-16}$$

This equation is widely accepted in the SPR peak determination for nanohole arrays.[11-14] According to this equation, the SPR wavelengths depend on structure of the nanohole arrays and dielectric properties of media. The following facts are worth noting: as the periodicity of nanohole array increases, its SPR peak shifts to longer wavelength for the same order mode; on the other hand, due to $|\varepsilon_m'| \gg \varepsilon_d$ at visible and near-infrared, ε_d dominates the combination term of dielectric constants whereby the SPR peak has higher wavelength when the nanohole array is in contact with the dielectric with higher ε_d.

References

1.   Maier, S. A., *Plasmonics: Fundamentals and Applications: Fundamentals and Applications*. Springer: 2007.

2.   Drude, P., Zur elektronentheorie der metalle. *Annalen der Physik* **1900,** *306* (3), 566-613.

3.   Ritchie, R., Plasma losses by fast electrons in thin films. *Physical Review* **1957,** *106* (5), 874.

4.   Raether, H., Surface plasmons on smooth surfaces. In *Surface Plasmons on Smooth and Rough Surfaces and on Gratings*, Springer Berlin Heidelberg: 1988; Vol. 111, pp 4-39.

5.   Johnson, P. B.; Christy, R.-W., Optical constants of the noble metals. *Phys Rev B* **1972,** *6* (12), 4370.

6.   Ebbesen, T. W.; Lezec, H. J.; Ghaemi, H. F.; Thio, T.; Wolff, P. A., Extraordinary optical transmission through sub-wavelength hole arrays. *Nature* **1998,** *391* (6668), 667-669.

7.   Barnes, W. L.; Dereux, A.; Ebbesen, T. W., Surface plasmon subwavelength optics. *Nature* **2003,** *424* (6950), 824-830.

8.   Genet, C.; Ebbesen, T., Light in tiny holes. *Nature* **2007,** *445* (7123), 39-46.

9.   Liu, H.; Lalanne, P., Microscopic theory of the extraordinary optical transmission. *Nature* **2008,** *452* (7188), 728-731.

10.   Ghaemi, H.; Thio, T.; Grupp, D. e. a.; Ebbesen, T. W.; Lezec, H., Surface plasmons enhance optical transmission through subwavelength holes. *Phys Rev B* **1998,** *58* (11), 6779.

11.   Brolo, A. G.; Gordon, R.; Leathem, B.; Kavanagh, K. L., Surface plasmon sensor based on the enhanced light transmission through arrays of nanoholes in gold films. *Langmuir* **2004,** *20* (12), 4813-4815.

12.   Lee, M. H.; Gao, H.; Henzie, J.; Odom, T. W., Microscale arrays of nanoscale holes. *Small* **2007,** *3* (12), 2029-2033.

13.   Stewart, M. E.; Mack, N. H.; Malyarchuk, V.; Soares, J. A.; Lee, T.-W.; Gray, S. K.; Nuzzo, R. G.; Rogers, J. A., Quantitative multispectral biosensing and 1D imaging using quasi-3D plasmonic crystals. *Proceedings of the National Academy of Sciences* **2006,** *103* (46), 17143-17148.

14.   Lee, S. H.; Johnson, T. W.; Lindquist, N. C.; Im, H.; Norris, D. J.; Oh, S. H., Linewidth‐Optimized Extraordinary Optical Transmission in Water with Template‐Stripped Metallic Nanohole Arrays. *Advanced Functional Materials* **2012,** *22* (21), 4439-4446.

Chapter 3

3 Universal Optical Performance Analysis

In this chapter, a universal model of performance analysis for nanoplasmonic sensors is established based on standard surface plasmon theory. From the analysis of nanohole arrays, a sensitivity formula is deduced by using the momentum matching condition of surface plasmon resonance excitation. This expression is applicable to general two-dimensional plasmonic nanostructures including periodic, quasiperiodic and aperiodic arrays. The analytical results calculated with this model are compared with the sensitivity data in previous publications which are subject to the same principle of surface plasmon resonance.

3.1 Performance Characteristics

To quantify and compare the performance of sensors, the most commonly used parameter is sensitivity, which indicates the sensor signal change responding to the measured quantity change. In surface plasmon resonance (SPR) sensing, spectral peak wavelength[1-2], intensity[3-4] and phase[5-6] have all been explored as the sensor signals, among which the peak wavelength given as Equation (2-16) in Chapter 2 is the most commonly employed signal for nanohole array sensors. Typically the SPR peak position shifts with the change of refractive index n of the surrounding dielectric environment. Thus refractive index sensing sensitivity is defined as

$$S = \frac{\Delta \lambda}{\Delta n} \tag{3-1}$$

Where $\Delta\lambda$ is the wavelength shift of SPR peak postion and n is the change of refractive index in the surrounding environment with dielectric constant $\varepsilon_d = n^2$.

In some cases, using sensitivity alone may have one drawback that a substantial broadening of the resonance peaks accompanies with the increase of sensitivity, thereby reducing the resolution and enlarging the limit of detection. On the other hand, contradiction may arise when we compare the sensitivities between in wavelength and energy domains.[7] To overcome above problems and take the resolution into account, a characteristic of figure of merit (FOM) is defined as[8]

$$FOM = \frac{S}{FWHM} \tag{3-2}$$

where S is the refractive index sensitivity and $FWHM$ is the full width at half-maximum of the corresponding SPR peak. It has been proved that the FOM in wavelength and energy scales are equivalent under certain condition.[7]

As an important characteristic, Q-factor or quality factor has been extensively used to describe how damped a resonator is in mechanics, electronics and optics. Q-factor is defined as

$$Q = \frac{\lambda}{FWHM} \tag{3-3}$$

where λ is resonant wavelength. However, in the research of SPR, it has been less used, compared to sensitivity and FOM. We will demonstrate it is of equal importance in the following analysis.

3.2   Performance Analysis of Nanohole Array Sensors

Owing to the simplicity of nanohole arrays, numerous configurations and geometries have been studied for SPR sensing applications. Given the above non-analytical characteristics, the performance of nanohole array sensors has generally been evaluated by various experiments and numerical simulations. Provided certain metallic material, nanohole array sensors with various configurations in terms of periodicity and pattern, e.g. square and hexagonal arrays, could have very distinct optical response. Overall, there is no obvious method to choose a configuration to maximize performances. Since different geometry parameters always couple together in sensor performance determination, it is complicated to optimize all of them at the same time. Therefore a structure-related performance analysis model could not be applicable to different geometries. This is the reason why most sensitivity analyses are based on experience expression and numerical methods. A performance model without explicit structure parameters might be applicable to various geometries of nanohole arrays.

3.2.1 Analytical Performance Modeling

In mathematics, if peak position λ_m from Equation (2-16) is directly differentiated against the refractive index n using Equation (3-1), the sensitivity S would retain the structure parameters of $P,$ i and j. Since these parameters exist as the same combination in S as that in λ_m, they can be cancelled together by dividing the sensitivity S to λ_m, $i.e.$ $\frac{S}{\lambda_m}$. Beyond mathematics, $\frac{S}{\lambda_m}$ should have an explicit physical origin to be a qualified characteristic.

Dividing FWHM upon numerator and denominator of $\dfrac{S}{\lambda_m}$, the result is exactly equal to

$\dfrac{FOM}{Q}$, which reveals its intrinsic meaning from a physical point of view.

By the derivation in Appendix I,

$$\frac{FOM}{Q} = \frac{S}{\lambda_m} = \frac{\varepsilon'_m}{n(\varepsilon'_m + n^2)} \qquad \text{(3-4)}$$

This expression suggests the ratio of sensitivity to peak wavelength depends on the dielectric properties of the metal and analyte. If the device is positioned in air ($n = 1$),

$$\frac{S}{\lambda_m} = \frac{\varepsilon'_m}{\varepsilon'_m + 1} \qquad \text{(3-5)}$$

For all the other two-dimensional Bravais lattices of nanoholes including oblique, rectangular, rhombic, and hexagonal arrays, as well as nanoslit arrays, the same relation can be obtained since all of them has similar expression for SPR peak wavelength, e.g.

$\lambda_m = \dfrac{P}{\sqrt{\frac{4}{3}(i^2 + ij + j^2)}} \sqrt{\dfrac{\varepsilon'_m \varepsilon_d}{\varepsilon'_m + \varepsilon_d}}$ for hexagonal nanohole arrays[9] and $\lambda_m = \dfrac{P}{i} \sqrt{\dfrac{\varepsilon'_m \varepsilon_d}{\varepsilon'_m + \varepsilon_d}}$ for

nanoslit arrays[10], in which geometric and dielectric parameters do not convolute with each other. This result suggests the ratio of sensitivity to peak wavelength is independent of the geometries of two-dimensional periodic nanohole arrays.

3.2.2 Analytical Expression of Performance Characteristics

From Equation (3-4), the sensitivity of nanohole array sensors can be explicitly defined in an analytical format,

$$S = \frac{\lambda_m}{n} \cdot \frac{\varepsilon'_m}{(\varepsilon'_m + n^2)} \tag{3-6}$$

This sensitivity expression explains why nanohole arrays of different patterns on the same metallic material with the same resonance wavelength show very similar sensitivities. The sensitivities plotted for Au and Ag in Figure 3-1 show a roughly linear increase as the peak position is shifted to longer wavelength. Despite different dielectric properties they own, Au and Ag have almost equal sensitivities in the same dielectric. Given $|\varepsilon'_m| \gg n^2$ at visible and near-infrared region, we can safely give an approximation $S \approx \frac{\lambda_m}{n}$, which confirms the SPR peaks at the same wavelength show higher sensitivity in the analyte with lower refractive index. In particular, $S \approx \lambda_m$ in air ($n=1$) and $S \approx 0.75\lambda_m$ in water ($n=1.33$). This implies that measurements in air are more sensitive compared with that in aqueous solution.
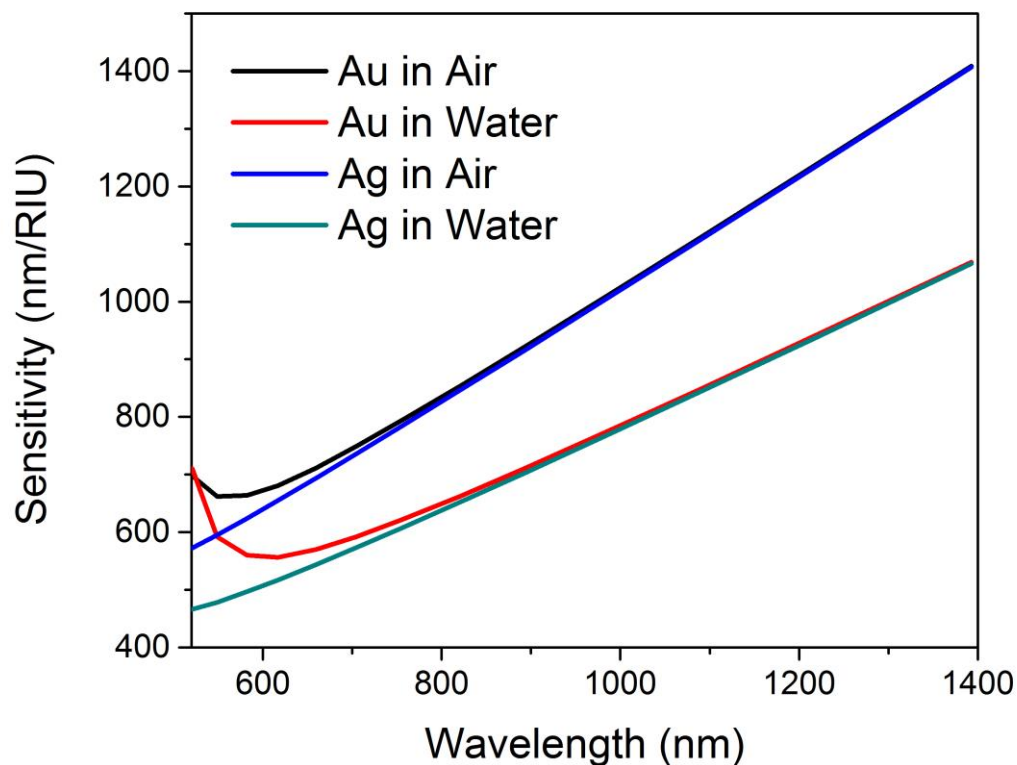
Figure 3-1 Sensitivity of Au and Ag nanohole array sensors in air and water respectively.

In addition, this analytical format of sensitivity can give us more insight into the interaction in plasmonic sensing. Intuitively, in the case of homogenous dielectric analyte, the sensitivity depends on the field distribution inside the dielectric in all three spatial dimensions. Since electromagnetic field of surface plasmon (SP) decays along the interface as well as in the perpendicular direction, a proper model should simultaneously consider both factors. The attenuation of SP field along both directions is respectively characterized by penetration depth and propagation length, which both show strong dependence on the SPR wavelength λ_m as discussed in Section 2.4. The longer penetration (propagation) of

the field at higher SPR wavelength provides a larger sensing volume to refractive index changes, thereby increasing the sensitivity. Therefore the presence of λ_m in Equation 3-6 originates from the overall field attenuations. Since the SPR linewidth is related to propagation length, i.e. longer propagation length implies a smaller FWHM, this sensitivity expression intrinsically contains the partial factor of FWHM which is involved in traditional FOM definition.

In the perpendicular direction, the field is distributed between the metal and dielectric according to Equation 2-11 and 2-12 in Chapter 2. It is their relative dielectric property that actually governs how SP field penetrates into the dielectric analyte, thereby determining the sensor's sensitivity. Thus, a relative penetration is defined by normalization of scalar penetration depth z_i as

$$\boldsymbol{p_i} = \frac{\boldsymbol{z_i}}{\sum \boldsymbol{z}} \tag{3-7}$$

which can represent the relative fraction of the SP field in the media. Accordingly, for dielectric,

$$\frac{z_2}{z_1+z_2} = \frac{\frac{c}{\omega}\sqrt{\frac{|\varepsilon_m'+\varepsilon_d|}{\varepsilon_d^2}}}{-\frac{c}{\omega}\sqrt{\frac{|\varepsilon_m'+\varepsilon_d|}{\varepsilon_m'^2}}+\frac{c}{\omega}\sqrt{\frac{|\varepsilon_m'+\varepsilon_d|}{\varepsilon_d^2}}} = \frac{\varepsilon_m'}{\varepsilon_m'+n^2} \tag{3-8}$$

Therefore the dielectric constant combination in Equation 3-6 comes from the relative field distribution in the perpendicular direction to the surface.

In brief, this analytic expression defines plasmonic sensitivity based on the primary physical facts of both electromagnetic field and dielectric property of media, rather than variable nanostructure geometry.

3.3   Comparison to Localized SPR Sensors

SPs on nanoparticles and in nanohole arrays clearly have the same physical origin and are both sensitive to the refractive index changes. Their sensing performance has been analyzed from simplified theoretical models for localized SPR. The sensitivity of localized SPR can be derived from a dipole polarizability resonance condition of an ellipsoidal particle in the quasistatic limit as,[11]

$$S_{LSPR} = \frac{2\varepsilon'_m}{n\frac{d\varepsilon'_m}{d\lambda}} \tag{3-9}$$

In this case, the sensitivity of nanoparticles is mainly dominated by the dielectric property and spectral position of the localized SPR, whereas the shape of the nanoparticle plays a secondary role, selecting the resonance wavelength. According to the above analysis, similar claim is valid for the case of nanohole array sensors, in which the structures of nanohole arrays serves the same purpose. The theoretical sensitivities of nanohole arrays and nanoparticles are plotted in Figure 3-2. The sensitivity of nanohole arrays is much higher in the visible range, whereas the nanoparticles' sensitivity is gradually approaching parallel to that of nanohole arrays at near-infrared. Hence the nanohole array sensors are in theory the better choices in terms of sensitivity in comparison to those based on nanoparticles.
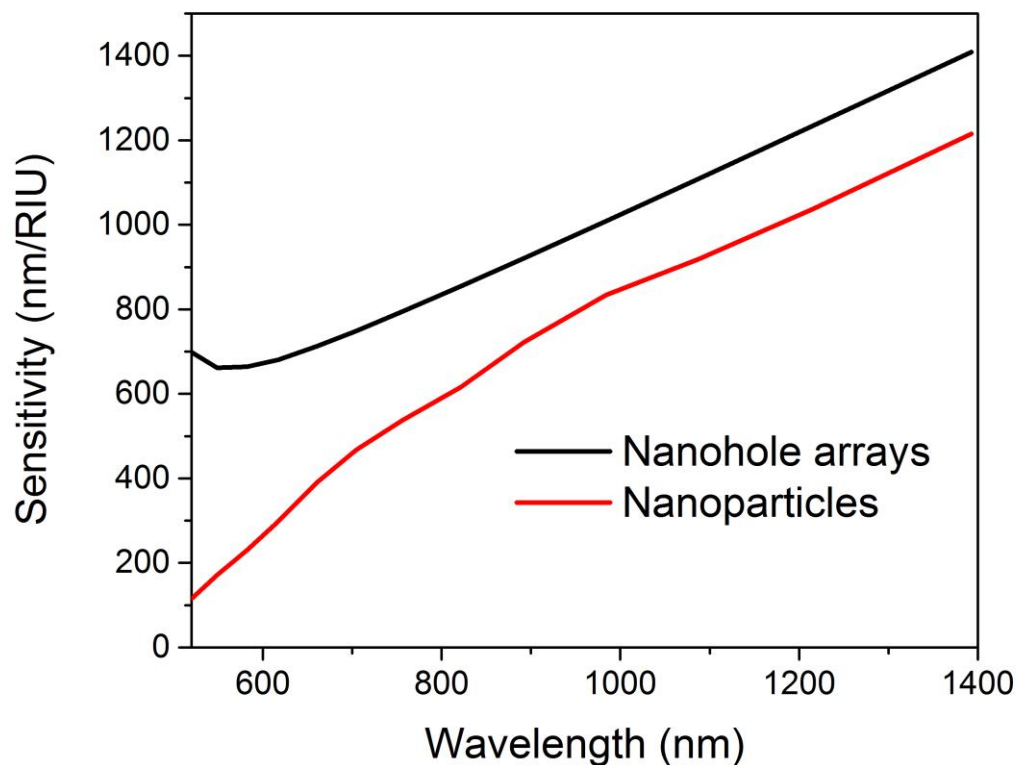
Figure 3-2 Theoretical sensitivities of nanohole arrays and nanoparticles in air.

3.4 Sensitivity Qualification

Sensitivities of plasmonic sensors have been independently measured by many experiment and numerical simulations using various two-dimensional metal nanostructures. Our theoretical results can be evaluated using those plasmonic sensors which are subject to the same principle of surface plasmon resonance. Thus a series of published data about sensitivity listed in Table 3-1, are chosen to compare with our theoretical values.

Table 3-1 Experimental or simulated sensitivities of two-dimensional plasmonic sensors

Publication	SPR wavelength (nm)	Metal/ Dielectric	Sensitivity (nm/RIU)
Large-scale plasmonic microarrays for label-free high-throughput screening[12]	880	Au/Water	615
Seeing protein monolayers with naked eye through plasmonic Fano resonances[13]	845	Au/water	690
Integrated nanoplasmonic-nanofluidic biosensors with targeted delivery of analytes [14]	889	Au/water	630
Attomolar protein detection using in-hole surface plasmon resonance[15]	720	Au/water	650
On-chip surface-based detection with nanohole arrays[16]	606	Au/water	333
Nanoholes as nanochannels: flow-through plasmonic sensing[17]	620	Au/water	324
A miniaturized sensor consisting of concentric metallic nanorings on the end facet of an optical fiber[18]	1200	Au/Alcohol	900

Focused ion beam fabrication of metallic nanostructures on end faces of optical fibers for chemical sensing applications[19]	670	Au/water	~500
EOT or Kretschmann configuration? Comparative study of the plasmonic modes in gold nanohole arrays [20]	710	Au/water	530
Screening plasmonic materials using pyramidal gratings[21]	650	Ag/water	410
Quantitative multispectral biosensing and 1D imaging using quasi-3D plasmonic crystals[3]	1023	Au/water	~700
Periodic nanohole arrays with shape-enhanced plasmon resonance as real-time biosensors[22]	850	Au/water	600
Template-stripped smooth Ag nanohole arrays with silica shells for surface plasmon resonance biosensing[23]	700	Ag/water	450
Linewidth-optimized extraordinary optical transmission in water with template-stripped metallic nanohole arrays[2]	720	Ag/water	494
FDTD in reference [2]	720	Ag/water	524
Nanohole-based surface plasmon resonance instruments with improved spectral resolution quantify a broad range of antibody-ligand binding kinetics[24]	710	Au/water	481

Real-time full-spectral imaging and affinity measurements from 50 microfluidic channels using nanohole surface plasmon resonance[25]	710	Ag/water	470
Ultrasmooth metallic films with buried nanostructures for backside reflection-mode plasmonic biosensing[26]	700	Au/water	410
Spectral sensitivity of two-dimensional nanohole array surface plasmon polariton resonance sensor[27]	1532	Au/ water	1520
Development of a mass-producible on-chip plasmonic nanohole array biosensor[28]	740	Au/ water	495
Rational design of high performance surface plasmon resonance sensors based on two-dimensional metallic hole arrays[29]	975	Au/ water	754
High-resolution surface plasmon resonance sensor based on linewidth-optimized nanohole array transmittance[30]	1510	Au/ water	1022
Sensitive biosensor array using surface plasmon resonance on metallic nanoslits[10]	805	Au/water	668
Comparisons of surface plasmon sensitivities in periodic gold nanostructures[31]	830	Au/water	650
Intensity sensitivity of gold nanostructures and its application for high-throughput biosensing[32]	790	Au/water	575

Optimization of periodic gold nanostructures for intensity-sensitive detection[33]	666	Au/water	478
Enhancing surface plasmon detection using template-stripped gold nanoslit arrays on plastic films[34]	693	Au/water	451
Optofluidic platform for real-time monitoring of live cell secretory activities using Fano resonance in gold nanoslits[35]	680	Au/water	470
Plasmonic nanohole arrays for monitoring growth of bacteria and antibiotic susceptibility test[36]	625	Au/water	409
Plasmonic gold mushroom arrays with refractive index sensing figures of merit approaching the theoretical limit[37]	1250	Ag/water	1015
Large-area subwavelength aperture arrays fabricated using nanoimprint lithography[38]	720	Ag/water	513

The above published sensitivities and the results calculated from our sensitivity formula are plotted against SPR wavelengths (Figure 3-3). It is observed that the experimental sensitivities are somewhat lower than theoretical values at the visible range. This degradation can be attributed to coupling effects from substrates and radiation damping induced by nanostructures in real cases, which have been both ignored in our model. In addition, some experimental peaks are red-shifted compared with the predicted values due to Fano-type interaction.[39] Therefore the sensitivity of experimental peak should be compared to that of a somewhat lower wavelength in our model, which would make our

prediction more precise. On the other hand, both sensitivities coincide well with each other in the near-infrared. Overall, our performance model predicts the range and trend of sensitivity change.
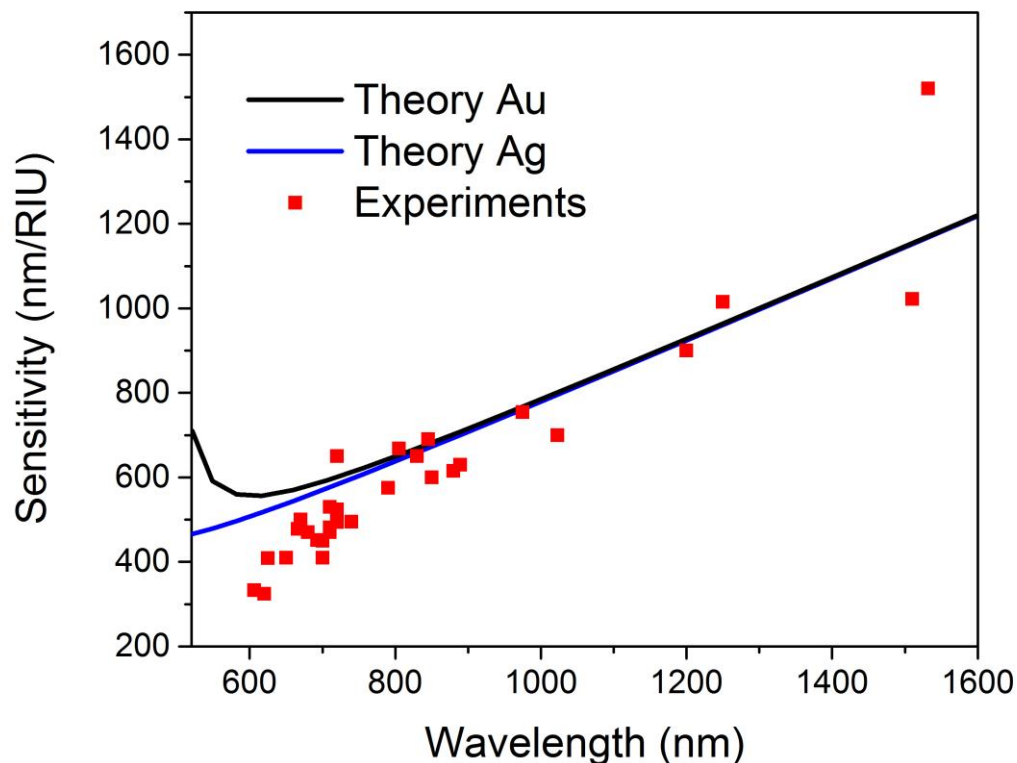
Figure 3-3 Theoretical and experimental sensitivities of two-dimensional nanoplasmonic sensors.

3.5 Generalization to Quasiperiodic and Aperiodic Structures

Revisiting the above sensitivity formula for periodic nanohole array sensors, we find it not only provides a geometry-irrelevant expression but also discloses the essence of plasmonic

sensing. Since the wave vector of SPs is always larger than that of light with the same frequency, a momentum gap exists between the SPs and light. An additional momentum G is always required to meet the resonance condition for the coupling of photons into SPs according to,

$$k_{inc} + G = k'_{sp} \tag{3-10}$$

where G is the reciprocal lattice vector for Bravais lattices. Above sensitivity analysis reveals it is SPR itself that essentially determines the sensor performances regardless of the way to produce it. Metal nanostructures only act as a coupling media to generate SPR rather than directly determine the final performances.

Beyond the Bravais lattices, quasicrystals (with long-range order but no short-range order) and aperiodic aperture arrays (without long-range or short-range order) were also demonstrated to support SPR.[40-46] Instead of reciprocal lattice vectors, quasicrystals and aperiodic structures are characterized by discrete Fourier transform vectors in their structure factors. The discrete Fourier transform vectors of quasicrystals have unusual n-fold rotational symmetry with n=5, 8, 12, and so on; the structure factor of aperiodic apertures possesses even more unusual rotational symmetry. Sharp transmission resonances appear at frequencies that closely match these discrete Fourier transform vectors. These vectors in reciprocal space are in fact equal to different wave-vectors k'_{sp}, corresponding to various SPR peak wavelengths in normal incident.[43] In this context, we can always eliminate these geometry-related parameters, i.e. general lattice vector for quasicrystals and aperiodic arrays, in a same manner as the deduction of sensitivity in Appendix 1. Hence our sensitivity expression is applicable to any two-dimensional

aperture arrays that have discrete Fourier transform vectors in their geometrical structure factor. It is expected that some non-periodic nanohole arrays would equally possess good optical performance thereby being used for sensing application.

3.6 Conclusions

In conclusion, a universal model of performance analysis for nanoplasmonic sensors is developed based on standard surface plasmon theory. Beginning with the analysis of nanohole arrays, a sensitivity formula is established using the momentum matching condition of SPR excitation for any tow-dimensional nanohole Bravais lattices. This expression includes no geometric parameters that normally appear in previous analytical methods, but only essential elements involved in SPR sensing. This quantitative model successfully explains a series of phenomena such as (1) sensitivity roughly linearly increase as the SPR position shifts to longer wavelength; (2) different patterns with the same SPR wavelength show very similar sensitivities; (3) nanostructures with different metals have similar sensitivity at the same wavelength; (4) SPR show higher sensitivity in the analyte with lower refractive index. The previously published sensitivity data are compared with the analytical results calculated with this expression, which is proved to be valid in performance analysis for plasmonic sensors. The comparison between nanohole arrays and nanoparticle LSPR sensors manifests the former has larger intrinsic sensitivity. The expression is further extended to general two-dimensional plasmonic nanostructure including quasiperiodic and aperiodic arrays.

References

1.   Henzie, J.; Lee, M. H.; Odom, T. W., Multiscale patterning of plasmonic metamaterials. *Nature nanotechnology* **2007,** *2* (9), 549-554.

2.   Lee, S. H.; Johnson, T. W.; Lindquist, N. C.; Im, H.; Norris, D. J.; Oh, S. H., Linewidth-Optimized Extraordinary Optical Transmission in Water with Template-Stripped Metallic Nanohole Arrays. *Advanced Functional Materials* **2012,** *22* (21), 4439-4446.

3.   Stewart, M. E.; Mack, N. H.; Malyarchuk, V.; Soares, J. A.; Lee, T.-W.; Gray, S. K.; Nuzzo, R. G.; Rogers, J. A., Quantitative multispectral biosensing and 1D imaging using quasi-3D plasmonic crystals. *Proceedings of the National Academy of Sciences* **2006,** *103* (46), 17143-17148.

4.   Tellez, G. A. C.; Tait, R. N.; Berini, P.; Gordon, R., Atomically flat symmetric elliptical nanohole arrays in a gold film for ultrasensitive refractive index sensing. *Lab on a Chip* **2013,** *13* (13), 2541-2546.

5.   Yavas, O.; Kocabas, C., Plasmon interferometers for high-throughput sensing. *Optics letters* **2012,** *37* (16), 3396-3398.

6.   Gao, Y.; Xin, Z.; Zeng, B.; Gan, Q.; Cheng, X.; Bartoli, F. J., Plasmonic interferometric sensor arrays for high-performance label-free biomolecular detection. *Lab on a Chip* **2013,** *13* (24), 4755-4764.

7.   Otte, M. A.; Sepulveda, B.; Ni, W.; Juste, J. P.; Liz-Marzán, L. M.; Lechuga, L. M., Identification of the optimal spectral region for plasmonic and nanoplasmonic sensing. *ACS Nano* **2009,** *4* (1), 349-357.

8.   Sherry, L. J.; Chang, S.-H.; Schatz, G. C.; Van Duyne, R. P.; Wiley, B. J.; Xia, Y., Localized surface plasmon resonance spectroscopy of single silver nanocubes. *Nano Letters* **2005,** *5* (10), 2034-2038.

9.   Thio, T.; Ghaemi, H.; Lezec, H.; Wolff, P.; Ebbesen, T., Surface-plasmon-enhanced transmission through hole arrays in Cr films. *JOSA B* **1999,** *16* (10), 1743-1748.

10.   Lee, K.-L.; Lee, C.-W.; Wang, W.-S.; Wei, P.-K., Sensitive biosensor array using surface plasmon resonance on metallic nanoslits. *Journal of biomedical optics* **2007,** *12* (4), 044023-044023-5.

11.   Miller, M. M.; Lazarides, A. A., Sensitivity of metal nanoparticle surface plasmon resonance to the dielectric environment. *The Journal of Physical Chemistry B* **2005,** *109* (46), 21556-21565.

12.   Chang, T.-Y.; Huang, M.; Yanik, A. A.; Tsai, H.-Y.; Shi, P.; Aksu, S.; Yanik, M. F.; Altug, H., Large-scale plasmonic microarrays for label-free high-throughput screening. *Lab on a Chip* **2011,** *11* (21), 3596-3602.

13.   Yanik, A. A.; Cetin, A. E.; Huang, M.; Artar, A.; Mousavi, S. H.; Khanikaev, A.; Connor, J. H.; Shvets, G.; Altug, H., Seeing protein monolayers with naked eye through plasmonic Fano resonances. *Proceedings of the National Academy of Sciences* **2011,** *108* (29), 11784-11789.

14.   Yanik, A. A.; Huang, M.; Artar, A.; Chang, T.-Y.; Altug, H., Integrated nanoplasmonic-nanofluidic biosensors with targeted delivery of analytes. *Applied Physics Letters* **2010,** *96* (2), 021101.

15.   Ferreira, J.; Santos, M. J.; Rahman, M. M.; Brolo, A. G.; Gordon, R.; Sinton, D.; Girotto, E. M., Attomolar protein detection using in-hole surface plasmon resonance. *Journal of the American chemical society* **2008,** *131* (2), 436-437.

16.   De Leebeeck, A.; Kumar, L. S.; de Lange, V.; Sinton, D.; Gordon, R.; Brolo, A. G., On-chip surface-based detection with nanohole arrays. *Analytical Chemistry* **2007,** *79* (11), 4094-4100.

17.   Eftekhari, F.; Escobedo, C.; Ferreira, J.; Duan, X.; Girotto, E. M.; Brolo, A. G.; Gordon, R.; Sinton, D., Nanoholes as nanochannels: flow-through plasmonic sensing. *Analytical Chemistry* **2009,** *81* (11), 4308-4311.

18.   Feng, S.; Darmawi, S.; Henning, T.; Klar, P. J.; Zhang, X., A miniaturized sensor consisting of concentric metallic nanorings on the end facet of an optical fiber. *Small* **2012,** *8* (12), 1937-1944.

19.   Dhawan, A.; Muth, J.; Leonard, D.; Gerhold, M.; Gleeson, J.; Vo-Dinh, T.; Russell, P., Focused ion beam fabrication of metallic nanostructures on end faces of optical fibers for chemical sensing applications. *Journal of Vacuum Science & Technology B* **2008,** *26* (6), 2168-2173.

20.   Couture, M.; Live, L. S.; Dhawan, A.; Masson, J.-F., EOT or Kretschmann configuration? Comparative study of the plasmonic modes in gold nanohole arrays. *Analyst* **2012,** *137* (18), 4162-4170.

21.   Gao, H.; Henzie, J.; Lee, M. H.; Odom, T. W., Screening plasmonic materials using pyramidal gratings. *Proceedings of the National Academy of Sciences* **2008,** *105* (51), 20146-20151.

22.   Lesuffleur, A.; Im, H.; Lindquist, N. C.; Oh, S.-H., Periodic nanohole arrays with shape-enhanced plasmon resonance as real-time biosensors. *Applied Physics Letters* **2007,** *90* (24), 243110.

23.   Im, H.; Lee, S. H.; Wittenberg, N. J.; Johnson, T. W.; Lindquist, N. C.; Nagpal, P.; Norris, D. J.; Oh, S.-H., Template-stripped smooth Ag nanohole arrays with silica shells for surface plasmon resonance biosensing. *ACS Nano* **2011,** *5* (8), 6244-6253.

24.   Im, H.; Sutherland, J. N.; Maynard, J. A.; Oh, S.-H., Nanohole-based surface plasmon resonance instruments with improved spectral resolution quantify a broad range of antibody-ligand binding kinetics. *Analytical Chemistry* **2012,** *84* (4), 1941-1947.

25.   Lee, S. H.; Lindquist, N. C.; Wittenberg, N. J.; Jordan, L. R.; Oh, S.-H., Real-time full-spectral imaging and affinity measurements from 50 microfluidic channels using nanohole surface plasmon resonance. *Lab on a Chip* **2012,** *12* (20), 3882-3890.

26.   Lindquist, N. C.; Johnson, T. W.; Jose, J.; Otto, L. M.; Oh, S. H., Ultrasmooth metallic films with buried nanostructures for backside reflection‐mode plasmonic biosensing. *Annalen der Physik* **2012,** *524* (11), 687-696.

27.   Pang, L.; Hwang, G. M.; Slutsky, B.; Fainman, Y., Spectral sensitivity of two-dimensional nanohole array surface plasmon polariton resonance sensor. *Applied Physics Letters* **2007,** *91* (12), 123112.

28.   Nakamoto, K.; Kurita, R.; Niwa, O.; Fujii, T.; Nishida, M., Development of a mass-producible on-chip plasmonic nanohole array biosensor. *Nanoscale* **2011,** *3* (12), 5067-5075.

29.   Zhang, L.; Chan, C. Y.; Li, J.; Ong, H. C., Rational design of high performance surface plasmon resonance sensors based on two-dimensional metallic hole arrays. *Optics express* **2012,** *20* (11), 12610-12621.

30.   Tetz, K. A.; Pang, L.; Fainman, Y., High-resolution surface plasmon resonance sensor based on linewidth-optimized nanohole array transmittance. *Optics letters* **2006,** *31* (10), 1528-1530.

31.   Lee, K.-L.; Wang, W.-S.; Wei, P.-K., Comparisons of surface plasmon sensitivities in periodic gold nanostructures. *Plasmonics* **2008,** *3* (4), 119-125.

32.   Lee, K.-L.; Wu, S.-H.; Wei, P.-K., Intensity sensitivity of gold nanostructures and its application for high-throughput biosensing. *Optics express* **2009,** *17* (25), 23104-23113.

33.   Lee, K.-L.; Wei, P.-K., Optimization of periodic gold nanostructures for intensity-sensitive detection. *Applied Physics Letters* **2011,** *99* (8), 083108.

34.   Lee, K.-L.; Chen, P.-W.; Wu, S.-H.; Huang, J.-B.; Yang, S.-Y.; Wei, P.-K., Enhancing surface plasmon detection using template-stripped gold nanoslit arrays on plastic films. *ACS Nano* **2012,** *6* (4), 2931-2939.

35.	Wu, S. H.; Lee, K. L.; Chiou, A.; Cheng, X.; Wei, P. K., Optofluidic Platform for Real‑Time Monitoring of Live Cell Secretory Activities Using Fano Resonance in Gold Nanoslits. *Small* **2013,** *9* (20), 3532-3540.

36.	Kee, J. S.; Lim, S. Y.; Perera, A. P.; Zhang, Y.; Park, M. K., Plasmonic nanohole arrays for monitoring growth of bacteria and antibiotic susceptibility test. *Sensors and Actuators B: Chemical* **2013,** *182*, 576-583.

37.	Shen, Y.; Zhou, J.; Liu, T.; Tao, Y.; Jiang, R.; Liu, M.; Xiao, G.; Zhu, J.; Zhou, Z.-K.; Wang, X., Plasmonic gold mushroom arrays with refractive index sensing figures of merit approaching the theoretical limit. *Nature communications* **2013,** *4*.

38.	Skinner, J. L.; Hunter, L. L.; Talin, A. A.; Provine, J.; Horsley, D. A., Large-area subwavelength aperture arrays fabricated using nanoimprint lithography. *Nanotechnology, IEEE Transactions on* **2008,** *7* (5), 527-531.

39.	Genet, C.; van Exter, M. P.; Woerdman, J., Fano-type interpretation of red shifts and red tails in hole array transmission spectra. *Opt Commun* **2003,** *225* (4), 331-336.

40.	Przybilla, F.; Genet, C.; Ebbesen, T., Enhanced transmission through Penrose subwavelength hole arrays. *Applied Physics Letters* **2006,** *89* (12), 121115.

41.	Rockstuhl, C.; Lederer, F.; Zentgraf, T.; Giessen, H., Enhanced transmission of periodic, quasiperiodic, and random nanoaperture arrays. *Applied Physics Letters* **2007,** *91* (15), 151109.

42.	Bravo-Abad, J.; Fernandez-Dominguez, A.; Garcı́a-Vidal, F.; Martı́n-Moreno, L., Theory of extraordinary transmission of light through quasiperiodic arrays of subwavelength holes. *arXiv preprint cond-mat/0606121* **2006**.

43.	Matsui, T.; Agrawal, A.; Nahata, A.; Vardeny, Z. V., Transmission resonances through aperiodic arrays of subwavelength apertures. *Nature* **2007,** *446* (7135), 517-521.

44.	Xue, J.; Zhou, W.-Z.; Dong, B.-Q.; Wang, X.; Chen, Y.; Huq, E.; Zeng, W.; Qu, X.-P.; Liu, R., Surface plasmon enhanced transmission through planar gold quasicrystals

fabricated by focused ion beam technique. *Microelectronic Engineering* **2009,** *86* (4), 1131-1133.

45.   Xue, J.; Dong, B.-Q.; Wang, X.; Yang, R.; Xu, Z.-C.; Chen, Y.; Huq, E.; Zeng, W.; Qu, X.-P.; Liu, R., Surface plasmon enhanced transmission through gold planar crystals with various aperture arrangements. *Microelectronic Engineering* **2010,** *87* (5), 1340-1343.

46.   Lubin, S. M.; Hryn, A. J.; Huntington, M. D.; Engel, C. J.; Odom, T. W., Quasiperiodic Moiré Plasmonic Crystals. *ACS Nano* **2013,** *7* (12), 11035-11042.

Chapter 4

4 Plasmonic Nanohole Array Sensors Fabricated by Template Transfer

Nanohole array type of surface plasmon resonance sensors provides a promising platform for label-free biosensing on the surface. For their extensive use, an efficient fabrication procedure to make nanoscale features on metallic films is required. We develop a simple and robust template-transfer approach to structure periodic nanohole arrays in optically thick Au films on poly(dimethylsiloxane) (PDMS) substrates. This technique significantly simplifies the process of sensor fabrication and reduces the cost of the device. An approach of spectral analysis is also developed for improving the sensor performance. The sensitivity of the resulting sensor to refractive index changes is 522 nm/RIU (refractive index unit) and the resolution is improved to 2×10^{-5} RIU, which are among the best reported values for localized surface plasmon resonance sensors. We also demonstrate the limit of detection of this sensor for cardiac troponin I.

4.1 Introduction

Surface plasmon resonance (SPR) sensing has become a widely applied optical approach to monitor biomolecular events not only for life science research, but also for drug discovery.[1] In principal, the resonant spectra of SPR vary with changes of the local refractive index induced by molecular binding. The common way of exciting SPR is to illuminate a thin Au film through an optical prism in a Kretschmann configuration.[2]

Commercially available SPR systems enable label-free interaction analysis in real-time and offer quantitative information on specificity, concentration, kinetics and affinity. Beyond propagating SPR, plasmonic nanostructures such as nanohole arrays on metal films can launch SPR.[3-4] In contrast to complicate optical design and precise alignment in prism-based SPR sensors, nanohole arrays exhibit enhanced extraordinary optical transmission (EOT) from normally incident light using a simple microscope setup.[5] The merits of nanohole arrays also include small detection volume and tuneable resonant wavelength.[6-8]

Nanoplasmonics has been developing fast because of recent nanofabrication advancements.[9-10] Existing techniques for fabrication of nanophotonic patterns can be classified into two main categories. One category is traditional methods including focused ion beam (FIB) milling,[11-13] electron beam lithography (EBL)[14-15] and deep UV lithography[16]. Performed with advanced techniques and large equipment, these methods are robust and can create structures with high resolution. However they are either time-consuming or require complex and expensive systems. On the other hand, template approaches involving soft lithography,[17] nanoimprint lithography,[18-19] colloidal lithography[20] and so on, can make nanostructures in a more efficient and cost-effective way due to the use of templates with relief patterns. Besides, recent developments in the coupling between plasmonic and photonic modes also show great promise in sensing application.[21-23] All of these techniques have facilitated fundamental studies of nanoplasmonics and also demonstrated the potential of sensing capability enhancement. However, applications to date have been mostly limited to model systems partly due to the high cost or low throughput of fabrication schemes. The field would greatly benefit from a simpler fabrication method without using any exposure tools, photomasks, or soft stamps.

Solid objects of different size, shape and composition have been transferred to various substrates by kinetically controlling adhesion between different interfaces.[24] This technique offers the capability to transfer nanostructures with high fidelity and productivity. However, the same approach has not been realized in the field of nanoplasmonics. Here for the first time we combine template transfer with precisely patterned Si substrates to fabricate nanohole array plasmonic sensors. This method enables creating intact and uniform nanoholes by only two simple steps. Sensors fabricated by the template transfer approach are featured in high sensitivity. Another merit is the template can be repeatedly used many times, thereby reducing the cost and time consumption of nanofabrication. In addition, this process does not require any additional resist processing, etching, or lift-off. Thus it can generate fresh surfaces without any contamination compared to other nanofabrication techniques based on chemistry processing. This is of great benefit especially in biological applications. Although our current work is focused on subwavelength holes in continuous Au films, the template transfer technique is equally applicable to fabrication of other nanoplasmonic architectures such as nanoparticles and nanorings.

4.2 Experimental Procedure

4.2.1 Fabrication of Si Template

The Si template of the nanohole array was patterned using EBL followed by deep ion etching (as shown in Figure 4-1a). A 100 nm thick poly(methyl methacrylate) (PMMA) resist was spin-coated on a Si wafer. An e-beam lithography system (LEO 1530 equipped with a nanopattern generation system) was used to pattern square arrays of circular

nanoholes with 200 nm diameter and 600 nm pitch on the PMMA layer. The features were then transferred to the Si substrate using a deep reactive ion etching machine (Alcatel 601E). After removing the PMMA mask in piranha solution (3:1 mixture of concentrated sulfuric acid and 30% hydrogen peroxide), the template is ready for Au deposition and transfer. Figure 4-1b shows the scanning electron microscope (SEM) image of the fabricated template. It is noted that alternative techniques other than EBL can also been employed to fabricate the template.
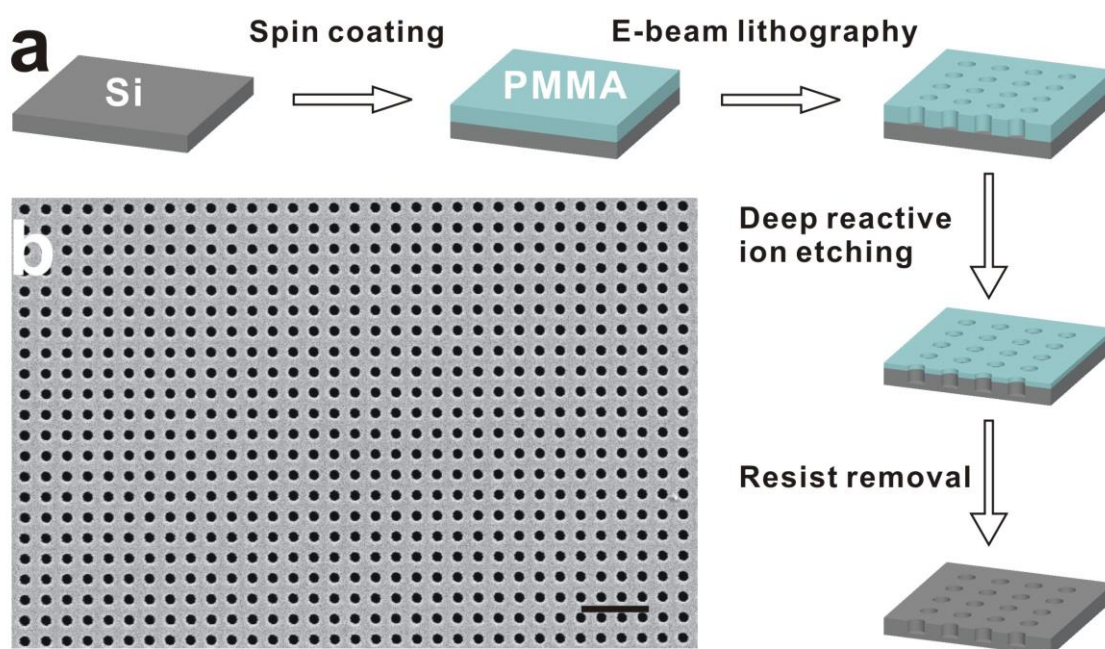

Figure 4-1 (a) Schematic for the fabrication process of Si templates. (b) Scanning electron microscope (SEM) image of the Si template with circular pits. Scale bar, 2 μm. The diameter of the nanoholes and the periodicity of the array are 200 and 600 nm, respectively.

4.2.2 Transfer of Au Nanohole Arrays

Nanohole array sensors are produced by template transfer of featured Au films, shown in Figure 4-2a. The template was thoroughly rinsed with ultrapure water and dried with N_2. A 100 nm thick Au film was then deposited onto it without adhesion layer at a deposition rate of 0.1 nm/s using electron-beam evaporation at ~5 $\times$ 10^{-6} Pa. Au nanohole arrays formed on the top surface of the template were then transferred to PDMS (Sylgard 184, Dow Corning) substrates. The use of PDMS is due to its optical transparency, simplicity of fabrication, low cost and biocompatibility. PDMS pre-polymer mixture (1:10) was cast on the patterned Au film and cured at room temperature to avoid distortion after polymerization. Because the cured PDMS is soft, cracks or wrinkles may occur on the pattern during peeling it from the template. Hence a microscope slide was attached to the PDMS layer as a backplane to prevent the film bending during the stripping process. Due to the weaker adhesion of Au to the Si surface than PDMS, detaching PDMS from the template resulted in transfer of the Au film with nanohole arrays onto the PDMS substrate.

Besides curing PDMS, we can also transfer the nanohole array with a flat PDMS slice by means of conformal contact to and removal from the template. In this method, the adhesion between the PDMS slice and the Au film depends on the separation rate. Peeling the structure away from the template at a sufficiently high velocity (typically faster than 10 cm/s)[24] leads to enough strong adhesion that can lift the Au film away from the template. Numerous trials here have confirmed that it is unnecessary to utilize special chemical or physical treatments to enhance the adhesion between Au films and PDMS slices. Figure 4-2b and c show the uniformity and roundness of the transferred Au nanohole array with

various magnified views. Because Si wafer can be very smooth, patterned Au surfaces have smoothness similar to that of the template, which can increase the propagation length of surface plasmons.[25] After cleaning with Au etchant followed by piranha solution, the template can be reused for a new cycle of transfer without damage. Currently the transfer is performed manually in the simplest implementation. For large scale fabrication, mechanical transfer tools such as liner and rotate stages can be assembled to manipulate substrates and templates, which can accomplish better control in terms of efficiency and quality. In combination with a large template capable of forming several tens of sensors for one time Au deposition, the cost can be reduced to less than $1 per nanohole array sensor.
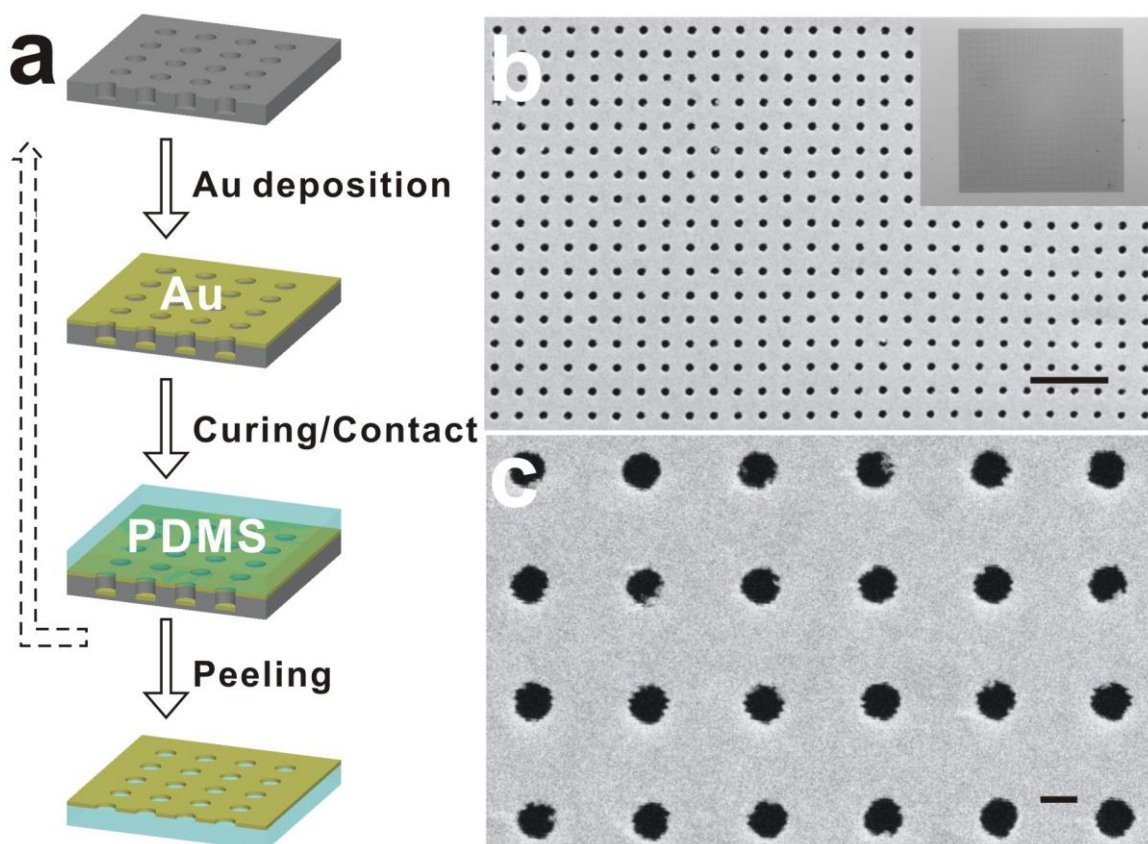
Figure 4-2 (a) Schematic for transfer of Au nanohole arrays from the Si template to PDMS substrates. (b) SEM image of the nanohole array transferred to PDMS. The scale bar is 2 μm. The inset shows an optical microscope image of total 40,000 holes in a 120 ×120 μm² area of Au film. (c) Enlarged SEM image. The scale bar is 200 nm.

4.2.3 Optical Measurement

Figure 4-3 shows the schematic of the setup for transmission measurement at normal incidence. A halogen light source was provided to illuminate the Au nanohole array

through a microscope objective (10×, NA = 0.25). The transmitted light was collected

under normal excitation with a fiber-coupled spectrometer (USB4000, Ocean optics). To

examine the bulk sensitivity of Au nanohole arrays to changes in the refractive index,

optical transmission spectra were measured as the sensor surface was covered with various

concentrations (5-20 wt %) of aqueous sucrose solution with refractive indexes ranging

from 1.3403 to 1.3639.
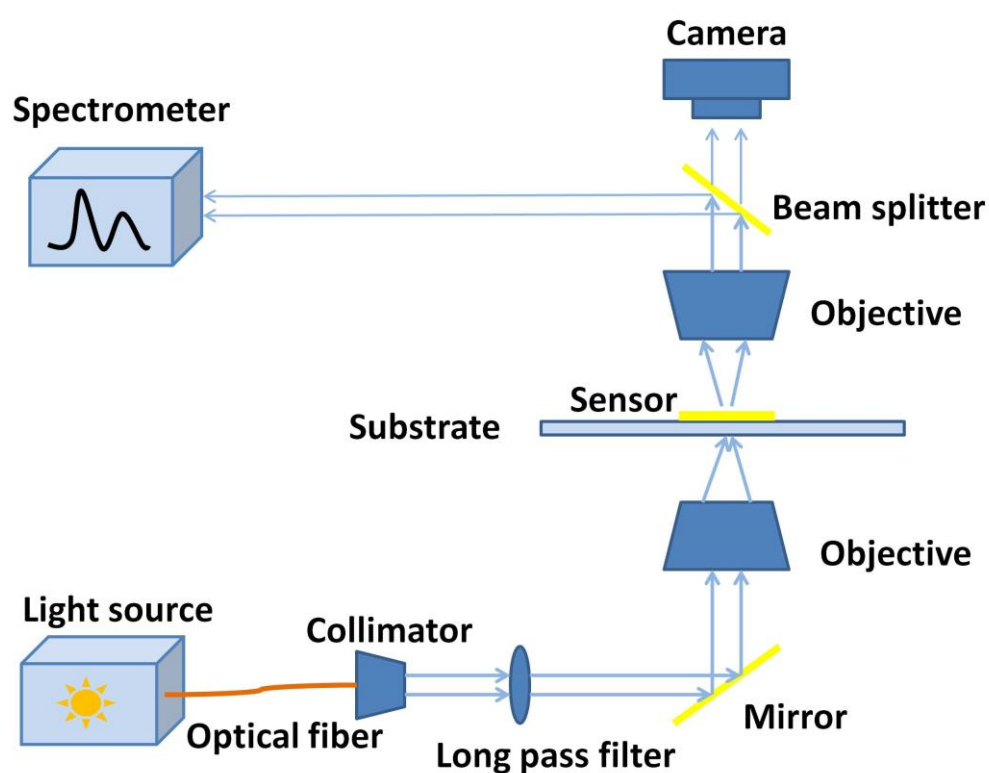
Figure 4-3 Schematic of the measurement setup to record the transmission spectra

at normal incident.

4.2.4 Cardiac Troponin-I Immunoassay

To demonstrate the performance of the nanohole array as a label-free biosensor, the cardiac troponin I (cTnI, 23876 Da, Sigma) was chosen as the analyte. The immunoassay for cTnI is schematically shown in Figure 4-4. Nanohole array sensors were firstly incubated in a 1 μM anti-cTnI (~26 kDa, Sigma) for 1 hour. Anti-cTnI physically adsorbed onto the Au surface at room temperature. 1% Bovine serum albumin (BSA, Sigma) was then used to block the surface to eliminate the nonspecific binding. The immunoreaction was performed by incubating the sensor in a 40 nM cTnI at room temperature for 1 hour. Before each spectrum acquisition, the sensor surface was washed with deionized water to remove the unbound residues and dried with N_2.

Figure 4-4 Schematic of immunoassay with the nanohole array sensor for cTnI.

4.3 Results and Discussions

4.3.1 Optical Properties

The sensing principle of plasmonic devices bases on the SPR sensitivity to the refractive index change adjacent to the metallic surface. Figure 4-5a and b show optical transmission s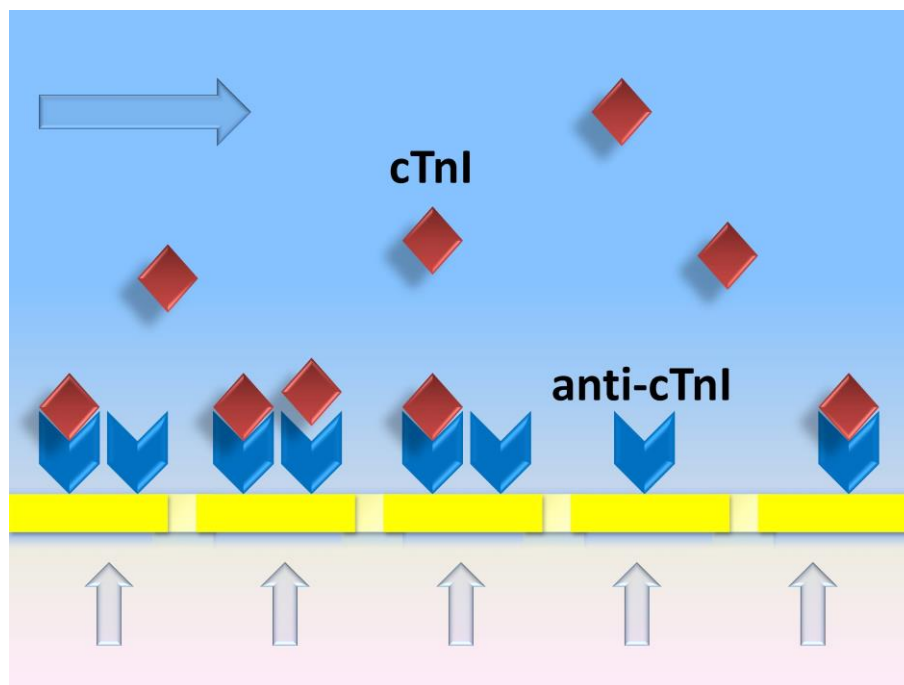pectra of these two types of Au nanohole arrays respectively, in sucrose solutions with different refractive indexes. Each curve was obtained by averaging 100 original spectra in order to decrease the noise level. It is noteworthy that the transmission efficiency for normal incidence is typically low due to diffraction losses. The multiple transmission maxima and minima originate from the couplings of the incident light and the surface plasmons on both sides of the Au nanohole film.[26] The positions of these peaks and troughs depend on array periodicity, film thickness, hole size and shape, as well as the refractive index of the surrounding medium. As the refractive indexes increase, the peak red-shifts occur at wavelengths of 765 nm and 743 nm for two sensors transferred by two different methods, respectively. These spectral shifts arise from the surface plasmons at the interface between Au and the aqueous solution. In contrast, the peaks around 570 nm almost remain at the same positions because they are subject to the SPR at the interface between Au and the PDMS substrate, which is not exposed to the sucrose solution. The minima near 650 nm in both cases are associated with Wood's anomalies due to light diffracted parallel to the Au surface and also remain stationary for refractive index changes.[26]
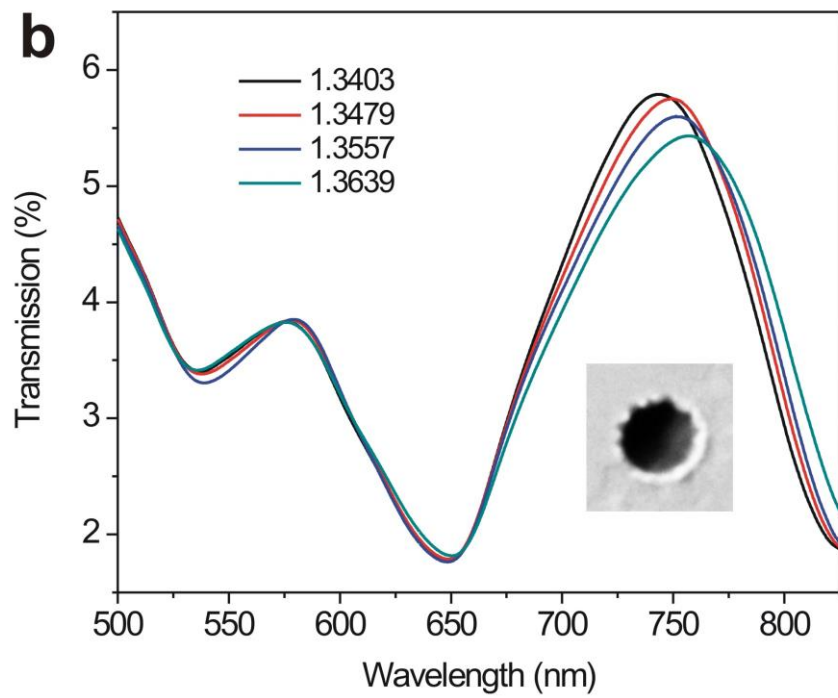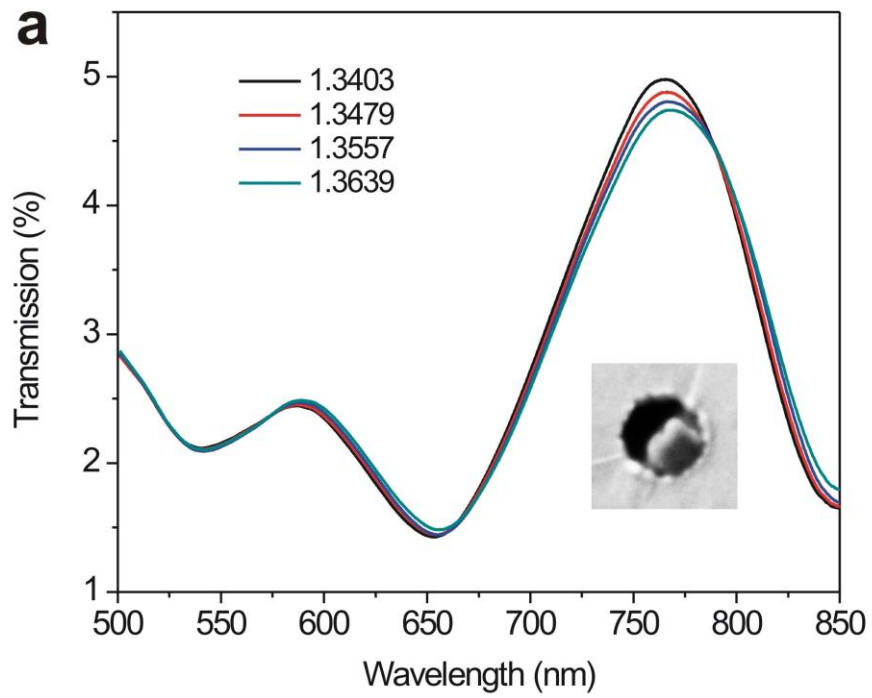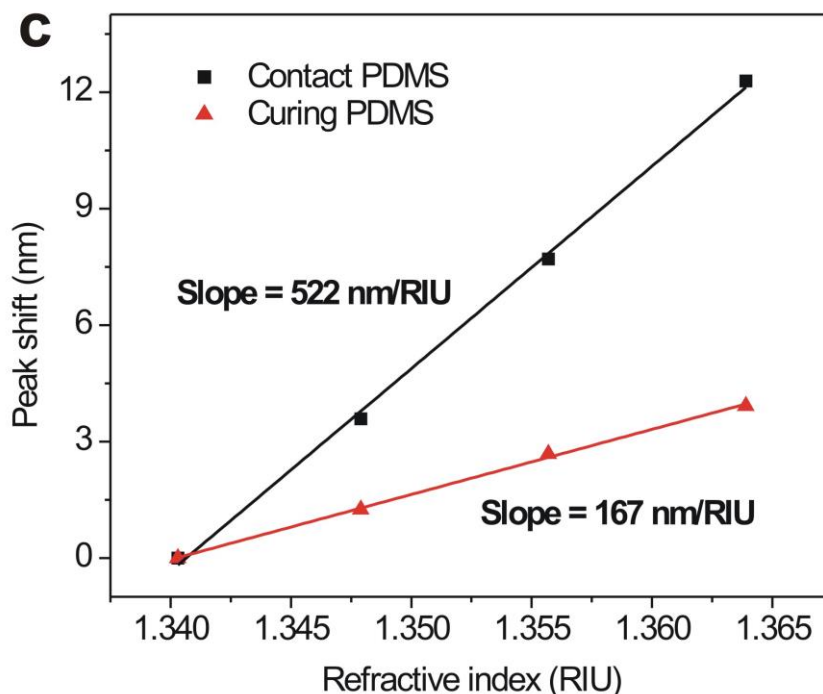
Figure 4-5(a) Transmission spectra of the nanohole array (hole diameter: 200 nm, periodicity: 600 nm) in a 100 nm Au film stripped by curing PDMS. The refractive indexes of sucrose solution covered on the Au film vary from 1.3403 to 1.3639. The SEM inset demonstrates the high magnified nanohole structure. After curing, PDMS blocks nanoholes, keeping their inner surfaces from external environment. (b) Transmission spectra of the nanohole array transferred by direct contact with a PDMS slice with the same feature as that in (a). The inset shows the enlarged SEM image of a hollow hole. (c) Bulk refractive index sensitivity measurements of the fabricated nanohole arrays. By fitting points of spectral shifts to linear curves, the bulk sensitivities are determined to be 167 nm/RIU for the peak at 765 nm in (a) and 522 nm/RIU for the peak at 743 nm in (b) respectively.

To optimize the sensing performance, we compared the sensitivities between nanohole array sensors transferred by curing PDMS and those transferred by contacting PDMS slices. Fig. 3c indicates that the measured spectral shifts of these peaks linearly respond to refractive index changes, as shown in Figure 4-5a and b. The measured spectral sensitivity of this transmission maximum is 167 nm/RIU for the nanohole array stripped after curing PDMS. However, the sensor formed by direct contact and detachment shows a 522 nm/RIU sensitivity in the corresponding maximum, which is a 3-fold increase compared to the former. We attribute this sensitivity enhancement to the high sensitivity of in-hole surface to refractive index changes, which is consistent with previous reports on both sensing confinement[27] and selective binding results[28]. In the scheme of cure-based transfer, PDMS flowed into the holes and finally clogged them, thereby disabling in-hole area to sense the refractive index changes induced by the alteration of sucrose concentrations. Besides, the presence of PDMS decreases the effective refractive index changes around the Au nanoholes. In contrast, the highly sensitive surface in the nanoholes detached with PDMS lamina was directly exposed to external dielectric environment and thus significantly enhanced the sensitivity. This bulk refractive index sensitivity is also higher than those of previous reported periodic nanohole arrays fabricated by FIB milling (400 nm/RIU),[5] EBL (393 nm/RIU)[14] and soft interference lithography (286 nm/RIU)[17].

4.3.2 Optimizing the Sensor Performance

One of key issues in the field of SPR sensing is how to improve the limit of detection by reducing the uncertainty in determining the resonance position.[29] Given that the recorded spectra are discrete and the wavelength resolution is limited by the spectrometer, it is

impossible to directly determine peak positions with higher precision than that of the spectrometer. In order to track the peak shift with high resolution, various peak position tracking algorithms were evaluated for conventional SPR or LSPR.[30-32] In our work, we developed an algorithm by fitting an original spectrum to a high degree polynomial by a least square procedure using the following equations:

$$T_{fit}(\lambda) = \sum_{k=0}^{n} p_k \lambda^k \tag{4-1}$$

$$R^2 = \sum_{\lambda_i \in S} \left[T(\lambda_i) - T_{fit}(\lambda_i) \right]^2 \tag{4-2}$$

$$\frac{\partial(R^2)}{\partial p_k} = 0 \tag{4-3}$$

where n is the polynomial degree, p_k is the coefficient defining the polynomial, T is recorded discrete transmission data, R^2 is the sum of the squares of the vertical deviations of a set of transmission data points in a wavelength span S, which is initially chosen as the full width at half-maximum of the peak. The peak position is calculated from the polynomial expression T_{fit}. This method minimizes the sum of the residual squares of the spectral points from the polynomial curve. Theoretically, it removes the resolution limitation imposed by the spectrometer and enables tracking peak positions with arbitrary precision. We applied this algorithm ($n = 9$) to tracking peak positions in above sensitivity determination, revealing a sharp linear relation between peak shifts and refractive index changes as shown in Figure 4-5c. An R-square value 0.998 of the linear curve fitting proves its feasibility and effectiveness in peak tracking.

The sensor's resolution in such case is mainly governed by the noise level, which can be estimated from the statistical standard deviation (SD) of peak positions calculated by the

above algorithm. Since the background shot noise of the nanohole system primarily comes from the light source and the spectrometer, it is possible to reduce the noise level by summing a number of spectra. By averaging up to 100 frames over 30 times, the spectral noise (SD) can be reduced from 0.27nm to 0.01 nm, as shown in Figure 4-6. This improvement is similar to that of the centroid algorithm[31] in terms of optimization level. However, our algorithm is simpler and thus more suitable for on-chip implementation. Using the measured bulk refractive index sensitivity of 522 nm/RIU, the best refractive index resolution of the system is better than 2×10^{-5} RIU, comparable to the state-of-art SPR sensors.[1]
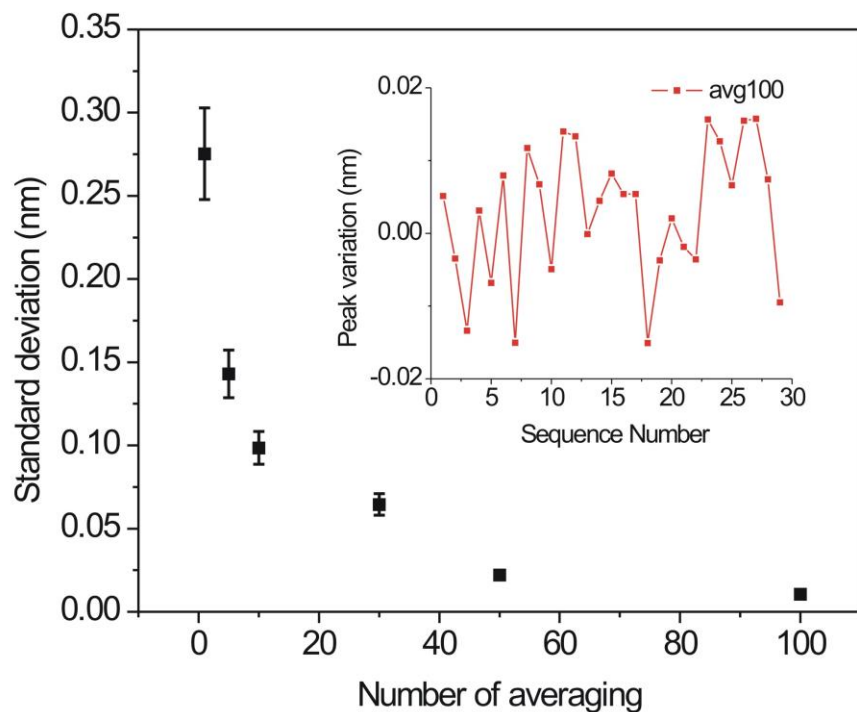
Figure 4-6 Background noise (SD) with the numbers of spectra averaging in tracking peak positions. The shot noise is reduced to 0.01 nm by averaging 100 transmission spectra. The inset shows a plot of variation of peak positions for 100 spectra averages.

4.3.3 Using Nanohole Arrays in Biosensing

cTnI is regarded as a critical biomarker in diagnosis of myocardial infarction owing to its presence only resulting from cardiac muscle tissue injury. Because the Au film is freshly stripped from the Si template with PDMS slices, it can be directly used for biosensing without cleaning the sensor surface with chemical solution, thereby reducing the possibility of contamination. Transmission spectra of the nanohole array sensor in the immunoassay for cTnI are presented in Figure 4-7a. It is noted that the transmission spectrum in air undergoes a remarkable change in comparison to that in liquid. The peak ascribed to

surface plasmons in the Au/liquid surface blue shifts to around 600 nm due to the decrease of refractive index. Meanwhile, two transmission maxima appear at the wavelength of 680 nm and 800 nm respectively. Molecular binding on the Au surface changes the local refractive index, which in turn shifts the positions of these spectral features. The spectral peak at 600 nm has a highest shift of 1.996 nm (as shown in Figure 4-7b) due to cTnI binding. We point out that no attempts at this stage have been made to optimize the platform performances for biosensing. However considering the noise level of 0.01 nm, the signal-to-noise ratio is ~200 for peak shifts upon cTnI binding. The analytical sensitivity is defined as the concentration at two standard deviations from a blank sample. It can be calculated the detection limit of current system is less than 0.4 nM. The detection resolution can be further improved by employing self-assembled linker layers on the Au surface and high S/N ratio optical detection systems.
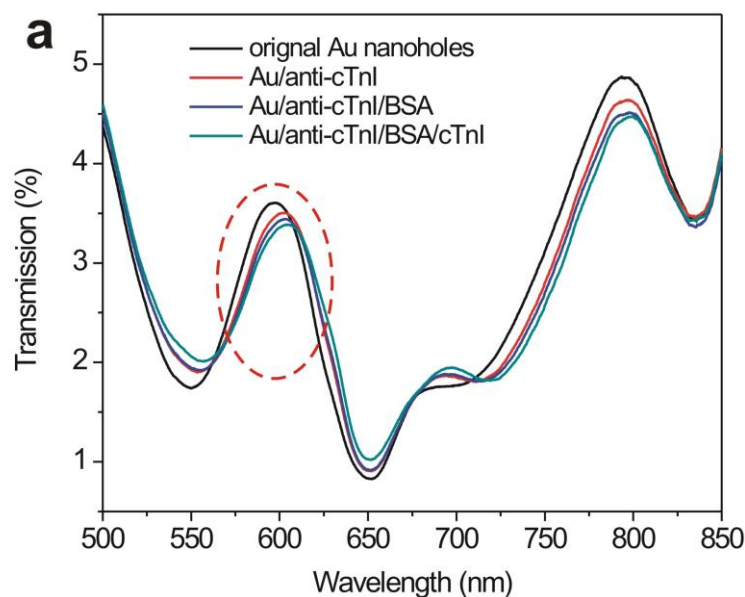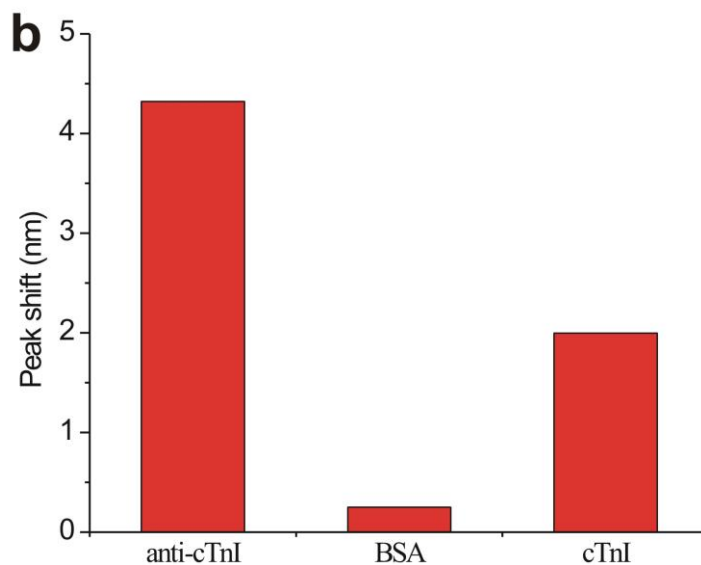
Figure 4-7 (a) Optical transmission spectra measurements of the Au nanohole array as a biosensor. The concentration of cTnI solution incubated on the sensor is 40 nM. (b) SPR shifts at 600 nm measured after the addition of anti-cTnI, BSA, and cTnI.

4.4 Conclusions

In summary, we have demonstrated a high-performance plasmonic sensor based on transmission through nanohole arrays fabricated by template transfer. This technique is capable of high-throughput and low-cost production as the templates can repeatedly duplicate nanohole arrays in a simple two-step process of Au evaporation and transfer. The simplicity of template transfer also permits the potential of direct integration of nanohole arrays into microfluidic systems. By comparing the sensitivity of sensors transferred by two methods, the in-hole surface is confirmed to enhance the detection ability of sensing refractive index changes. The sensor has a 522nm/RIU sensitivity and can resolve

refractive index changes down to 2×10^{-5} RIU via effective peak position tracking and spectra averaging without requiring any temperature control. Furthermore, this instrument is capable of quantifying cTnI at relatively low concentrations only with a standard microscope and off-the-shelf optical components. All of these advantages enable the nanohole array sensor to be a promising option for nanoplasmonics biosensing.

References

1.   Homola, J., Surface plasmon resonance sensors for detection of chemical and biological species. *Chemical Reviews* **2008,** *108* (2), 462-493.

2.   Homola, J., Present and future of surface plasmon resonance biosensors. *Analytical and Bioanalytical Chemistry* **2003,** *377* (3), 528-539.

3.   Ebbesen, T. W.; Lezec, H. J.; Ghaemi, H. F.; Thio, T.; Wolff, P. A., Extraordinary optical transmission through sub-wavelength hole arrays. *Nature* **1998,** *391* (6668), 667-669.

4.   Barnes, W. L.; Dereux, A.; Ebbesen, T. W., Surface plasmon subwavelength optics. *Nature* **2003,** *424* (6950), 824-830.

5.   Brolo, A. G.; Gordon, R.; Leathem, B.; Kavanagh, K. L., Surface plasmon sensor based on the enhanced light transmission through arrays of nanoholes in gold films. *Langmuir* **2004,** *20* (12), 4813-4815.

6.   Gordon, R.; Sinton, D.; Kavanagh, K. L.; Brolo, A. G., A New Generation of Sensors Based on Extraordinary Optical Transmission. *Accounts of Chemical Research* **2008,** *41* (8), 1049-1057.

7.   Gordon, R.; Brolo, A. G.; Sinton, D.; Kavanagh, K. L., Resonant optical transmission through hole-arrays in metal films: physics and applications. *Laser Photonics Rev* **2010,** *4* (2), 311-335.

8.   Sannomiya, T.; Scholder, O.; Jefimovs, K.; Hafner, C.; Dahlin, A. B., Investigation of Plasmon Resonances in Metal Films with Nanohole Arrays for Biosensing Applications. *Small* **2011,** *7* (12), 1653-1663.

9.   Henzie, J.; Lee, J.; Lee, M. H.; Hasan, W.; Odom, T. W., Nanofabrication of Plasmonic Structures*. *Annual Review of Physical Chemistry* **2009,** *60* (1), 147-165.

10.   Stewart, M. E.; Anderton, C. R.; Thompson, L. B.; Maria, J.; Gray, S. K.; Rogers, J. A.; Nuzzo, R. G., Nanostructured plasmonic sensors. *Chemical Reviews* **2008,** *108* (2), 494-521.

11.   Stark, P. R. H.; Halleck, A. E.; Larson, D. N., Short order nanohole arrays in metals for highly sensitive probing of local indices of refraction as the basis for a highly multiplexed biosensor technology. *Methods* **2005,** *37* (1), 37-47.

12.   Ji, J.; Yang, J.-C.; Larson, D. N., Nanohole arrays of mixed designs and microwriting for simultaneous and multiple protein binding studies. *Biosensors and Bioelectronics* **2009,** *24* (9), 2847-2852.

13.   Lesuffleur, A.; Im, H.; Lindquist, N. C.; Oh, S.-H., Periodic nanohole arrays with shape-enhanced plasmon resonance as real-time biosensors. *Applied Physics Letters* **2007,** *90* (24), 243110.

14.   Sharpe, J. C.; Mitchell, J. S.; Lin, L.; Sedoglavich, N.; Blaikie, R. J., Gold Nanohole Array Substrates as Immunobiosensors. *Analytical Chemistry* **2008,** *80* (6), 2244-2249.

15.   Yanik, A. A.; Huang, M.; Artar, A.; Chang, T.-Y.; Altug, H., Integrated nanoplasmonic-nanofluidic biosensors with targeted delivery of analytes. *Applied Physics Letters* **2010,** *96* (2), 021101.

16.   Peng, K.-Q.; Wang, X.; Li, L.; Wu, X.-L.; Lee, S.-T., High-Performance Silicon Nanohole Solar Cells. *Journal of the American chemical society* **2010,** *132* (20), 6872-6873.

17.   Henzie, J.; Lee, M. H.; Odom, T. W., Multiscale patterning of plasmonic metamaterials. *Nature nanotechnology* **2007,** *2* (9), 549-554.

18.   Malyarchuk, V.; Hua, F.; Mack, N.; Velasquez, V.; White, J.; Nuzzo, R.; Rogers, J., High performance plasmonic crystal sensor formed by soft nanoimprint lithography. *Optics express* **2005,** *13* (15), 5669-5675.

19.   Turker, B.; Guner, H.; Ayas, S.; Ekiz, O. O.; Acar, H.; Guler, M. O.; Dana, A., Grating coupler integrated photodiodes for plasmon resonance based sensing. *Lab on a Chip* **2011,** *11* (2), 282-287.

20.   Larsson, E. M.; Alegret, J.; Käll, M.; Sutherland, D. S., Sensing Characteristics of NIR Localized Surface Plasmon Resonances in Gold Nanorings for Application as Ultrasensitive Biosensors. *Nano Letters* **2007,** *7* (5), 1256-1263.

21.   Boriskina, S. V.; Reinhard, B. M., Adaptive on-chip control of nano-optical fields with optoplasmonic vortex nanogates. *Optics express* **2011,** *19* (22), 22305-22315.

22.   Etsuo, M.; Yaerim, L.; Youjiro, K.; Akiko, T.; Mari, K.; Shigenori, F.; Jean-Jacques, D., Sensitivity to refractive index of high-aspect-ratio nanofins with optical vortex. *Nanotechnology* **2012,** *23* (50), 505502.

23.   Ho, Y.-L.; Lee, Y.; Maeda, E.; Delaunay, J.-J., Coupling of localized surface plasmons to U-shaped cavities for high-sensitivity and miniaturized detectors. *Optics express* **2013,** *21* (2), 1531-1540.

24.   Meitl, M. A.; Zhu, Z.-T.; Kumar, V.; Lee, K. J.; Feng, X.; Huang, Y. Y.; Adesida, I.; Nuzzo, R. G.; Rogers, J. A., Transfer printing by kinetic control of adhesion to an elastomeric stamp. *Nature materials* **2006,** *5* (1), 33-38.

25.   Nagpal, P.; Lindquist, N. C.; Oh, S.-H.; Norris, D. J., Ultrasmooth Patterned Metals for Plasmonics and Metamaterials. *Science* **2009,** *325* (5940), 594-597.

26.   Chang, S.-H.; Gray, S.; Schatz, G., Surface plasmon generation and light transmission by isolated nanoholes and arrays of nanoholes in thin metal films. *Optics express* **2005,** *13* (8), 3150-3165.

27.   Ferreira, J.; Santos, M. J.; Rahman, M. M.; Brolo, A. G.; Gordon, R.; Sinton, D.; Girotto, E. M., Attomolar protein detection using in-hole surface plasmon resonance. *Journal of the American chemical society* **2008,** *131* (2), 436-437.

28.   Feuz, L.; Jönsson, P.; Jonsson, M. P.; Höök, F., Improving the limit of detection of nanoscale sensors by directed binding to high-sensitivity areas. *ACS Nano* **2010,** *4* (4), 2167-2177.

29.   Unger, A.; Kreiter, M., Analyzing the Performance of Plasmonic Resonators for Dielectric Sensing. *The Journal of Physical Chemistry C* **2009,** *113* (28), 12243-12251.

30.   Knut, J.; Ralph, S.; Ingemar, L.; Bo, L., Surface plasmon resonance: instrumental resolution using photo diode arrays. *Measurement Science and Technology* **2000,** *11* (11), 1630.

31.   Dahlin, A. B.; Tegenfeldt, J. O.; Höök, F., Improving the Instrumental Resolution of Sensors Based on Localized Surface Plasmon Resonance. *Analytical Chemistry* **2006,** *78* (13), 4416-4423.

32.   Garet, G. N.; Marek, P.; Jirí, H., Data analysis for optical sensors based on spectroscopy of surface plasmons. *Measurement Science and Technology* **2002,** *13* (12), 2038.

Chapter 5

5   Plasmonic Optical Fiber

Surface plasmon resonance (SPR) on metal nanostructures offers a promising route for manipulation and interrogation of light in the subwavelength regime. However, the utility of SPR structures is largely limited by currently used complex nanofabrication methods and relatively sophisticated optical components. In this chapter, to relieve these restrictions, plasmonic optical fibers are constructed by transferring periodic metal nanostructures from patterned templates onto endfaces of optical fibers using an epoxy adhesive. Patterned metal structures are generally extended from two-dimensional (2D) nanohole arrays to one-dimensional (1D) nanoslit arrays. By controlling viscosity of the adhesive layer, diverse surface topographies of metal structures are realized with the same template. We design a special plasmonic fiber that simultaneously implements multimode refractive index sensing (transmission and reflection) with remarkably narrow linewidth (6.6 nm) and high figure of merit (60.7), which are both among the best reported values for SPR sensors. We demonstrate a real-time immunoassay relying on plasmonic fiber for the first time. Plasmonic optical fibers also take advantages of consistent optical responses, excellent stability during fiber bending and capability of spectrum filtering. These features enable our plasmonic fibers to open up an alternative avenue for the general community in biosensing and nanoplasmonics.

5.1 Introduction

Surface plasmon resonance (SPR) is collective oscillation resulting from the coupling of electromagnetic waves with free electrons at the metal/dielectric interfaces. Such interaction in metal nanostructures leads to significant field enhancement phenomena such as the extraordinary optical transmission (EOT).[1] Since electromagnetic fields are concentrated and channelled beyond the diffraction limit, SPR can be used to detect light-matter interactions and produce special spectra in an extremely compact dimension. This unique aspect gives rise to a wealth of plasmonic applications from label-free biosensing, chemical imaging, surface-enhanced spectroscopies[2] to colour generation[3]. However, functional plasmonic devices are usually confined to planar substrates and rely on bulky optical infrastructures such as lasers, prisms and/or microscopes for operation. Broad applications of such optical setups are still restricted due to the use of their optical elements for focusing and alignment. For instance, analytes have to be collected and transferred from their in situ environment to laboratory settings. As a result, such procedures may have changed the original states of analytes and probably induced large deviation from the real values to be detected, especially for biosensing. A miniaturized, portable and accessible plasmonic platform is highly desirable for practical application.[4]

Among numerous optical platforms, optical fiber serves as a versatile medium due to its advantages of lightweight, small size, cost effectiveness, flexibility and robustness. The implementation of active plasmonic elements on optical fibers can thus significantly simplify the optical design and release their dependence on some sophisticated optical elements, making the nanoplasmonic sensors with great versatility and accessibility. This

would allow us to perform remote and *in vivo* tasks such as biological sensing in living organisms. This combination would have the possibility to far extend the scope of plasmonics utilization in biological and chemical community.

However, small dimension and large aspect ratio of the optical fiber render it challenging to deploy metal nanostructures on the endface. Generally two strategies have been explored to fabricate plasmonic nanostructures on fiber facets. One direction is in situ patterning the endface of the optical fiber. As a common nanofabrication method, electron-beam lithography (EBL) was used to fabricate metal nanorings[5], nanodots[6] and hybrid nanostructures[7] on fibers due to its high resolution. However, EBL requires special apparatus to host the optical fiber; nevertheless spin-coating is still susceptible to produce an uneven resist layer around the perimeter on small facets.[7] Focused ion beam (FIB) was utilized to mill nanohole arrays on various types of optical fibers.[8-9] The drawbacks of FIB milling are the potential for substrate contamination by ions[10] and its low yield. Optical fiber surface-enhanced Raman scattering (SERS) sensors were demonstrated using nanoimprint lithography to replicate nanostructures of the cicada wing[11-12] and the anodized aluminum oxide (AAO)[12]. This method needs precise translation stages and cameras for accurate alignment during imprinting. Since metal is coated after imprinting and covers the entire tip surface, it is impossible to form the duty-cycle structures via this method.

The other strategy separates pattern generation from optical fibers and then transfers the as-prepared metal structures onto the fiber tips. This division avoids the difficulty of directly patterning structures on unusual substrates like optical fibers incompatible with conventional fabrication. For instance, arbitrary metal nanoscale features were stripped via

a sacrificial thiol-ene film from a patterned substrate and then transferred to the optical fiber facets.[13-14] This approach is serial and each array must be written individually by EBL. Another facile method depends on nanoskiving using a microtome to section thin metal nanostructures embedded in epoxy.[15] However, this skiving technique is not capable of producing large areas of structured films due to its high level cutting force. Besides, defects could occur because of the mechanical stresses of sectioning and creases on the slabs might take place during transfer.[15] Moreover, metal structures transferred by both methods could easily break away from the fiber tips in harsh conditions for lack of robust bonding. None of these plasmonic fibers have been applied to real-time biosensing.

In this chapter, we develop plasmonic optical fibers patterned with various periodic metal nanostructures on the tips by a template transfer method. This facile approach allows for realizing high-quality and large-area general plasmonic structures from nanohole arrays to nanoslit arrays on optical fibers by two extremely simple steps: deposition and transfer.[16-17] The realization of final plasmonic structures only depends on the patterns of used templates. Besides, distinct surface topographies of transferred metal structures are achieved with the same template by controlling the viscosity of the adhesive layer. The reuse of the templates and robustness of this technique ensure high yield. Using an Au nanohole array fiber, we demonstrate a high-performance refractive index nanoprobe simultaneously in transmission-reflection multimode. Furthermore, we report the first real-time immunoassay using the plasmonic optical fiber as a practical application in biosensing perspectives. The plasmonic fiber also shows high stability during bending and unique spectrum filtering property.

5.2   Results and Discussion

5.2.1 Fabrication and Characterization of Plasmonic Fiber

The fabrication procedure of plasmonic optical fibers is summarized in Figure 5-1a. Diverse nanostructures such as nanoholes and nanoslits are pre-patterned on Si templates, on which Au is vertically deposited by electron-beam evaporation. During the Au deposition on the Si template, corresponding metal nanostructures are naturally formed. A thermal-curing epoxy as an adhesion layer is applied onto one polished facet of an optical fiber and then heated to become sticky. Afterwards, the template coated with Au is attached to the epoxy adhesive. The fiber ferrule acts as a holder to support the template on top until the epoxy is completely cured by way of heating. The Au on the reliefs of the template is left on the fiber endface via detaching the template. The intact and uniform metal pattern covers the entire fiber tips typically in diameter of several millimeters, as shown in Fig. 1b. This entire coverage eliminates the edge effect in many methods based on spin-coating.[7, 13-14] Distinct color can be observed from different angles due to diffraction by coupling white light into the fiber from the distal end without metal. This fabrication can be equally applied to complex fiber structures. For instance, a six-around-one plasmonic fiber bundle is demonstrated on the right-bottom in Figure 5-1b, which allows for carrying more signal than a single assembly and thus lowering the random noise. This multiple-in-one design can also facilitate high-throughput multiplex screening in a parallel and compact fashion.
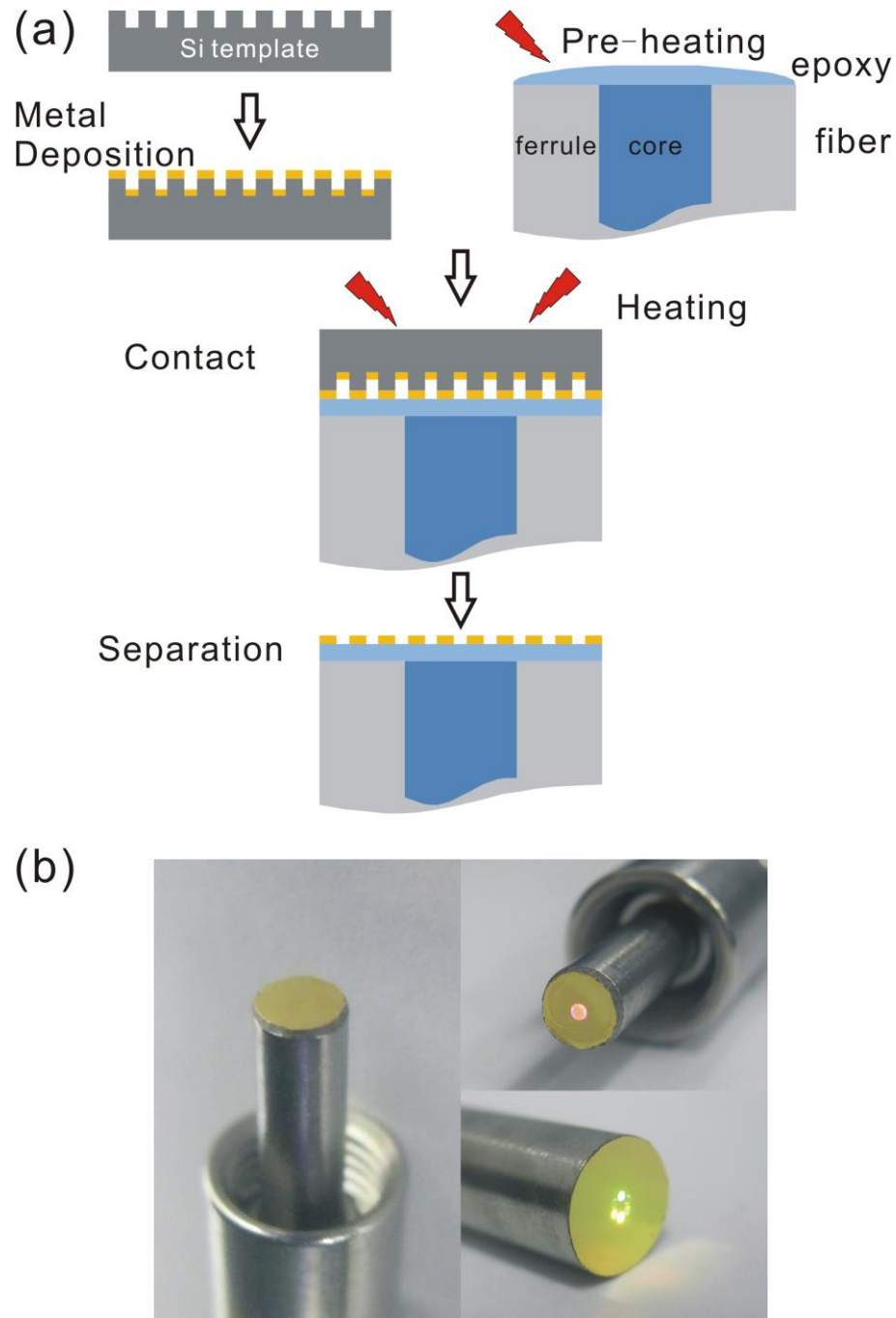
Figure 5-1 (a) Schematic of the fabrication process of plasmonic optical fiber by patterning the fiber endface. The metal is deposited on the pre-patterned Si template with the designed nanostructure. After pre-heating the epoxy adhesive on the fiber tip to be sticky, the template is attached to and detached from the fiber tip, resulting

in the transfer of the metal on relief to the fiber facet. (b) Photographs of plasmonic optical fibers with Au nanostructures on the tips. Two fibers on the right are illuminated by coupling white light from the distant ends. Diameters of the fiber cores are all 600 μm; diameters of the fiber tips are 3.2 mm (left and right-top) and 6.7 mm (right-bottom) respectively.

Various Au nanostructures on the fiber endfaces are demonstrated in scanning electron microscopy (SEM) images in Figure 5-2a-c, including the hexagonal nanohole array, the square nanohole array and the nanoslit array respectively. Fine grain boundary on the Au film shown in Figure 5-2a visually implies a minimal surface roughness similar to that of Si wafer, which facilitate the surface plasmon propagation.[18-19] The photographs of diffraction patterns produced by the corresponding plasmonic fibers are shown in Figure 5-2d-f when white light is coupled from the ends without patterns. Both SEM images and diffraction patterns confirm the high quality of plasmonic structures that cover the entire facets of the optical fibers without defects.
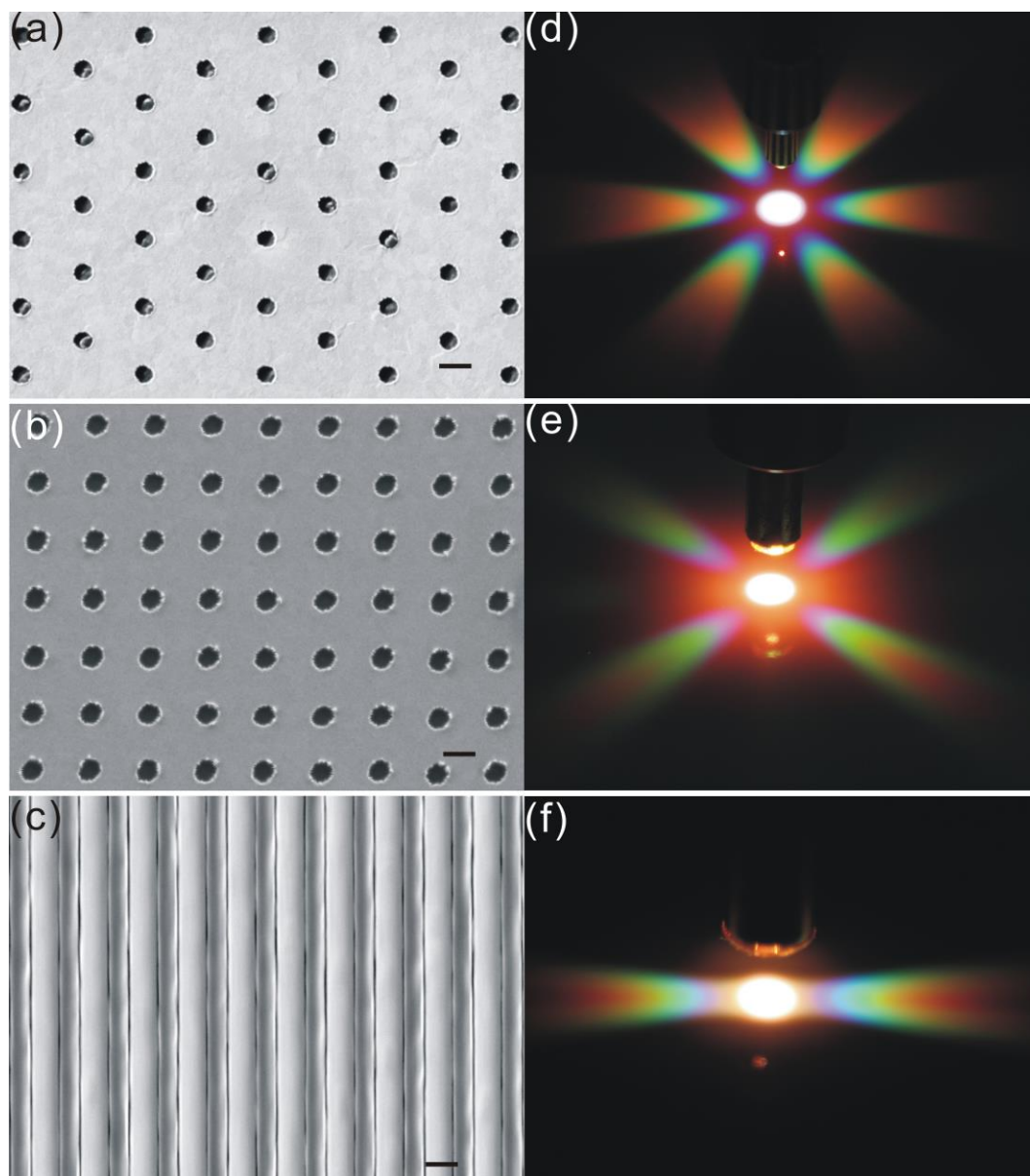
Figure 5-2 (a-c) SEM images of the Au hexagonal nanohole array, square nanohole array and nanoslit array on the fiber tips. The periodicities of the nanostructures are 700 nm, 600 nm and 500 nm, respectively. All scale bars are 500 nm. (d-f) Photographs of the far-field optical diffraction patterns produced by correspondingly illuminating (a-c) with white light coupled from the other bare ends of plasmonic fibers.

Furthermore, metal nanostructures on different parts of a template can be selectively transferred to optical fibers to form diverse topographies. As mentioned above, pre-heating increases the viscosity of the epoxy adhesive so that the epoxy would only touch the reliefs on the template surface. In turn, only the metal on the reliefs are consequently transferred to the fiber tip. In contrast, the uncured original epoxy with a low viscosity could flow into the pits on the template due to capillary force, resulting in the transfer of the entire metal on both reliefs and pits. Figure 5-3a shows an array of Au nanoslits, between which the cured epoxy is exposed. Its continuous counterpart nanoridges transferred from the same template is shown in Figure 5-3b aligned with Figure 5-3a. By removing the Au on the ridges, the epoxy underneath is distinctly revealed. This variation of the transfer method allows for manufacture of three-dimensional (3D) hybrid nanostructures on the fiber[7] in a simple way.
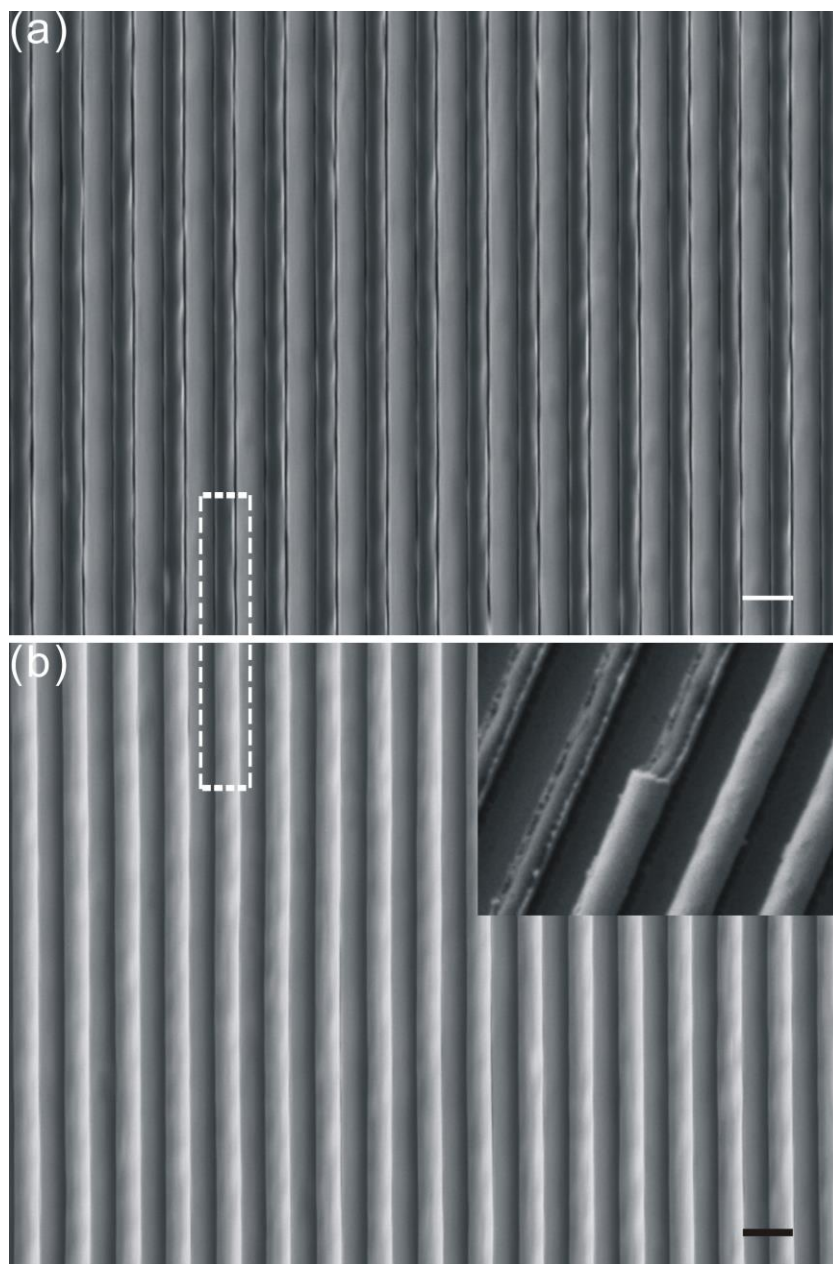
Figure 5-3 SEM images of the Au periodic nanoslits transferred from the same template with (a) and without (b) the step of pre-heating the epoxy adhesive on the fiber tip. Two images are aligned vertically for comparison. The dash rectangle highlights the distinct parts for better visualization. The inset in (b) reveals the epoxy under the Au nanoridges. All scale bars are 500 nm.

To obtain the transmission and reflection at the same time, we build a fiber assembly comprising three single fibers connected together by a Y-shape splitter, schematically shown in Figure 5-4a. The Au hexagonal nanohole array with 700 nm period in Figure 5-2a is attached to the common end as a SPR sensor. The reason to choose the hexagonal hole array is it can reduce the resonance cross-talk compared to the square hole array with the same lattice constant.[3] On the other hand, the array periodicity of 700 nm is chosen to position SPR peak in the accessible range of our spectrometer when aqueous solutions flow over. In this multimode configuration, the light transmitted through the nanohole array is directly collected by a face-to-face configured single fiber coupled to a spectrometer (transmission mode); meanwhile reflected signal is redirected through one of bifurcated legs into the other spectrometer (reflection mode). When this multimode plasmonic fiber naturally works in reflection mode only, no alignment or flow cell is required and thus it could get into human body, which would enable remote and *in vivo* biomolecule sensing. Figure 5-5 and Figure 5-6 show different plasmonic fibers integrated with special designed flow cells working in various modes.
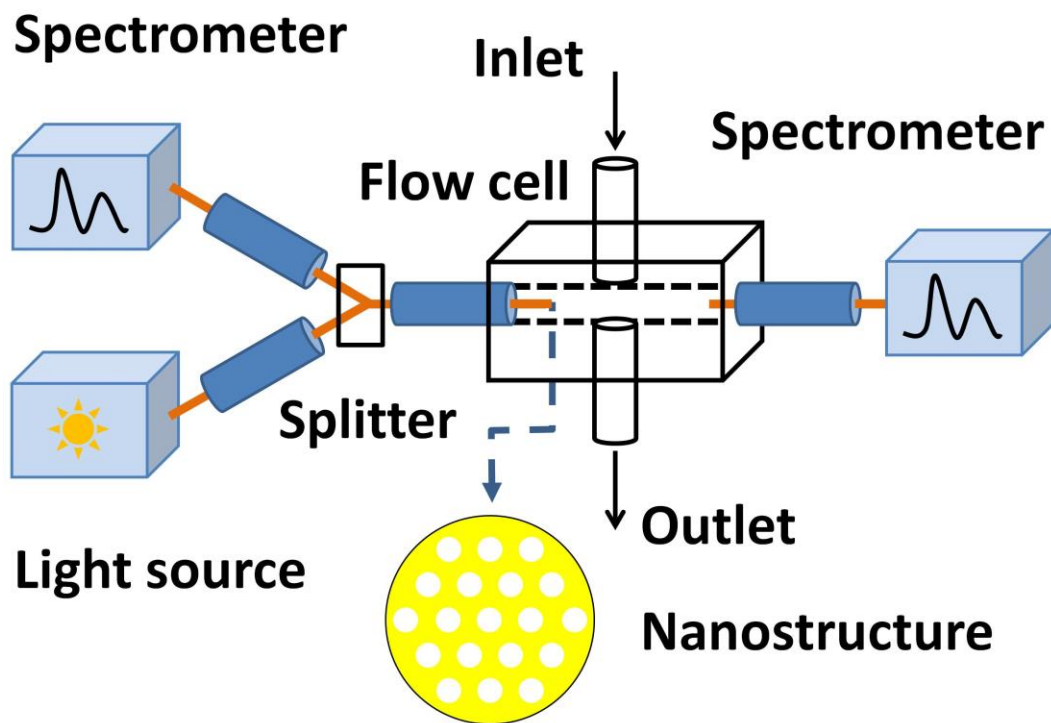
Figure 5-4 Diagram of a Y-shape plasmonic fiber mounted in a flow cell for multimode sensing simultaneously in transmission and reflection.
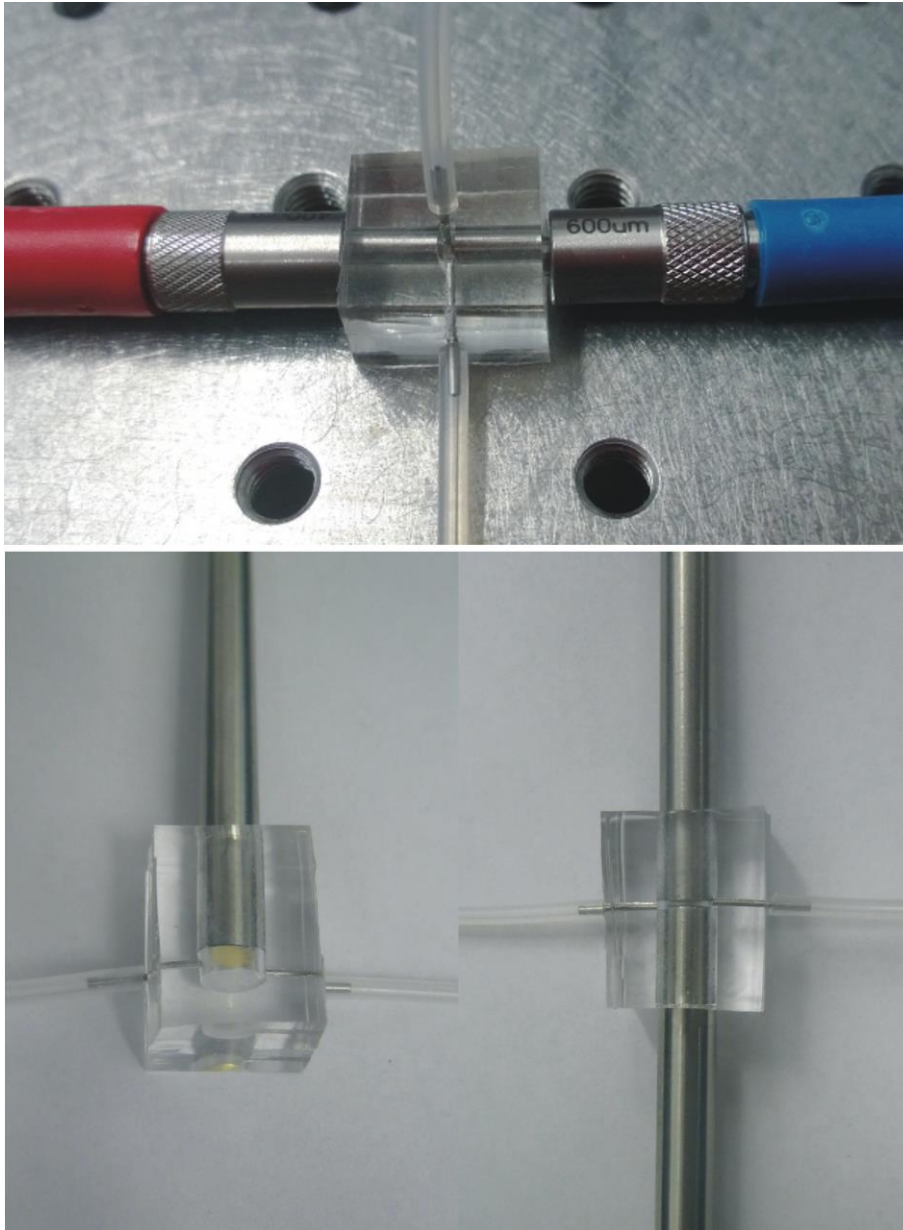
Figure 5-5 Plasmonic optical fibers working in multimode (top and bottom-right) or reflection mode only (bottom-left).
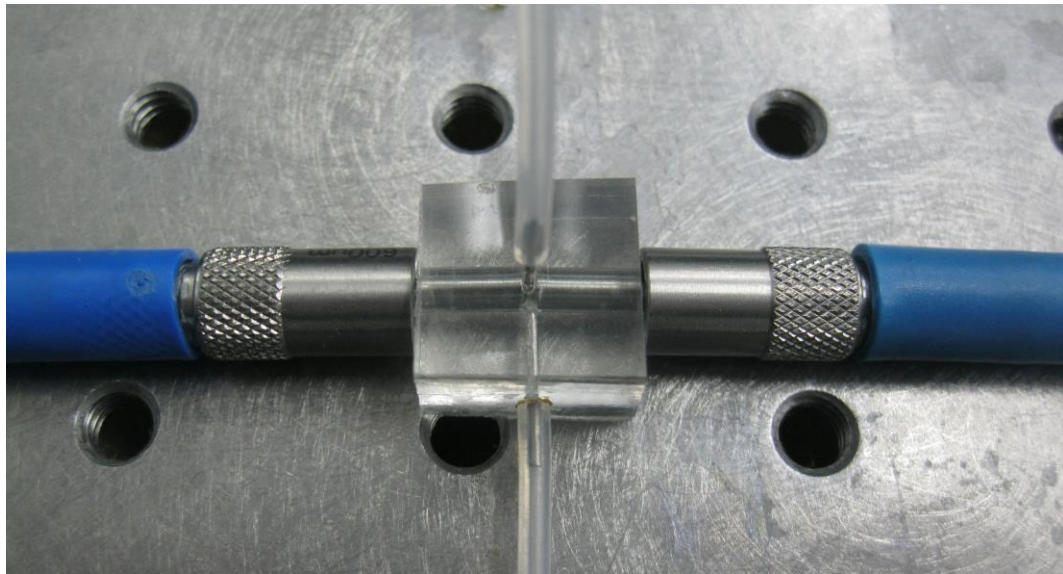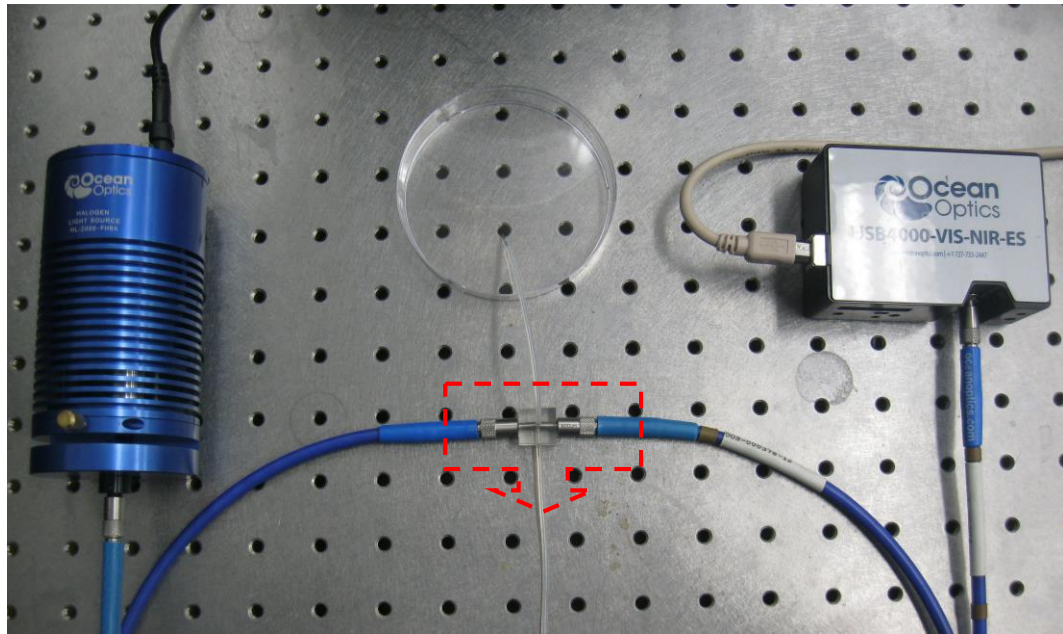
Figure 5-6 A transmission plasmonic optical fiber.

5.2.2 Spectroscopic Analysis and Simulation

The normalized transmission (as well as its finite-difference time-domain simulation, FDTD) and reflection spectra are plotted in Figure 5-7. SPR peaks can be clearly identified around 700 nm in these spectra. The experimental transmission exhibits overall agreement with the simulated result in shape and position; whereas the spectral linewidth of the resonance in experiment is slightly broader than simulation because of the divergence of incident light.[5] The transmission for plane Au film (100 nm thickness) transferred from Si wafer without structures is also recorded for comparison. The single peak at 500 nm comes from of direct light transmission through the gold film, which could be attributed to the interaction between the conduction band and the d-band of Au.[20] This maximum emerges at the same position near 500 nm in the nanohole array transmissions as well, and overlaps with two small peaks between 500 nm and 600 nm.
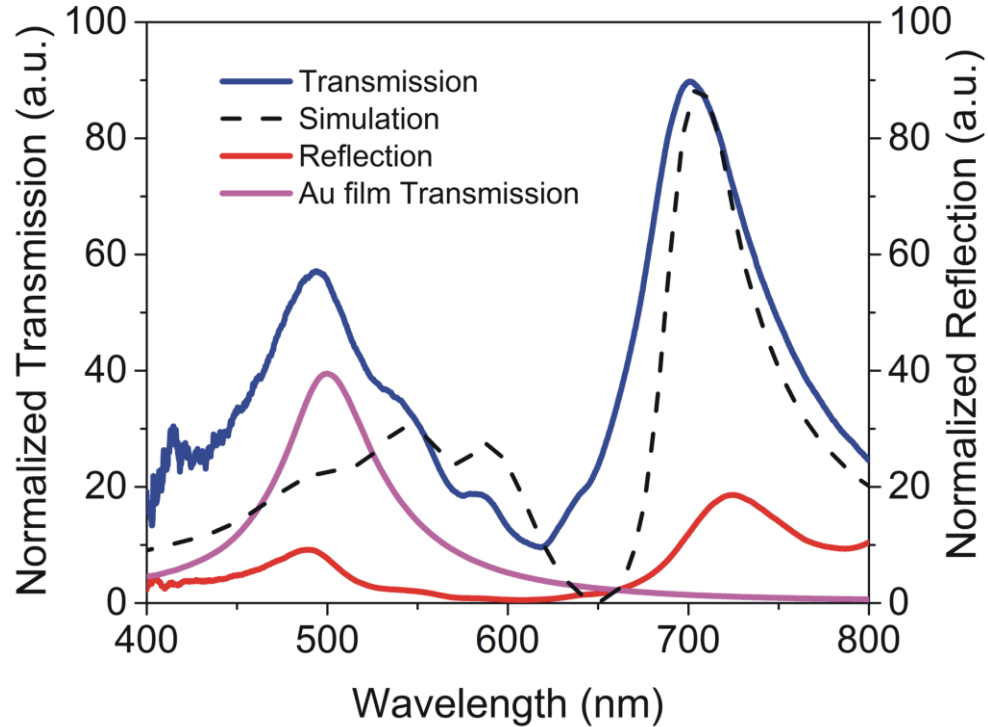
Figure 5-7 Normalized Au nanohole array spectra for transmission and its simulation as well as reflection, and the Au film transmission spectrum.

A near-field profile is required to understand the physics associated with the spectral features of the plasmonic nanostructure in detail. The simulated electric field distributions shown in Figure 5-8 are extracted at peak wavelengths of 494 nm, 538 nm, 585 nm and 698 nm in x-z plane and at epoxy/Au interface. The strong intensity at the center of hole (Figure 5-8a and e) confirms the nature of direct transmission around 500 nm. The pattern of field distribution from Figure 5-8b indicates that the peak at 538 nm is mediated by a coupling oscillation between air/Au and epoxy/Au interface. The extension of electric field beyond the edge of hole at epoxy/Au interface (Figure 5-8f) further implies an out-of-plane character of the oscillation. In contrast, in-plane oscillations at 585 nm (Figure 5-8c) and

698 nm (Figure 5-8d) indicate the localized surface plasmon excitations. The field profile for 585 nm given in Figure 5-8g displays a hexapole feature along the edge of the nanohole; whereas the dipole mode oscillation (Figure 5-8h) leads to strong coupling of the incident light near 700 nm, which effectively traps the light and results in an enhanced transmission.
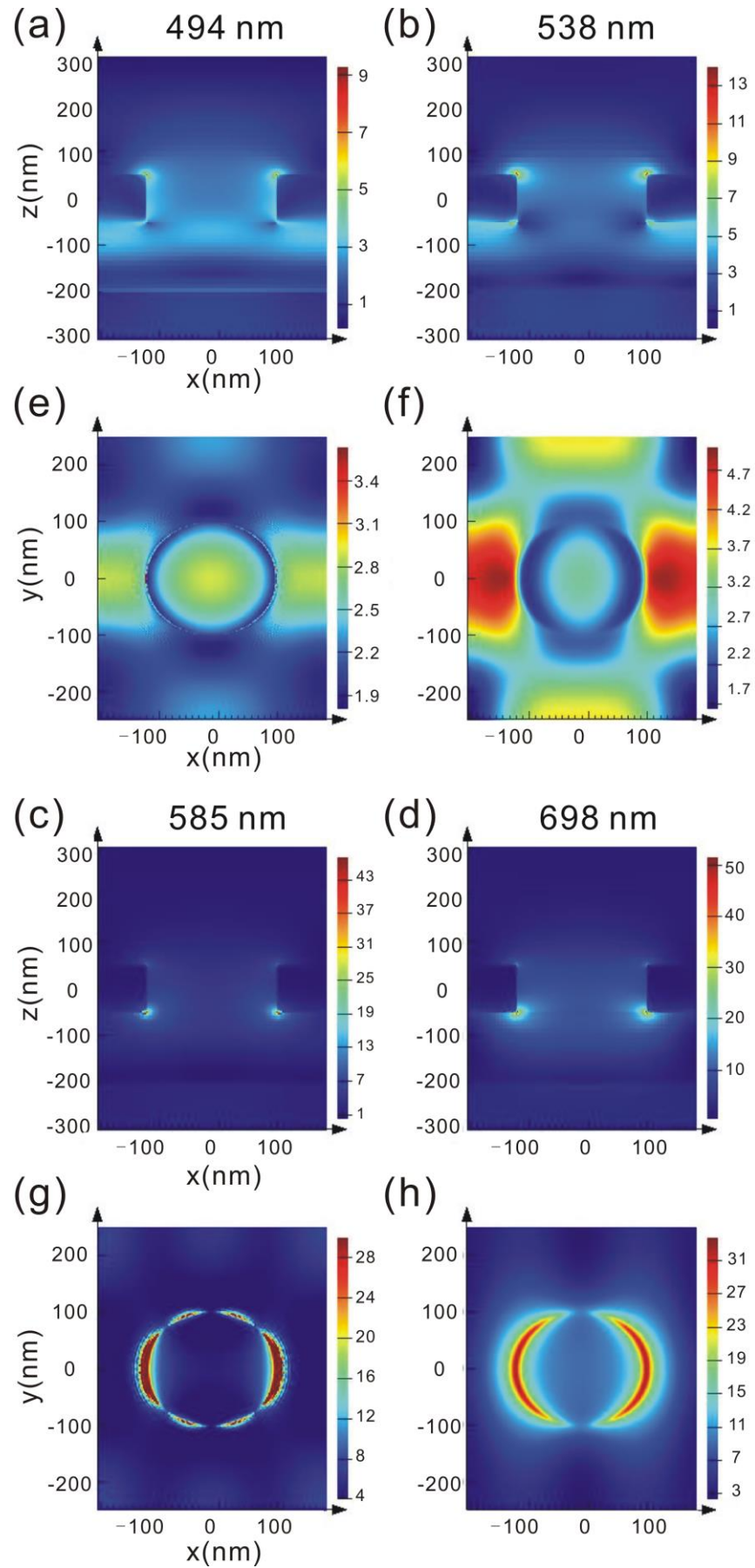
Figure 5-8 Electric field profiles at peak wavelengths of 494 nm, 538 nm, 585 nm and 698 nm in x-z plane (a,b,c,d, respectively) and at epoxy/Au interface (e,f,g,h, respectively).

5.2.3 Optical Performance

The plasmonic fiber is characterized as a refractive index probe using different concentrations of NaCl solutions through a fluidic channel. When the fiber tip is exposed to the solutions, narrow peaks and troughs are simultaneously recorded over reflection (Figure 5-9a) and transmission (Figure 5-10a) spectra between 820 nm and 920 nm. All the maxima and minima proportionally shift to longer wavelengths as the refractive index n increases. The refractive index sensitivities (Figure 5-9b and Figure 5-10b) are obtained by linearly fitting three peak shifts in reflection, as well as two peak shifts and two trough shifts in transmission. The highest sensitivities for transmission and reflection are 595 nm/RIU (refractive index unit) and 497 nm/RIU, respectively. The overall performance of a SPR sensor is dominated by both the sensitivity of the resonance and its spectral linewidth.[21] The full width at half maximum (FWHM) of the resonance with 401 nm/RIU sensitivity in reflection is narrowed down to 6.6 nm in 20% NaCl solution, comparable to the recorded narrowest resonance linewidth of 4.29 nm.[22] Accordingly, figure of merit (FOM), defined as the refractive index sensitivity divided by the corresponding FWHM,[21] achieves 60.7 which is four times higher than the previously reported value for Au nanohole arrays on planar substrates.[23]

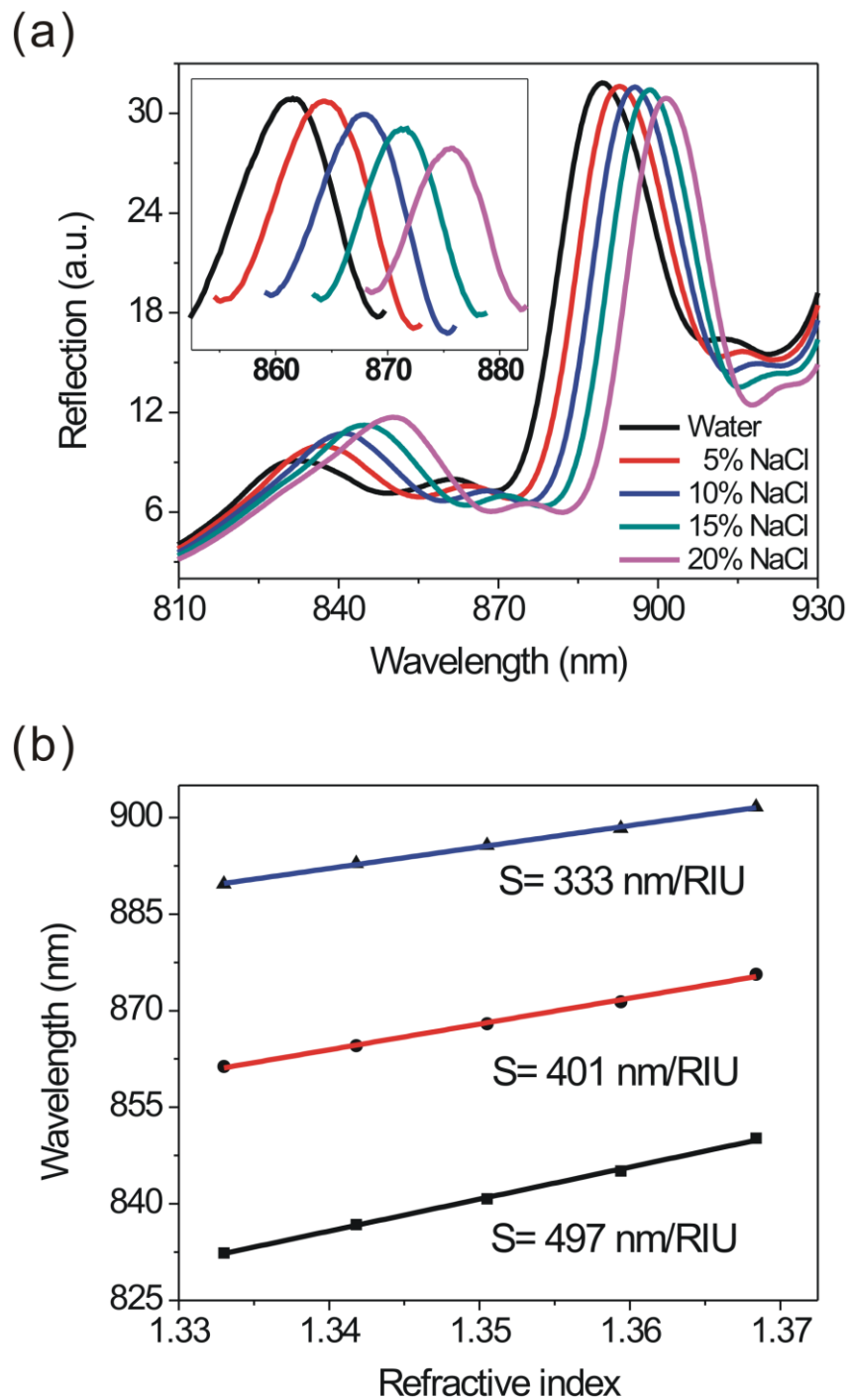**Figure 5-9 Reflection spectra (a) measured in water and NaCl solutions. The inset in (a) is a magnified view of the narrowest resonances in reflection. Refractive index sensitivities (b) obtained by linear fitting three peak shifts in (a).**
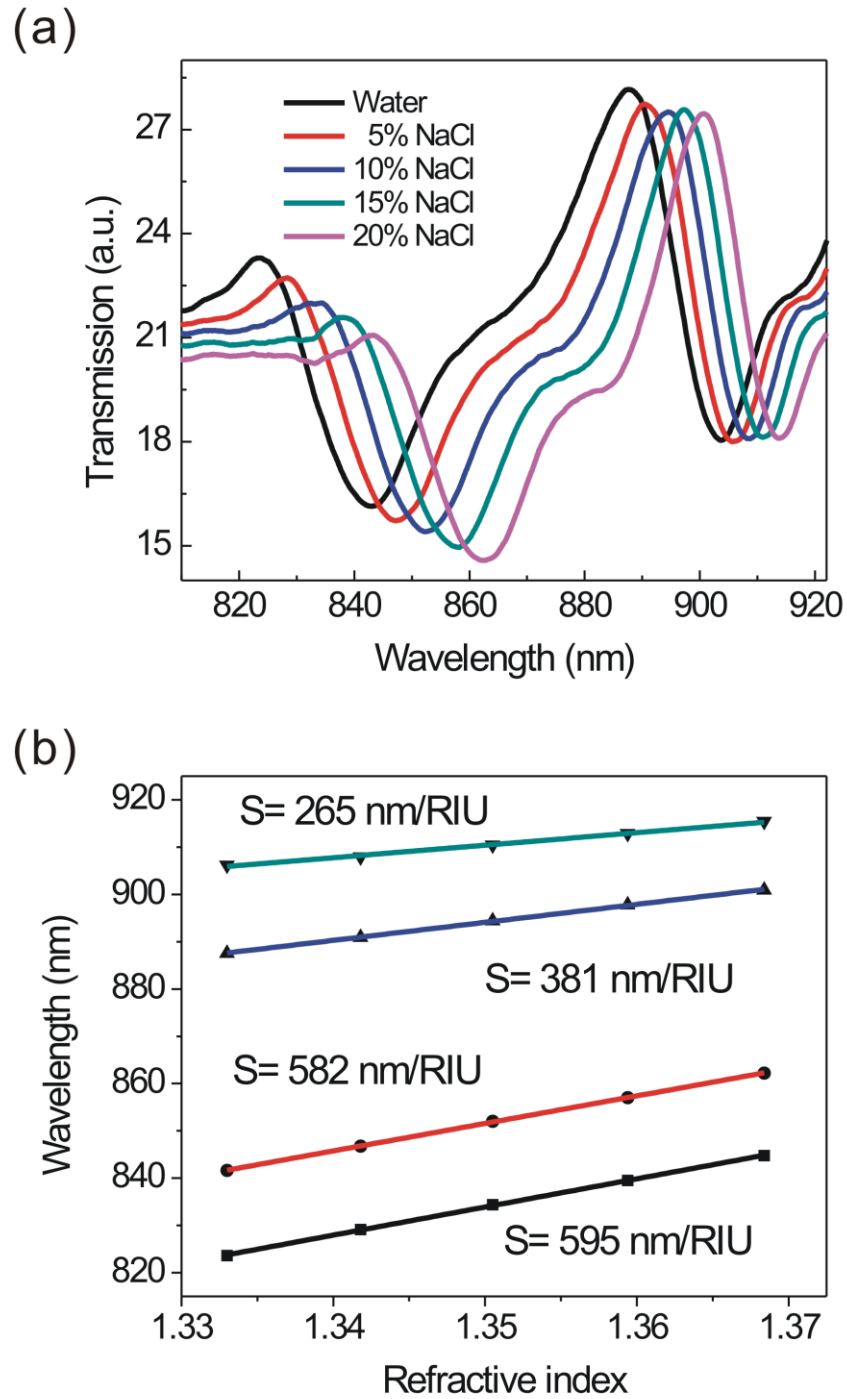
Figure 5-10 Transmission spectra (a) measured in water and NaCl solutions and refractive index sensitivities (b) obtained by linear fitting two peak shifts and two trough shifts in (a).

5.2.4 Self-Assembled Monolayer (SAM)

To examine the fiber sensor's response to molecular adsorption on its endface, a self-assembled monolayer (SAM) is formed by immersing the fresh fabricated fiber tip into an alkyl thiol (480.18 g/mol) solution. Due to the increase of the external refractive index, n, the 500 nm peak has a slight blue-shift in comparison with the original spectrum, as shown in Figure 5-11. This shift presumably results from the adsorption of SAM molecules and morphology change on the Au thin film.[24] In contrast, the peak at 700 nm shifts 10 nm to longer wavelengths and exhibits characteristic of SPP–Bloch waves (BW).[25-26] Additional small peaks present between 500 nm and 700 nm are related to high order resonance modes. Since the light illuminates the array in all possible directions confined by the core diameter and numerical aperture of the fiber, the resonant modes become more complex than those obtained only at normal incidence.
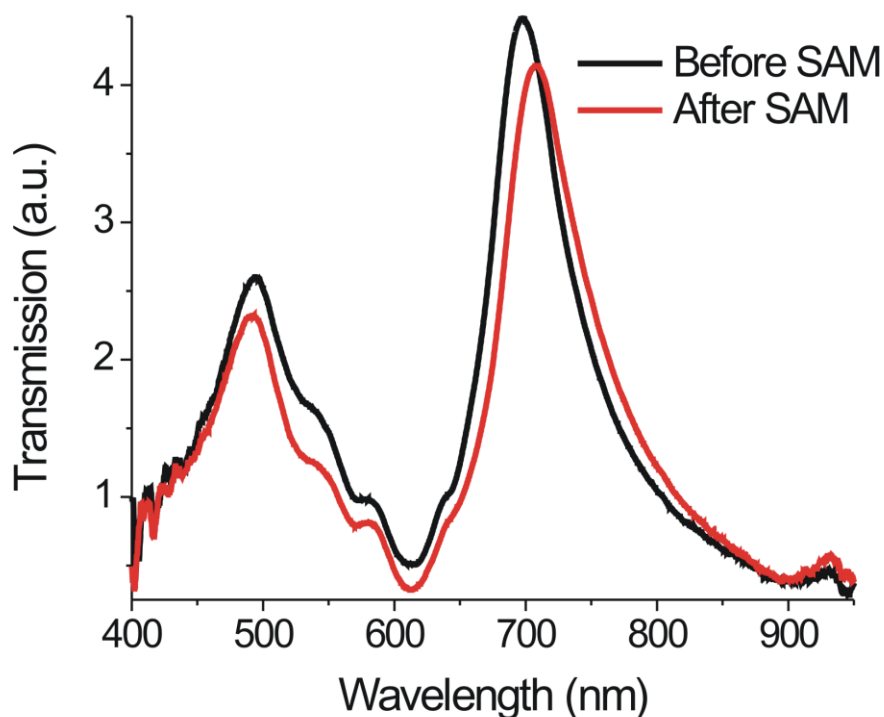
Figure 5-11 Optical transmission spectra of nanohole array fibers for SAM assembly.

5.2.5 Real-Time Biosensing

To demonstrate the feasibility of our plasmonic fiber for label-free and real-time biosensing, we further perform the immunoassay between BSA and anti-BSA, which has been extensively investigated.[27-29] Peak shifts (Figure 5-12) are used to monitor their specific binding on the surface by the plasmonic fiber platform. We directly pick up the wavelength of the transmission maximum around 830 nm in each spectrum as the peak wavelength rather than use any algorithm to track it. The PBS buffer is first injected into the flow cell to define the baseline of peak wavelength. As the surface of freshly transferred SPR sensor is extremely clean, the signal is immediately steady. A 50 μg/ml BSA solution in PBS

buffer then flows over the Au surface on the fiber tip. A peak shift $\Delta\lambda$ of 0.73 nm is observed upon BSA monolayer assembly. A subsequent PBS wash has little effect on the fiber response, which implies the robustness of BSA monolayer. Then, a 4.3 µg/ml anti-BSA solution is pumped into the flow cell. After washing out the unbound anti-BSA molecules by PBS rinse, the binding of anti-BSA to BSA on the surface finally results in a 0.53 nm peak shift.

We can obtain the effective BSA layer thickness d using a well-established quantitative formula,[27]

$$\Delta\lambda = S(n_1 - n_2)\left(1 - e^{-\frac{2d}{l}}\right) \tag{5-1}$$

where S is the bulk refractive index sensitivity of 595nm/RIU obtained in the optical performance experiment, n_1 and n_2 are the respective refractive index of protein layer and buffer solution, and l is the SP field penetration depth in buffer solution. Given the refractive index of BSA is 1.57,[27] the recorded 0.73 nm peak shift corresponds to an effective thickness of 0.95 nm. Using the volume density of BSA (1.3 g/cm^3),[27] the surface density of this saturated protein monolayer is calculated to be 1.24×10^{-7} g/cm^2. It is noted that BSA adsorptions on Au and some polymers with the most adsorptive surfaces show very similar saturation density ($(1.2\text{-}1.8) \times 10^{-7}$ g/cm^2).[28-29]
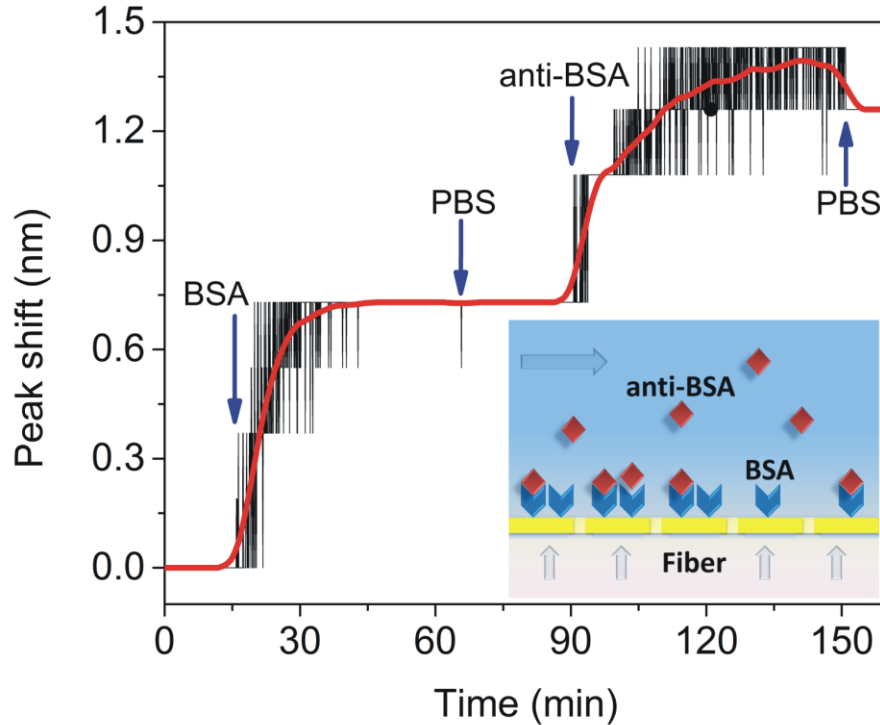
Figure 5-12 Real-time peak shifts upon BSA assembly on the plasmonic fiber tip and subsequent binding between BSA and anti-BSA. The red line is a fitted curve for better visualization.

Peak fluctuation of raw data results from the relative low resolution (~ 0.2 nm) of our spectrometer, which is unable to differentiate subtle change of binding status by direct peak pick-up. However, we indeed capture the real-time kinetic features during biomolecular binding in detail. Using complex algorithms can improve the resolution at the expense of considerable computation; in contrast, this simple peak pick-up method requires minimum calculation for such massive spectra data. This advantage would facilitate the on-chip real-time spectroscopy analysis by using our plasmonic fiber integrated with portable spectrometer.

5.2.6 Stability, Consistency and Optimization

The minimum bend radius is of critical importance to handle the fiber-optic based system. The intensity spectra of our plasmonic fiber demonstrate excellent stability in fiber bending test (Figure 5-13). The bending inspection begins with the long-term bend radius (24 cm) of the original fiber (multimode, 600 μm core diameter). The resonance wavelength is determined by a previous peak position tracking algorithms.[16] As bend radius of the fiber is gradually changed from 24 cm to 15 cm, the drifts (no more than 0.15 nm) of the resonance wavelength are negligible, considering that the resolution of our spectrometer is ~0.2 nm. The large shift about 0.5 nm occurs until bend radius approaches the short-term bend radius (12 cm) of the original fiber. This test proves that our plasmonic fiber has the same bend radius as that of original fiber. Such flexibility allows our plasmonic fiber to easily conform to various external environments in real world application.
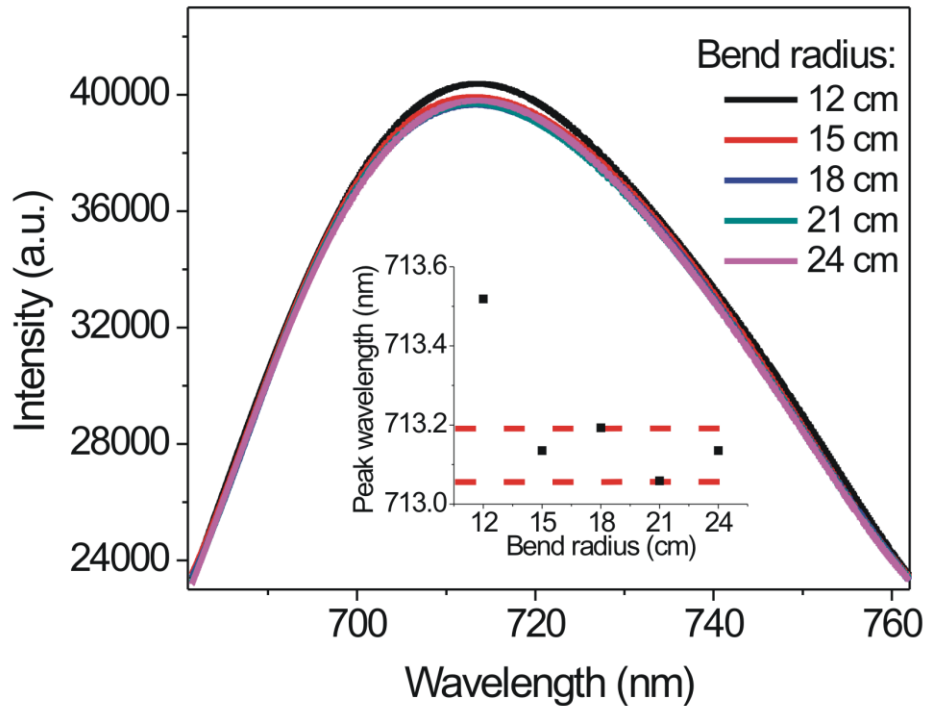
Figure 5-13 Intensity spectra of a plasmonic fiber for various bending radii from 24 cm to 12 cm. The inset shows the fluctuation of the resonance wavelengths.

The plasmonic fibers with metal structures replicated from one same template have almost same spectral features due to high quality replication. Figure 5-14 shows the transmission spectra of two nanohole array integrated optical fibers with various core diameters (400 μm and 600 μm) in air. The tiny peak position variation (less than 0.5 nm) for different diameter fibers verifies the excellent consistency of optical response of our nanoplasmonic fibers.
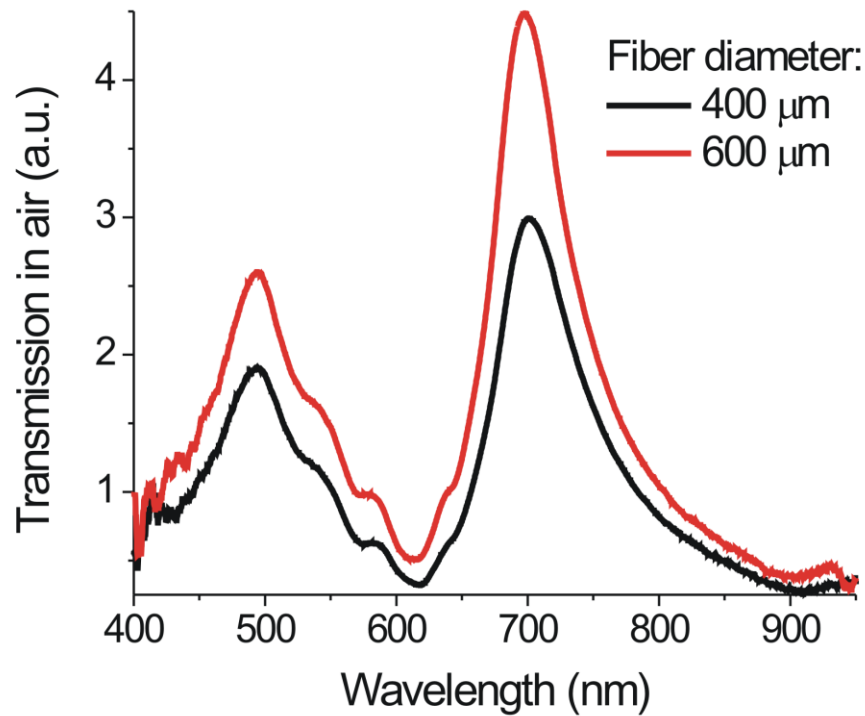
Figure 5-14 Optical transmission spectra of nanohole array fibers with various core diameters in air.

We also preliminarily implement spectrum filtering by connecting multiple plasmonic fibers end-to-end. Their linkage thus allows for filtering the small spectral features and narrowing the linewidth of the transmission peaks. The normalized results of spectrum filtering are demonstrated in Figure 5-15 for comparison. When two same fibers are linked, the small peaks between 500 nm to 600 nm almost vanish due to filtering. By coupling triple fibers, the FWHM of the resonance peak around 700 nm is substantially narrowed down to 58.2 nm, almost half of that for single fiber (~100 nm). These effects further optimize the spectral character and potentially improve the optical performance (e.g. Q factor) of our plasmonic fibers.
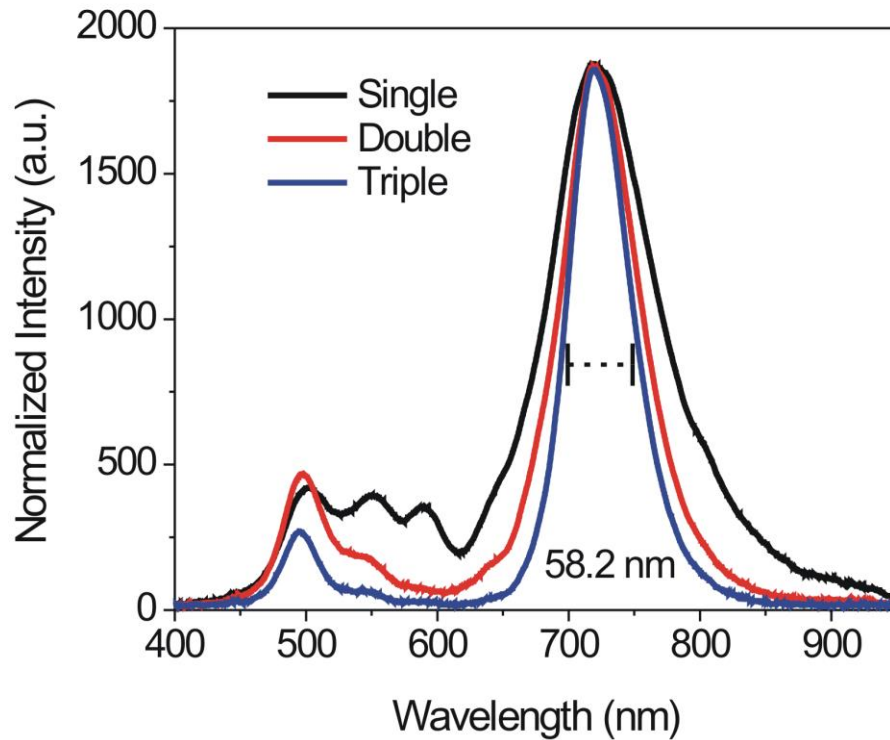
Figure 5-15 Normalized spectra for single, double and triple plasmonic fibers connected end-to-end. The resonance around 700 nm is narrowed down to 58.2 nm in triple coupling.

5.3 Materials and Methods

5.3.1 Metal Deposition and Transfer

A custom electron-beam evaporator was used to deposit 100 nm thick Au onto the Si template without adhesion layer. The deposition rate of 1 Å/s was maintained at ~5 ×10^{-6} Pa. 1 μL thermal-curing optical epoxy (301, Epoxy Technology Inc.) was applied on one endface of the optical fiber and pre-heated for 10 min under a halogen lamp to be sticky. After attaching the template to the fiber facet, the Au on the reliefs of the template firmly

adhered to the fiber tip via 2 h heating. The Au nanostructures were then transferred by detaching the template from the fiber endface. After cleaning with Au etchant followed by chlorinated solvents, the template can be reused for a new cycle of transfer without damage.

5.3.2 Fabrication of Flow Cell

The fluidic flow cell was fabricated by casting polydimethylsiloxane (PDMS) to surround a round steel rod with the same diameter as that of the fiber tip. The steel rod was first layed in a petri dish with two ends supported. The PDMS was then cast and cured at 70 ℃ overnight. After pulling the rod out of the PDMS channel, the flow cell was cut to proper length to accommodate the fiber tips.

5.3.3 Bulk Refractive Index Sensing

Refractive index solutions were made by adding NaCl into the deionized water to obtain various concentrations (5%, 10%, 15% and 20%) with n (1.3418, 1.3505, 1.3594, and 1.3684, respectively). Different index solutions were injected through the flow cell sequentially using a syringe pump. Reflection and transmission spectra were simultaneously recorded by averaging 100 acquisitions with two portable spectrometers (USB4000, Ocean Optics Inc.) respectively.

5.3.4 Biomelecular Sensing

BSA, anti-BSA and PBS buffer were purchased from Sigma-Aldrich. Solutions (PBS, BSA, PBS, anti-BSA and PBS) were sequentially injected into the flow cell using a syringe pump at a flow rate of 30 μL/min. The circulation times are 15 min, 50 min, 25 min, 60 min and

15 min, respectively. Each spectrum is recoded with a temporal resolution of 2 s (10 ms integration time and 200 frame averaging).

5.3.5 FDTD Simulations

FDTD simulations were done using a commercial software, FDTD solutions (Lumerical Solutions Inc.). The simulation contained a single nanohole with periodic boundaries within the plane of the Au film and perfectly matched layers in the boundaries parallel to the Au film. Three same linearly polarized light were configured along each main translation direction of the hexagonal array to simulate the unpolarized light tranmitted by the optical fiber. The refractive indices of the epoxy adhesive was set to be 1.52.

5.4   Conclusions

In conclusion, we have implemented plasmonic optical fibers patterned with general metal nanostructures on the endfaces by a simple and effective transfer method. Surface topography of metal structures can be controlled by adjusting the viscosity of adhesive layers. The specially designed multimode plasmonic fiber can work in transmission and reflection at the same time in refractive index sensing. The resonance of the fiber features spectrally narrow linewidth of 6.6 nm and high figure of merit of 60.7. For the first time, we introduce the real-time biosensing using the plasmonic optical fiber as a practical application. In addition, the spectra of our fibers possess great stability to resist mechanical bending. The linked plasmonic fibers show great potential for the improvement of optical performance and the realization of optical multiple-filter. All these advantages present our

plasmonic optical fiber as a versatile platform in the wide field of biosensing and nanoplasmonics.

Reference

1.   Ebbesen, T. W.; Lezec, H. J.; Ghaemi, H. F.; Thio, T.; Wolff, P. A., Extraordinary optical transmission through sub-wavelength hole arrays. *Nature* **1998,** *391* (6668), 667-669.

2.   Stewart, M. E.; Anderton, C. R.; Thompson, L. B.; Maria, J.; Gray, S. K.; Rogers, J. A.; Nuzzo, R. G., Nanostructured plasmonic sensors. *Chemical Reviews* **2008,** *108* (2), 494-521.

3.   Xu, T.; Shi, H.; Wu, Y. K.; Kaplan, A. F.; Ok, J. G.; Guo, L. J., Structural colors: from plasmonic to carbon nanostructures. *Small* **2011,** *7* (22), 3128-3136.

4.   Walt, D. R., Miniature analytical methods for medical diagnostics. *Science* **2005,** *308* (5719), 217-219.

5.   Feng, S.; Darmawi, S.; Henning, T.; Klar, P. J.; Zhang, X., A miniaturized sensor consisting of concentric metallic nanorings on the end facet of an optical fiber. *Small* **2012,** *8* (12), 1937-1944.

6.   Lin, Y.; Zou, Y.; Lindquist, R. G., A reflection-based localized surface plasmon resonance fiber-optic probe for biochemical sensing. *Biomed. Opt. Express* **2011,** *2* (3), 478-484.

7.   Consales, M.; Ricciardi, A.; Crescitelli, A.; Esposito, E.; Cutolo, A.; Cusano, A., Lab-on-fiber technology: toward multifunctional optical nanoprobes. *ACS Nano* **2012,** *6* (4), 3163-3170.

8.   Dhawan, A.; Muth, J. F., Engineering surface plasmon based fiber-optic sensors. *Materials Science and Engineering: B* **2008,** *149* (3), 237-241.

9.   Dhawan, A.; Muth, J.; Leonard, D.; Gerhold, M.; Gleeson, J.; Vo-Dinh, T.; Russell, P., Focused ion beam fabrication of metallic nanostructures on end faces of optical fibers

for chemical sensing applications. *Journal of Vacuum Science & Technology B* **2008,** *26* (6), 2168-2173.

10.   Fu, Y.; Bryan, N. K. A., Investigation of physical properties of quartz after focused ion beam bombardment. *Applied Physics B* **2005,** *80* (4-5), 581-585.

11.   Kostovski, G.; White, D.; Mitchell, A.; Austin, M.; Stoddart, P., Nanoimprinted optical fibres: Biotemplated nanostructures for SERS sensing. *Biosensors and Bioelectronics* **2009,** *24* (5), 1531-1535.

12.   Kostovski, G.; Chinnasamy, U.; Jayawardhana, S.; Stoddart, P. R.; Mitchell, A., Sub‑15nm Optical Fiber Nanoimprint Lithography: A Parallel, Self‑aligned and Portable Approach. *Advanced Materials* **2011,** *23* (4), 531-535.

13.   Smythe, E. J.; Dickey, M. D.; Whitesides, G. M.; Capasso, F., A technique to transfer metallic nanoscale patterns to small and non-planar surfaces. *ACS Nano* **2008,** *3* (1), 59-65.

14.   Smythe, E. J.; Dickey, M. D.; Bao, J.; Whitesides, G. M.; Capasso, F., Optical antenna arrays on a fiber facet for in situ surface-enhanced Raman scattering detection. *Nano Letters* **2009,** *9* (3), 1132-1138.

15.   Lipomi, D. J.; Martinez, R. V.; Kats, M. A.; Kang, S. H.; Kim, P.; Aizenberg, J.; Capasso, F.; Whitesides, G. M., Patterning the tips of optical fibers with metallic nanostructures using nanoskiving. *Nano Letters* **2010,** *11* (2), 632-636.

16.   Jia, P.; Jiang, H.; Sabarinathan, J.; Yang, J., Plasmonic nanohole array sensors fabricated by template transfer with improved optical performance. *Nanotechnology* **2013,** *24* (19), 195501.

17.   Jia, P.; Yang, J., Integration of large-area metallic nanohole arrays with multimode optical fibers for surface plasmon resonance sensing. *Applied Physics Letters* **2013,** *102* (24), 243107-243107-3.

18.   Nagpal, P.; Lindquist, N. C.; Oh, S.-H.; Norris, D. J., Ultrasmooth Patterned Metals for Plasmonics and Metamaterials. *Science* **2009,** *325* (5940), 594-597.

19.   Lee, S. H.; Johnson, T. W.; Lindquist, N. C.; Im, H.; Norris, D. J.; Oh, S. H., Linewidth-Optimized Extraordinary Optical Transmission in Water with Template-Stripped Metallic Nanohole Arrays. *Advanced Functional Materials* **2012,** *22* (21), 4439-4446.

20.   McMahon, J. M.; Henzie, J.; Odom, T. W.; Schatz, G. C.; Gray, S. K., Tailoring the sensing capabilities of nanohole arrays in gold films with Rayleigh anomaly-surface plasmon polaritons. *Optics express* **2007,** *15* (26), 18119-18129.

21.   Sherry, L. J.; Chang, S.-H.; Schatz, G. C.; Van Duyne, R. P.; Wiley, B. J.; Xia, Y., Localized surface plasmon resonance spectroscopy of single silver nanocubes. *Nano Letters* **2005,** *5* (10), 2034-2038.

22.   Yanik, A. A.; Cetin, A. E.; Huang, M.; Artar, A.; Mousavi, S. H.; Khanikaev, A.; Connor, J. H.; Shvets, G.; Altug, H., Seeing protein monolayers with naked eye through plasmonic Fano resonances. *Proceedings of the National Academy of Sciences* **2011,** *108* (29), 11784-11789.

23.   Henzie, J.; Lee, M. H.; Odom, T. W., Multiscale patterning of plasmonic metamaterials. *Nature nanotechnology* **2007,** *2* (9), 549-554.

24.   Khriachtchev, L.; Heikkilä, L.; Kuusela, T., Red photoluminescence of gold island films. *Applied Physics Letters* **2001,** *78* (14), 1994-1996.

25.   Chang, S.-H.; Gray, S.; Schatz, G., Surface plasmon generation and light transmission by isolated nanoholes and arrays of nanoholes in thin metal films. *Optics express* **2005,** *13* (8), 3150-3165.

26.   Thio, T.; Ghaemi, H.; Lezec, H.; Wolff, P.; Ebbesen, T., Surface-plasmon-enhanced transmission through hole arrays in Cr films. *JOSA B* **1999,** *16* (10), 1743-1748.

27.   Jung, L. S.; Campbell, C. T.; Chinowsky, T. M.; Mar, M. N.; Yee, S. S., Quantitative interpretation of the response of surface plasmon resonance sensors to adsorbed films. *Langmuir* **1998,** *14* (19), 5636-5648.

28.   Silin, V.; Weetall, H.; Vanderah, D. J., SPR studies of the nonspecific adsorption kinetics of human IgG and BSA on gold surfaces modified by self-assembled monolayers (SAMs). *Journal of colloid and interface science* **1997,** *185* (1), 94-103.

29.   Gölander, C.-G.; Kiss, E., Protein adsorption on functionalized and ESCA-characterized polymer films studied by ellipsometry. *Journal of colloid and interface science* **1988,** *121* (1), 240-253.

Chapter 6

6 Freestanding Metal Nanomembrane as Plasmonic Sensor

In this chapter, large-area freestanding metal nanomembranes with periodic nanohole arrays are implemented using a novel fabrication approach. This technique is also capable of fabrication of freestanding nanoslits. The freestanding metal nanomembranes are characterized by SEM to demonstrate high quality and uniformity. The transmission of the freestanding nanomembrane show higher efficiency compared to that of nanohole arrays with same features on the substrate.

6.1 Introduction

Freestanding nanomembranes have been a theoretical and experimental interest for several decades since they combine nanoscale thickness and features with macroscopic lateral dimensions at the same time.[1] Several cutting-edge freestanding ultrathin membranes made by inorganic matter (*i.e.* silicon[2-3], metals[4], nanoparticles[5], graphene[6-7], PDMS[8]), organic materials (*i.e.* epoxy resin[9]) and hybrid composite[10-12] have been implemented. These freestanding membranes are emerging as critical elements in various sensing devices, such as mechanical, chemical and thermal sensors. In the scope of plasmonic sensing, freestanding metal membranes as miniature passive plasmonic sensors are highly desirable in that they can be attached to unconventional substrates incompatible to conventional fabrication methods. To date, several technique have been achieved for the fabrication of

freestanding nanoscale membranes, including spin-coating[13], layer-by-layer assembly[14-18], and monolayer self-assembled[19-20]. However, these approaches are not applicable to metal. The synthesis of large-area freestanding metal nanomembranes with submicron features is still a challenge and remains to be explored.

6.2 Fabrication of Freestanding Metal Nanostructures

6.2.1 Preparation for Fabrication

Based on the template transfer method, we develop a new process that is capable of fabrication of large-area freestanding metal nanostructures. In the previous method, once metal structures are transferred to the target substrate, they would permanently stay on the cured adhesive layer of insoluble epoxy. Thus a soluble adhesive is in demand for releasing the transferred metal nanostructures. Accordingly, instead of epoxy, we choose polyvinylpyrrolidone (PVP) which is a water-soluble polymer and has good adhesion to various metals. On the other hand, the PVP adhesive has to be thick enough to avoid flowing into the nanoholes.

On the other hand, a special holder is required to support the margin of released metal membranes in order to make them freestanding. First, the holder should consist of a flexible support (to make conformal contact with metal membranes) and a hard base (to avoid the deformation of the entire frame during handling). Meanwhile, the surface of the support which contacts with the membrane has to be smooth; otherwise, even small roughness would result in wrinkles, which could extend from the interface to the freestanding part for such thin membrane. In addition, the inner edge of the support has to be round to form

smooth line of contact to avoid localized strain. Based on these considerations, PDMS and flat glass-bottom petri dish are good choices for the support and hold respectively. A precisely machined round steel cylinder with diameter of 5 mm is first positioned perpendicularly on the glass at the bottom of petri dish. Thereafter PDMS is cast into the petri dish and cured at 75 °C for 2 hour. After levering the glass from the bottom and pulling the steel rod out of PDMS, we obtain a membrane holder with a throughout hole in PDMS on the bottom of petri dish.

6.2.2 Fabrication Procedure

Figure 6-1 summarizes the procedure for fabrication of freestanding metal nanomembranes. The Si template with the pattern of nanohole array is first deposited with 100 nm Au using e-beam deposition to form metal nanomembrane. Then PVP water solution (40% m/m) is dropped on the top of the template with Au nanostructures. After evaporation of water, the dried adhesive along with the Au membrane is levered from the template using a razor. Thereafter the Au membrane is attached to the PDMS in the holder to completely cover the throughout hole. The holder is then placed above a beaker to keep the PVA adhesive in contact with water. After PVA is gradually dissolved again, the holder with the metal nanomembrane is carefully pulled out of water. The metal nanomembrane above the hole on the holder becomes freestanding after water evaporation as shown in Figure 6-2. The diameter of the round membrane is 5 mm. Besides membranes, freestanding nanoslits are also implemented by the same approach using the template with nanoslit relief on the surface.
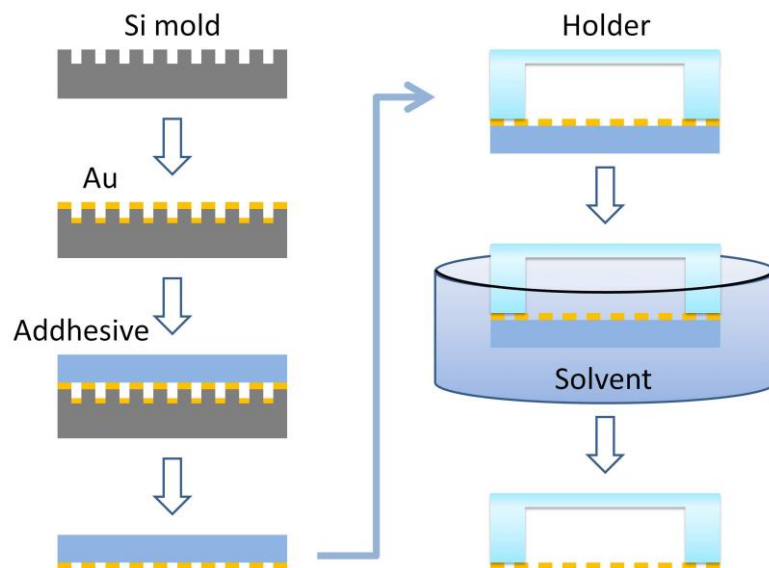
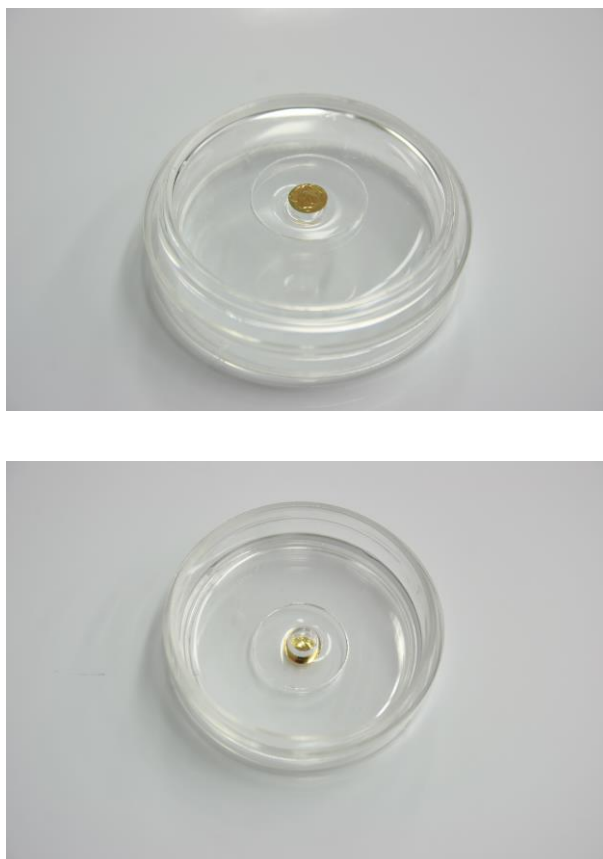**Figure 6-1 Fabrication procedure for freestanding metal nanomembranes.**

Figure 6-2 Freestanding Au nanomembrane on the PDMS holder in a petri dish.

Any material in sufficiently thin form becomes flexible whereby the membrane can conformably contact to uneven surfaces. Meanwhile, van der Waals force is strong enough to maintain the attachment of such thin metal nanomembranes on substrates. To demonstrate the freestanding metal membranes are transferrable, we lay them onto different substrates. The Figure 6-3 shows a metal membrane attached on the inner wall of a glass bottle without using any adhesive, which is impossible to be implemented by means of any conventional methods.

Figure 6-3 Au nanohole membrane attached on the inner wall of a glass bottle.

6.3 Characterization

To make sure the transferred metal nanostructures is intact and as same as that on the template, we characterize them with SEM. Figure 6-4 demonstrates a freestanding Au

nanomembrane of a hexagonal nanohole array with periodicity of 700 nm and diameter of 200 nm. The freestanding membrane has smooth surface and same well-ordered pattern as that of the template. To know about the in-hole morphology, we cut off a piece from the membrane using FIB milling. Figure 6-5 displays the cross-section of the nanomembrane, on which the throughout holes are opening on both surfaces of the membrane.
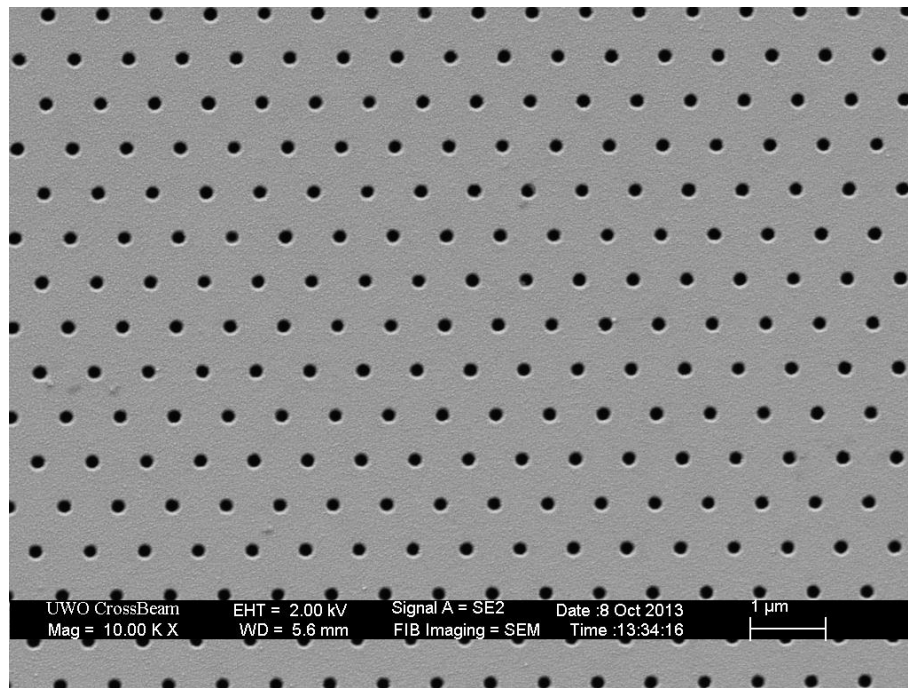

Figure 6-4 Freestanding Au membrane with a hexagonal nanohole array with periodicity of 700 nm and diameter of 200 nm.
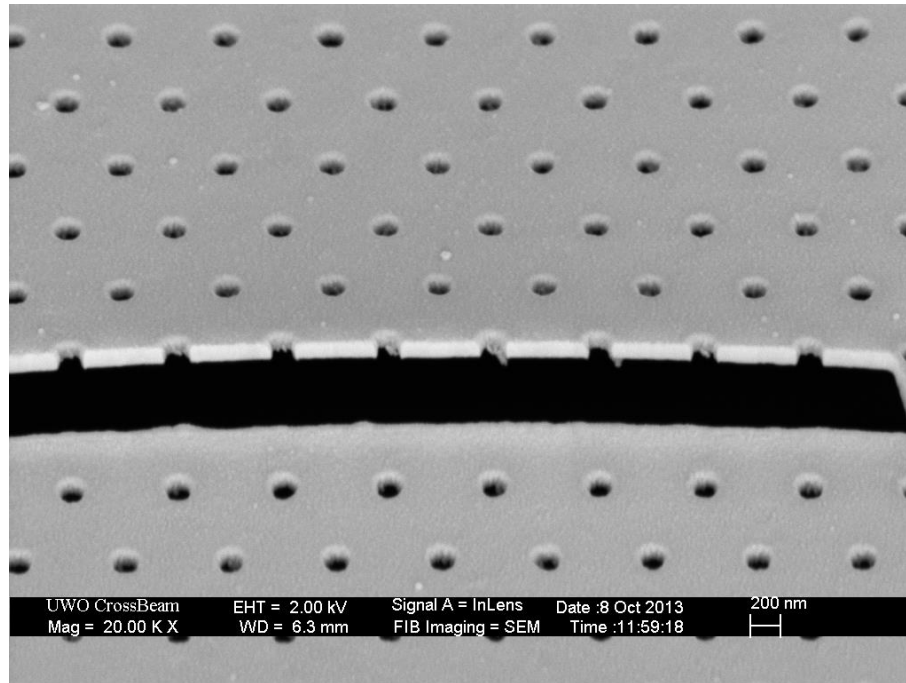
Figure 6-5 A cross-section of freestanding Au nanomembrane cut by FIB milling.

When we cut out a narrow and long slit intersecting with 32 holes along one of the main translation axes, the edge of the long slit immediately bends up. It is noticed that the width of slit surprisingly becomes bigger and bigger after many times of electron imaging. We believe these interesting phenomena in such small dimension are worth further investigation on mechanical and electrical properties of these large-area freestanding metal nanomembranes.
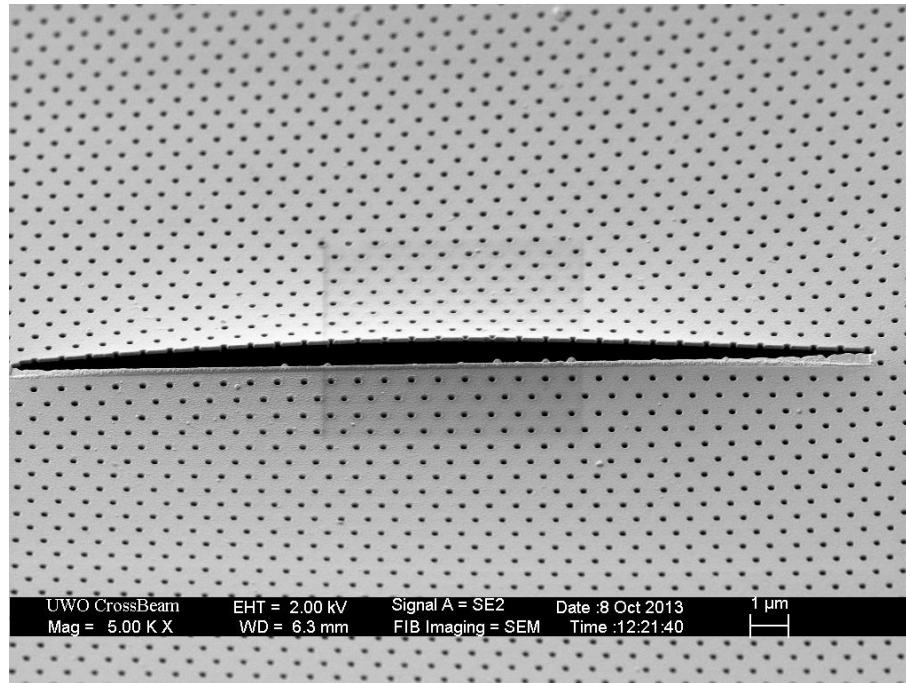
Figure 6-6 A narrow and long slit cut by FIB milling. The edge is bent owing to strain release. After repeatedly imaging with SEM, the slit becomes wider than that at the beginning.
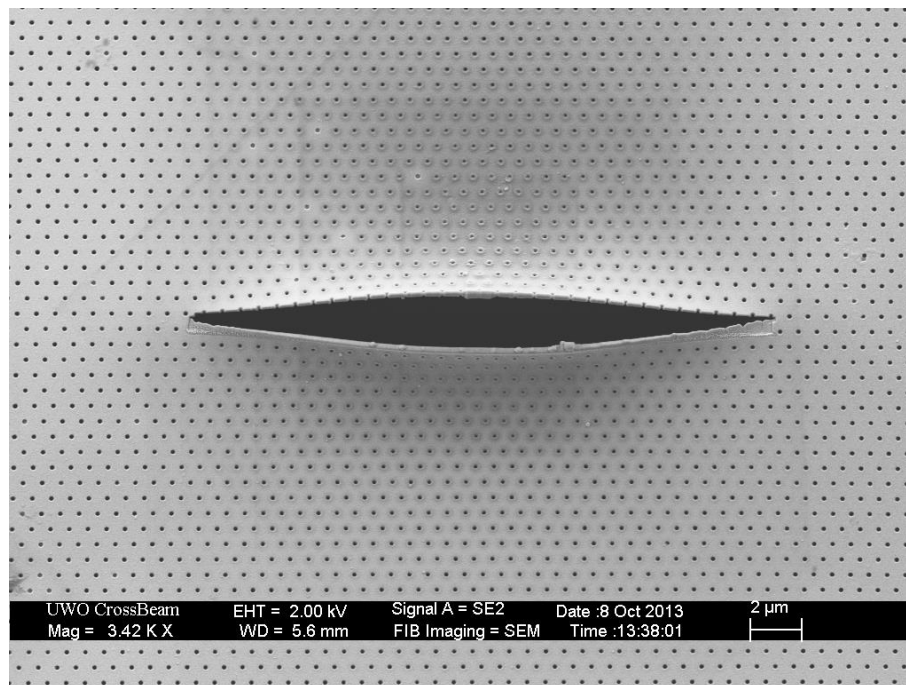
SEM images of freestanding nanoslits are shown in Figure 6-7, in which most slits stick together and separation appears due to unbalanced stresses on either side of some slits.

Figure 6-7 Freestanding nanoslits. The width of the silts is 400 nm.

Besides SEM imaging, we also use atomic force microscopy (AFM) to characterize the roughness of the Au freestanding nanomembrane. All AFM experiments were performed on a Dimension V AFM equipped with Nanoscope controller V (Veeco, Inc.). We obtain AFM images (Figure 6-8) at different regions of the membrane to make sure it is intact and smooth.
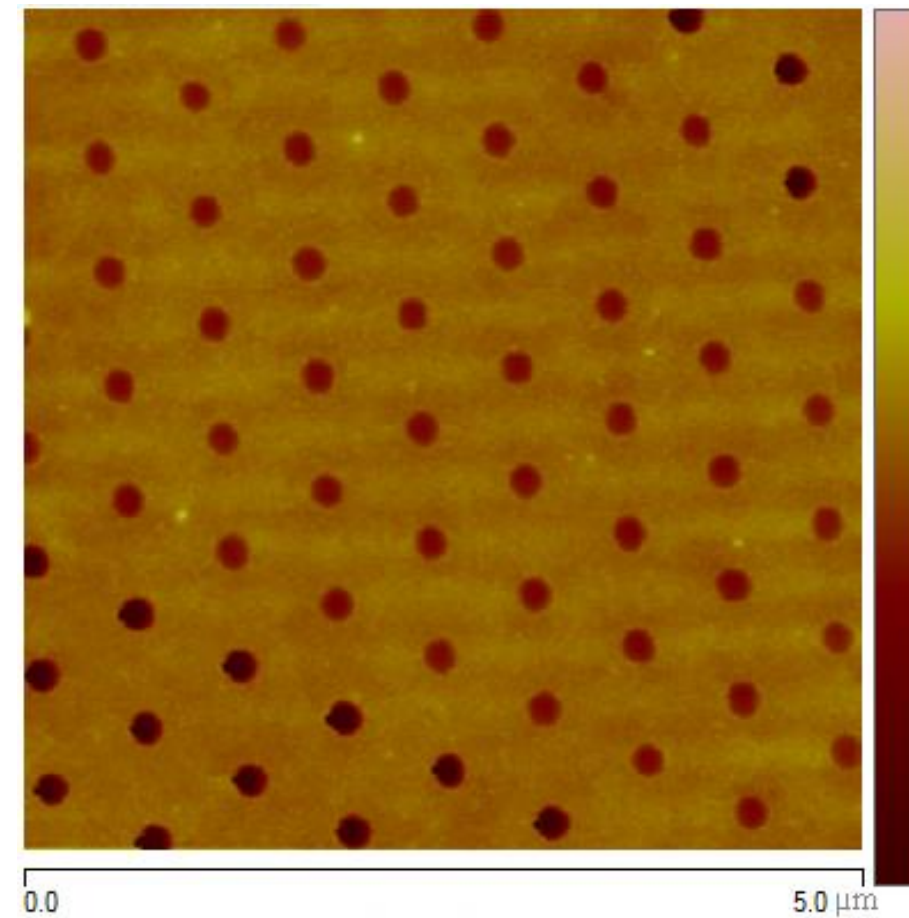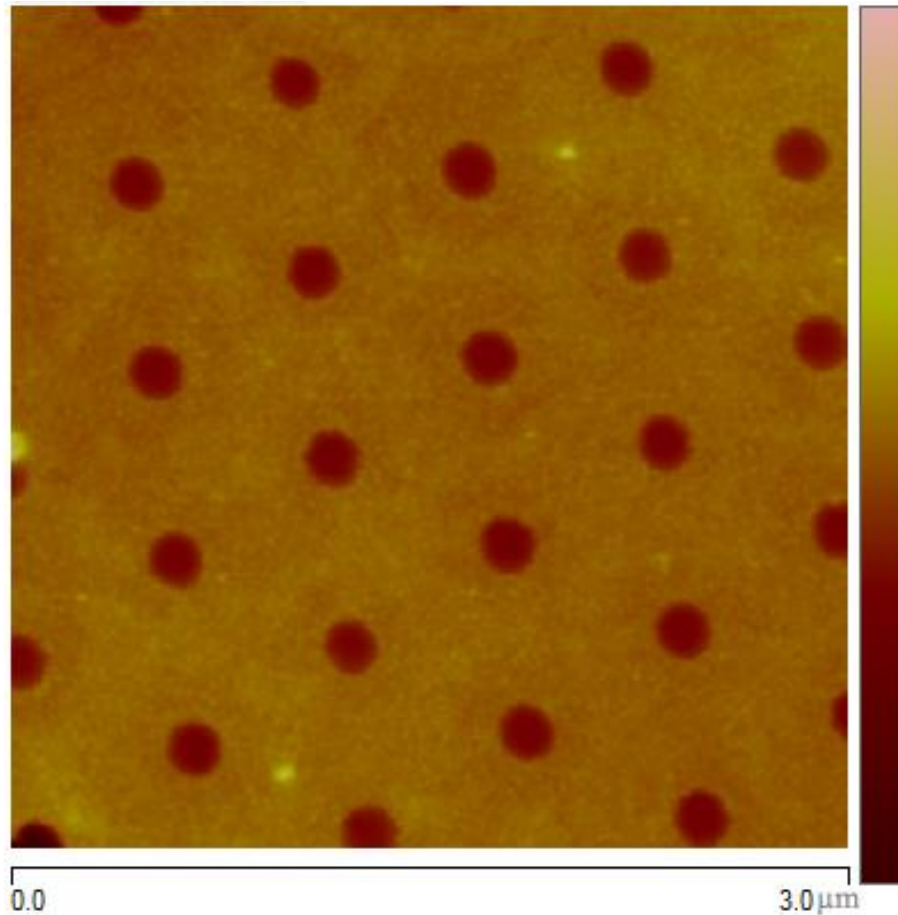
Figure 6-8 AFM images of a freestanding nanohole membrane.

6.4   Optical Property

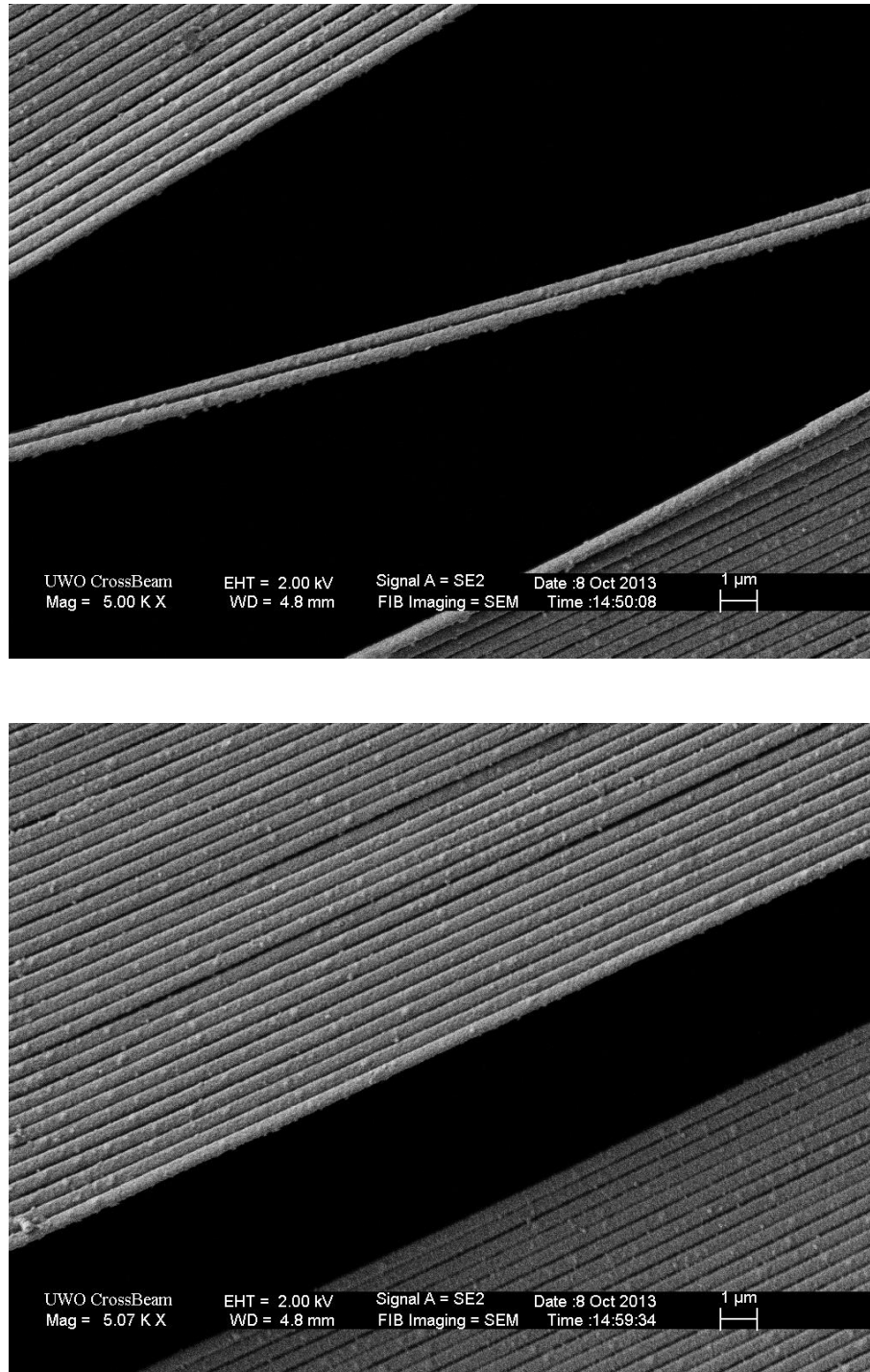We record the transmission spectra of the same Au nanohole array membrane in freestanding format and on the substrate (refractive index 1.45). SPR transmission efficiency significantly increases in the freestanding nanomembrane compared to the nanohole array on the substrate, as shown in Figure 6-9. In the substrate case, dielectric materials with different dielectric constants on either side of the nanohole array film lead to the SPR at different wavelength. In contrast, the uniform dielectric environment in the freestanding case matches SP energy on both surfaces, thereby resulting in the coincidence

of the SPR on both surfaces and remarkable enhancement of the transmission intensity. According to the sensitivity analysis in Chapter 3, this field enhancement would significantly increase the performance of plasmonic sensors.
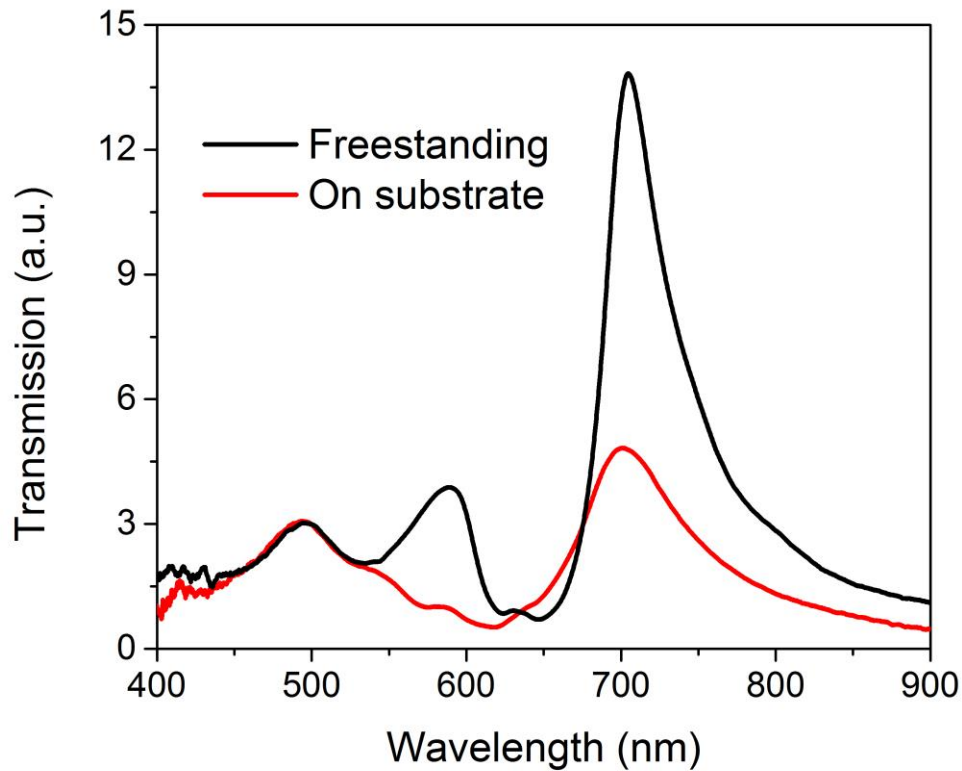
Figure 6-9 Transmission spectra of the same nanohole array membrane in freestanding format and on the substrate.

6.5   Conclusion

In summary, a novel fabrication scheme is developed based on the previous template transfer technique for freestanding metal nanomembranes. This method is also applicable for freestanding nanoslit fabrication. The created nanomembrane with the periodic

nanohole array features high uniformity in large area. Some interesting behaviors during characterization imply this freestanding metal nanomembrane has special mechanical and electrical properties. In comparison to the same nanohole array on the substrate, the freestanding nanohole array show much higher transmission intensity, which would enhance the plasmonic sensing performance.

References

1.   Rogers, J.; Lagally, M.; Nuzzo, R., Synthesis, assembly and applications of semiconductor nanomembranes. *Nature* **2011,** *477* (7362), 45-53.

2.   Striemer, C. C.; Gaborski, T. R.; McGrath, J. L.; Fauchet, P. M., Charge-and size-based separation of macromolecules using ultrathin silicon membranes. *Nature* **2007,** *445* (7129), 749-753.

3.   Roberts, M. M.; Klein, L. J.; Savage, D. E.; Slinker, K. A.; Friesen, M.; Celler, G.; Eriksson, M. A.; Lagally, M. G., Elastically relaxed free-standing strained-silicon nanomembranes. *Nature materials* **2006,** *5* (5), 388-393.

4.   Jin, J.; Wakayama, Y.; Peng, X.; Ichinose, I., Surfactant-assisted fabrication of free-standing inorganic sheets covering an array of micrometre-sized holes. *Nature materials* **2007,** *6* (9), 686-691.

5.   Mueggenburg, K. E.; Lin, X.-M.; Goldsmith, R. H.; Jaeger, H. M., Elastic membranes of close-packed nanoparticle arrays. *Nature materials* **2007,** *6* (9), 656-660.

6.   Lee, C.; Wei, X.; Kysar, J. W.; Hone, J., Measurement of the elastic properties and intrinsic strength of monolayer graphene. *Science* **2008,** *321* (5887), 385-388.

7.   Kim, K. S.; Zhao, Y.; Jang, H.; Lee, S. Y.; Kim, J. M.; Kim, K. S.; Ahn, J.-H.; Kim, P.; Choi, J.-Y.; Hong, B. H., Large-scale pattern growth of graphene films for stretchable transparent electrodes. *Nature* **2009,** *457* (7230), 706-710.

8.   Kang, E.; Ryoo, J.; Jeong, G. S.; Choi, Y. Y.; Jeong, S. M.; Ju, J.; Chung, S.; Takayama, S.; Lee, S. H., Large‐Scale, Ultrapliable, and Free‐Standing Nanomembranes. *Advanced Materials* **2013,** *25* (15), 2167-2173.

9.   Watanabe, H.; Kunitake, T., A Large, freestanding, 20 nm thick nanomembrane based on an epoxy resin. *Advanced Materials* **2007,** *19* (7), 909-912.

10.   Vendamme, R.; Onoue, S.-Y.; Nakao, A.; Kunitake, T., Robust free-standing nanomembranes of organic/inorganic interpenetrating networks. *Nature materials* **2006,** *5* (6), 494-501.

11.   Jiang, C.; Markutsya, S.; Pikus, Y.; Tsukruk, V. V., Freely suspended nanocomposite membranes as highly sensitive sensors. *Nature materials* **2004,** *3* (10), 721-728.

12.   Markutsya, S.; Jiang, C.; Pikus, Y.; Tsukruk, V. V., Freely Suspended Layer-by-Layer Nanomembranes: Testing Micromechanical Properties. *Advanced Functional Materials* **2005,** *15* (5), 771-780.

13.   Mattsson, J.; Forrest, J.; Börjesson, L., Quantifying glass transition behavior in ultrathin free-standing polymer films. *Physical Review E* **2000,** *62* (4), 5187.

14.   Mallwitz, F.; Laschewsky, A., Direct Access to Stable, Freestanding Polymer Membranes by Layer‐by‐Layer Assembly of Polyelectrolytes. *Advanced Materials* **2005,** *17* (10), 1296-1299.

15.   Tang, Z.; Kotov, N. A.; Magonov, S.; Ozturk, B., Nanostructured artificial nacre. *Nature materials* **2003,** *2* (6), 413-418.

16.   Mamedov, A. A.; Kotov, N. A.; Prato, M.; Guldi, D. M.; Wicksted, J. P.; Hirsch, A., Molecular design of strong single-wall carbon nanotube/polyelectrolyte multilayer composites. *Nature materials* **2002,** *1* (3), 190-194.

17.   Huck, W. T.; Stroock, A. D.; Whitesides, G. M., Synthesis of geometrically well defined, molecularly thin polymer films. *Angewandte Chemie International Edition* **2000,** *39* (6), 1058-1061.

18.   Mamedov, A. A.; Kotov, N. A., Free-standing layer-by-layer assembled films of magnetite nanoparticles. *Langmuir* **2000,** *16* (13), 5530-5533.

19.   Eck, W.; Küller, A.; Grunze, M.; Völkel, B.; Gölzhäuser, A., Freestanding Nanosheets from Crosslinked Biphenyl Self‐Assembled Monolayers. *Advanced Materials* **2005,** *17* (21), 2583-2587.

20.   Xu, H.; Goedel, W. A., Polymer-silica hybrid monolayers as precursors for ultrathin free-standing porous membranes. *Langmuir* **2002,** *18* (6), 2363-2367.

Chapter 7

7 Thesis Summary and Future Direction

This thesis focuses on two important aspects of surface plasmonic resonance sensing: theoretical analysis and sensor engineering. A performance analysis model has been proposed and plasmonic optical sensors in three modalities are respectively have been implemented. They are summarized according to the thesis structures as follows. In the end, a few future directions are discussed.

7.1 Thesis Summary

A universal performance analysis model for nanoplasmonic sensors is proposed in Chapter 3 based on surface plasmon theory introduced in Chapter 2. A sensitivity expression is established using the momentum matching condition of SPR excitation for any tow-dimensional nanohole Bravais lattices. The formula only consists of parameters relative to essential elements involved in SPR sensing. A series of phenomena in plasmonic sensing are successfully explained using this quantitative model, including (1) sensitivity roughly linearly increase as the SPR position shifts to longer wavelength; (2) different patterns with the same SPR wavelength show very similar sensitivities; (3) nanostructures with different metals have similar sensitivity at the same wavelength; (4) SPR peaks show higher sensitivity in the analyte with lower refractive index. The nanohole arrays are proved to have larger intrinsic sensitivity compared to nanoparticle LSPR sensors. The expression is also applicable to general two-dimensional plasmonic nanostructure including quasiperiodic and aperiodic arrays. The analytical model is proved to be valid in plasmonic

sensors performance analysis by the comparison between the published sensitivity data and the analytical results calculated with this model.

Chapter 4 present a high-performance on-chip plasmonic sensor based on transmission through nanohole arrays fabricated by template transfer in a simple two-step process of Au evaporation and transfer. This novel approach is capable of low-cost and high-throughput fabrication of plasmonic nanostructures since the templates can be repeatedly used. By the sensitivity comparison between two nanohole array sensors with different morphology, the in-hole surface is verified to have higher sensitivity. The sensor with a 522nm/RIU sensitivity can resolve refractive index changes down to 2×10^{-5} RIU via spectra averaging and an effective peak position tracking algorithm. Moreover, this instrument is employed to detect cTnI at a relatively low concentration.

Plasmonic optical fibers with general metal nanostructures from nanohole arrays to nanoslit arrays on the endfaces are implemented by a simple and effective transfer method in Chapter 5. By adjusting the viscosity of adhesive layers, surface topography of metal structures can be controlled. The specially designed plasmonic fiber can work in multimode (transmission and reflection) at the same time in refractive index sensing. This plasmonic fiber features remarkably narrow linewidth of 6.6 nm and high figure of merit of 60.7. A real-time biosensing is demonstrated using the plasmonic optical fiber for the first time. Furthermore, the plasmonic fibers possess great stability to resist mechanical bending. The linked plasmonic fibers are capable of improving optical performance and achieving optical multiple-filter.

In Chapter 6, large-area freestanding metal nanomembranes are achieved using novel fabrication scheme based on the template transfer method. This technique is same applicable to freestanding nanoslit fabrication. The formed freestanding Au nanomembrane with the periodic nanohole array is qualified with high uniformity. Some interesting behaviors during characterization suggest this freestanding metal nanomembrane has special mechanical and electrical properties. The freestanding nanohole array exhibit remarkably higher transmission intensity in comparison to the same nanohole array on the substrate. This feature qualifies the freestanding metal nanomembrane as a high performance plasmonic sensor.

7.2 Thesis Contribution

The two major contributions of this thesis are summarized:

- A universal performance analysis model is established for general two-dimensional plasmonic sensors. This model is based on the fundamental facts of surface plasmon theory. The sensitivity expression discloses the relationship between plasmonic sensor performance and essential physics of surface plasmon.

- Plasmonic optical sensors are engineered into high-performance on-chip sensors, plasmonic optical fibers and freestanding nanomembranes. These three modalities possess different applicability to fulfill various plasmonic sensing tasks in respective scenarios.

7.3 Future Direction

The plasmonic optical sensors implemented in this thesis will be utilized in more biological and biochemical application, especially in detection and monitoring of those disease-

related biomarkers. For instance, the plasmonic optical fiber can be employed for in-vivo biosensing in urine or saliva. This would be a valuable tool to be capable of provide real-time information related to disease process.

Although the biosensors based on SPR provides ultrahigh sensitivity, compactness, and multiplexing capabilities, the major drawback is they lack molecular specificity. Since their operation completely relies on SPR responses to the refractive index changes at the metal/dielectric interface, this type of signals are incapable of discriminating between specific and nonspecific binding, which may result in false positives. On the other hand, surface-enhanced Raman spectroscopy (SERS) combines the advantage of SPR field enhancement with unique spectral features of Raman signal. To enable molecular specificity, the plasmonic sensors proposed in this thesis will act as SERS substrates to provide valuable spectroscopy tools for the identification of chemical and biological samples.

Appendices

Appendix 1 Derivation of Sensitivity for a Periodic Nanohole Array Sensor

Given differentiation in a relatively narrow wavelength range, we neglect the spectral dispersion of the metallic material, *e.g.* ε_m does not change in a very narrow λ range in the following deduction.

$$S/\lambda = \frac{1}{\lambda} \lim_{n \to n_0} \frac{\lambda - \lambda_0}{n - n_0}$$

$$= \frac{1}{\frac{a_0}{\sqrt{i^2 + j^2}} \left(\frac{\varepsilon_m' n^2}{\varepsilon_m' + n^2}\right)^{1/2}} \lim_{n \to n_0} \frac{\frac{a_0}{\sqrt{i^2 + j^2}} \left(\frac{\varepsilon_m' n^2}{\varepsilon_m' + n^2}\right)^{1/2} - \frac{a_0}{\sqrt{i^2 + j^2}} \left(\frac{\varepsilon_m' n_0^2}{\varepsilon_m' + n_0^2}\right)^{1/2}}{n - n_0}$$

$$= \frac{1}{\left(\frac{\varepsilon_m' n^2}{\varepsilon_m' + n^2}\right)^{1/2}} \lim_{n \to n_0} \frac{\left(\frac{\varepsilon_m' n^2}{\varepsilon_m' + n^2}\right)^{1/2} - \left(\frac{\varepsilon_m' n_0^2}{\varepsilon_m' + n_0^2}\right)^{1/2}}{n - n_0}$$

$$= \frac{1}{\left(\frac{\varepsilon_m' n^2}{\varepsilon_m' + n^2}\right)^{1/2}} \lim_{n \to n_0} \frac{\frac{\varepsilon_m' n^2}{\varepsilon_m' + n^2} - \frac{\varepsilon_m' n_0^2}{\varepsilon_m' + n_0^2}}{(n - n_0) \left[\left(\frac{\varepsilon_m' n^2}{\varepsilon_m' + n^2}\right)^{1/2} + \left(\frac{\varepsilon_m' n_0^2}{\varepsilon_m' + n_0^2}\right)^{1/2}\right]}$$

$$= \frac{1}{\left(\frac{\varepsilon_m' n^2}{\varepsilon_m' + n^2}\right)^{1/2}} \lim_{n \to n_0} \frac{\frac{\varepsilon_m' n^2(\varepsilon_m' + n_0^2) - \varepsilon_m' n_0^2(\varepsilon_m' + n^2)}{(\varepsilon_m' + n^2)(\varepsilon_m' + n_0^2)}}{(n - n_0) \left[\left(\frac{\varepsilon_m' n^2}{\varepsilon_m' + n^2}\right)^{1/2} + \left(\frac{\varepsilon_m' n_0^2}{\varepsilon_m' + n_0^2}\right)^{1/2}\right]}$$

$$= \frac{1}{\left(\frac{\varepsilon_m' n^2}{\varepsilon_m' + n^2}\right)^{1/2}} \lim_{n \to n_0} \frac{\frac{\varepsilon_m'^2(n^2 - n_0^2)}{(\varepsilon_m' + n^2)(\varepsilon_m' + n_0^2)}}{(n - n_0) \left[\left(\frac{\varepsilon_m' n^2}{\varepsilon_m' + n^2}\right)^{1/2} + \left(\frac{\varepsilon_m' n_0^2}{\varepsilon_m' + n_0^2}\right)^{1/2}\right]}$$

$$= \frac{1}{\left(\frac{\varepsilon_m' n^2}{\varepsilon_m' + n^2}\right)^{1/2}} \lim_{n \to n_0} \frac{\frac{\varepsilon_m'^2(n + n_0)}{(\varepsilon_m' + n^2)(\varepsilon_m' + n_0^2)}}{\left(\frac{\varepsilon_m' n^2}{\varepsilon_m' + n^2}\right)^{1/2} + \left(\frac{\varepsilon_m' n_0^2}{\varepsilon_m' + n_0^2}\right)^{1/2}}$$

$$= \frac{1}{\left(\dfrac{\varepsilon_m' n^2}{\varepsilon_m' + n^2}\right)^{1/2}} \cdot \frac{\dfrac{2\varepsilon_m'^2 n}{(\varepsilon_m' + n^2)^2}}{2\left(\dfrac{\varepsilon_m' n^2}{\varepsilon_m' + n^2}\right)^{1/2}} = \frac{\varepsilon_m'}{n(\varepsilon_m' + n^2)}$$

That is

$$S/\lambda = \frac{\varepsilon_m'}{n(\varepsilon_m' + n^2)}$$

Appendix 2 Copyright permission for using article "Integration of large-area metallic nanohole arrays with multimode optical fibers for surface plasmon resonance sensing"

<u>**License Number**</u>	<u>**3342050970317**</u>
Order Date	Mar 04, 2014
Publisher	AIP Publishing LLC
Publication	Applied Physics Letters
Article Title	Integration of large-area metallic nanohole arrays with multimode optical fibers for surface plasmon resonance sensing
Author	Peipei Jia,Jun Yang
Online Publication Date	Jun 19, 2013
Volume number	102
Issue number	24
Type of Use	Thesis/Dissertation
Requestor type	Author (original article)
Format	Electronic
Will you be translating?	No
Title of your thesis / dissertation	PLASMONIC OPTICAL SENSOR: PERFORMANCE ANALYSIS AND ENGINEERING FOR BIOSENSING
Expected completion date	Mar 2014

Appendix 3 Copyright permission for using article "Plasmonic nanohole array sensors fabricated by template transfer with improved optical performance"

Assignment of copyright form - IOP Publishing Limited

3. Author Rights

3.1 IOP grants the Named Authors the rights specified in 3.2, 3.3 and 3.4. All such rights must be exercised for non-commercial purposes, if possible should display citation information and IOP's copyright notice, and for electronic use best efforts must be made to include a link to the online abstract in the Journal. Exercise of the rights in 3.3 and 3.4 additionally must not use the final published IOP format but the Named Author's own format (which may include amendments made following peer review, but not any editing, typesetting or other changes made by IOP) (the "Accepted Manuscript").

3.2 The rights are:

3.2.1 To make copies of the Article (all or part) for teaching purposes;

<u>3.2.2 To include the Article (all or part) in a research thesis or dissertation;</u>

3.2.3 To make oral presentation of the Article (all or part) and to include a summary and/or highlights of it in papers distributed at such presentations or in conference proceedings; and

3.2.4 All proprietary rights other than copyright.

Curriculum Vitae

Name:	Peipei Jia
Post-secondary Education and Degrees:	Shandong University Jinan, Shandong, China 2000-2004 B.A. Zhejiang University, Hangzhou, Zhejiang, China 2004-2006 M.A. Shandong University Jinan, Shandong, China 2008-2010 Ph.D. Candidate The University of Western Ontario London, Ontario, Canada 2010-2014 Ph.D. Candidate
Honours and Awards:	University Undergraduate Student Scholarship Shandong University 2001-2002, 2002-2003 Post-graduate Study Abroad Scholarship Ministry of Education of the P.R. China 2010-2013
Related Work Experience	Teaching Assistant The University of Western Ontario 2010-2014

Publications:

- **Peipei Jia** and Jun Yang, "Integration of large-area metallic nanohole arrays with multimode optical fibers for surface plasmon resonance sensing", *Appl. Phys. Lett.*, Vol. 102, 243107, 2013.

- **Peipei Jia**, Hao Jiang, Jayshri Sabarinathan and Jun Yang, "Plasmonic nanohole array sensors fabricated by template transfer with improved optical performance", *Nanotechnology*, Vol. 24, 195501, 2013.

- **Peipei Jia** and Jun Yang "Biophotonics and Its Applications in Lab-on-a-Chip or BioMEMS Platforms", a chapter in the book: *Optical Nano and Micro Actuator Technology*.

- Yinyao Zhu, **Peipei Jia**, Huilong Duan, Xudong Lu "Integration of Medical Information Systems Based on Virtual Database and Web Services", Proceedings of the 3rd International Conference on Bioinformatics and Biomedical Engineering, 2009.

- Jiye An, Xudong Lu, Huilong Duan, Haomin Li and **Peipei Jia**, 'An Act Indexing Information Model for Clinical Data Integration', Proceedings of the 1st IEEE International Conference on Bioinformatics and Biomedical Engineering, 2007.

- **Peipei. Jia**, "Service-Oriented Architecture Integration of Medical Information Systems", Master dissertation, Zhejiang University, 2006.